An Engineered Inter-domain Disulfide Bridge in Flavocytochrome b_2: Insights into the Role of Domain Mobility

Katy J Drewette

Thesis presented for the degree of Doctor of Philosophy

University of Edinburgh

2006

For my Mum and Dad

"Logic will get you from A to B. Imagination will take you everywhere."

Albert Einstein

Declaration

The work presented in this thesis is the original work of the author, except where specific reference is made to other sources. It has not been submitted in part, or in whole, for any other degree.

Katy J Drewette

Acknowledgements

Many thanks go to my supervisors Prof Steve Chapman and Prof Graeme Reid, without whom, this PhD would not have been possible. Your help and guidance has been invaluable, especially when I was having doubts at the end of my first year. Special thanks also to Dr Caroline Miles for her help and patience carrying out Site-directed mutagenesis, Dr Simon Daff for his knowledge of enzyme kinetics and Dr Chris Mowat for his invaluable help to gather and process X-ray crystallographic data and ultimately provide a great crystal structure. I would also like to give particular thanks to Prof Lesley Yellowlees for her support and encouragement throughout my PhD, Dr Emma Rothery for her help when I started in the lab, and also Miss Chiara Bruckmann for help in solving the 'multimer problem' and obtaining crystals from which a structure was solved.

Very many thanks also to all the members of the Chapman, Daff, Yellowlees and Reid groups, both past and present, who have made the lab an enjoyable place to work. My greatest thanks to the friends I have made during my time at Edinburgh University. It would not have been the same without you.

Most of all I would like to thank my Mum and Dad and family for their support and encouragement over the past three years, and Grandpa Smith, who I know would have been extremely proud of this academic achievement.

Abstract

Flavocytochrome b_2 from the yeast *Saccharomyces cerevisiae* is a L-lactate:cytochrome *c* oxidoreductase. The crystal structure of this homotetrameric enzyme has been solved to 2.4 Å (Xia & Mathews, 1990). Each subunit consists of two distinct domains; a small (100 residue) N-terminal cytochrome domain containing a *b*-type heme, and a larger (411 residue) C-terminal domain containing flavin mononucleotide (FMN). Substrate dehydrogenation occurs at the FMN, which is then re-oxidised by stepwise transfer of electrons via the b_2-heme to cytochrome *c*. The two domains are connected by a hinge sequence, running from residues 89 to 103. It has been proposed that the most likely role of this hinge region is to confer inter-domain mobility, allowing movement of the cytochrome domain with respect to the flavin domain (White *et al.*, 1993). This proposal is supported by a number of observations from crystallography (Xia & Mathews, 1990) and NMR spectroscopy (Labeyrie *et al.*, 1988). In light of these observations key questions arise – why is there inter-domain mobility in flavocytochrome b_2 and is it important for catalysis? Previous experiments involving "hinge-swap" enzyme (White *et al.*, 1993) as well as more subtle mutations involving insertions/deletions to the hinge region (Sharp *et al*, 1994, 1996) have illustrated the importance of maintaining the structural integrity of the hinge for efficient inter-domain communication.

An alternative approach to examine the importance of domain mobility is to try and restrict it. In this work a disulfide-bridge was engineered in a position, such that the two domains would be fixed in close proximity. Site-directed mutagenesis was used to make the double mutation, N42C:K324C. The crystal structure of the N42C:K324C mutant enzyme was solved to 3.0 Å resolution. An inspection of this structure has confirmed the existence of the imposed disulfide-bridge. In addition, the four b_2-heme domains of the tetramer are ordered, indicating their limited mobility. Ellman assays were used to chemically confirm the existence of a disulfide-bridge between positions 42 and 324.

Steady-state kinetic analyses with L-lactate, using ferricyanide $[Fe(CN)_6]^{3-}$ and cytochrome *c* as electron acceptors were carried out in both the closed (disulfide-bridged form) and open (disulfide-bridge cleaved after addition of dithiothreitol)

forms of the mutant enzyme. The formation of the disulfide-bridge causes a 15-fold decrease in k_{cat} with both electron acceptors. Since $[Fe(CN)_6]^{3-}$ can accept electrons from both the FMN and b_2-heme while cytochrome *c* can only accept electrons from the b_2-heme this indicates that it is the rate of FMN reduction by L-lactate that is primarily affected by disulfide-bridge formation.

Pre-steady-state kinetic analyses with L-lactate are consistent with the steady-state data. The formation of the disulfide-bridge makes it impossible to measure the rate constant for FMN reduction directly while b_2-heme reduction shows a rate constant some 450-fold less than in the open form. This is because FMN reduction is very slow and so the flavin is re-oxidised immediately by the subsequent electron transfer to the b_2-heme. If flavin to b_2-heme electron transfer is much faster then b_2-heme reduction will be limited by the rate of formation of reduced flavin. Thus, disulfide-bridge formation substantially lowers the rate of FMN reduction.

Pre-steady-state experiments were carried out with wild-type enzyme and the closed and open forms of the N42C:K324C mutant enzyme to measure their second-order rate constants for the reaction with sulfite. This molecule possesses the ability to form an adduct with the flavin prosthetic group of flavocytochrome b_2 without subsequent transfer of electrons to the b_2-heme. As such, it is a useful tool to investigate accessibility to the active site. Strikingly, the value of k_2 for the closed form of the N42C:K324C mutant enzyme is more than 60-fold lower than that for the open form. Clearly, the rate of sulfite entry to the active site is dramatically slowed by formation of the disulfide-bridge. In addition, binding experiments with sulfite were carried out. The K_d for the closed form of the mutant enzyme is some 6-fold higher than for the open form, indicating that binding of sulfite to the flavin is not favoured in the disulfide-bridged enzyme.

The bimolecular reaction of the closed and open forms of the N42C:K324C mutant enzyme with cytochrome *c* was studied using pre-steady-state techniques. The second-order rate constants for the closed and open forms of the mutant enzyme were found to be very similar, but still 15-fold lower than wild-type enzyme. This suggests that domain movement plays no role in cytochrome *c* reduction, but the imposed cysteine mutations affect the efficiency of this process.

Abbreviations and Units

1. Amino Acids

Both the single and three letter notations are used.

Amino acid	Three letter code	Symbol
Alanine	Ala	A
Arginine	Arg	R
Asparagine	Asn	N
Aspartic acid	Asp	D
Cysteine	Cys	C
Glutamic acid	Glu	E
Glutamine	Gln	Q
Glycine	Gly	G
Histidine	His	H
Isoleucine	Ile	I
Leucine	Leu	L
Lysine	Lys	K
Methionine	Met	M
Phenylalanine	Phe	F
Proline	Pro	P
Serine	Ser	S
Threonine	Thr	T
Tryptophan	Trp	W
Tyrosine	Tyr	Y
Valine	Val	V

2. Mutations

When referring to amino acid substitutions as a result of site-directed mutagenesis, two different notations are used. Using the example of substitution of asparagine 42 by cysteine in flavocytochrome b_2, then the two representations would be;

Asn42→Cys or N42C

3. Nucleotides

When reference is made to nucleotide sequence, the abbreviations used are:

A	adenine
C	cytosine
G	guanine
T	thymine
U	uracil

4. Kinetic Parameters

K_m	Michaelis constant
k_{cat}	Rate constant at saturation
k_{et}	Rate of electron transfer
k_{lim}	Limiting rate constant
k_{max}	Maximal rate constant
K_i	Inhibition constant
K_d	Dissociation constant

5. Standard Units

m	metre	**°C**	degree Celsius
g	gram	**M**	molar
s	second	**V**	volt
l	litre	**Å**	Angstrom

6. Other Abbreviations

Abs	Absorbance
ADP	Adeosine diphosphate
ATP	Adenosine-5'-triphosphate
Da	Daltons
dH_2O	deionised water
dsDNA	Double stranded deoxyribonucleic acid
DMSO	Dimethyl sulfoxide
DTT	Dithiothreitol
ε_χ	Extinction coefficient at wavelength χ
EBI	European Bioinformatics Institute
E. coli	*Escherichia coli*
EDTA	Ethylenediaminetetraacetic acid
EPR	Electron Paramagnetic Resonance Spectroscopy
ER	Endoplasmic reticulum
ESRF	European Synchotron Radiation Facility
EtOH	Ethanol
FAD	Flavin adenine dinucleotide
FMN	Flavin mononucleotide
ΔG	Free energy change
H. anomola	*Hansenula anomala*
I	Ionic strength
LB	Luria Bertani
MES	2-[N-morpholino]ethanesulfonic acid
NMR	Nuclear magnetic resonance spectroscopy
NADH	β-Nicotinamide adenine dinucleotide
PAGE	Polyacrylamide Gel Electrophoresis
PDB	Protein Data Bank
PDI	Protein Disulfide Isomerase
PDS	2, 2'-Dipyridyl disulfide
PEG	Polyethylene glycol
S. cerevisiae	Saccharomyces cerevisiae
SDM	Site-directed mutagenesis

SDS	Sodium dodecyl sulfate
TAE	Tris /acid/EDTA
Tris	Tris(hydroxymethyl)aminomethane
UV	Ultraviolet
Vis	Visible

Contents

List of Figures

Chapter 3 Biochemical and Structural Characterisation of the N42C:K324C Mutant Flavocytochrome b_2 77

List of Tables

Chapter

Introduction

Chapter 1
Introduction

1.1 Electron Transfer in Proteins

Biological electron transfer takes place within all living organisms and is an essential means by which processes such as respiration and photosynthesis can take place. Adenosine triphosphate (ATP) is the central character in bioenergetics. It is the immediate source of energy that powers cellular work. The release of this energy, however, must be carried out in an efficient manner. Just as the explosion of a petrol tank would not drive a car very far, neither, would the oxidation of glucose in a single explosive step harvest enough energy for cellular respiration. In eukaryotic cells, glucose and other organic fuels are broken down gradually in a series of electron transfer steps which utilize many respiratory complexes in the mitochondrial inner membrane (Figure 1.1). Electrons removed from an organic fuel are transported by NADH through this electron transport chain. The electrons can then cascade down a potential gradient, losing a small amount of energy with each step until they finally reach oxygen, the terminal electron acceptor. This also takes place in the cell membrane of bacteria, where electrons are transferred from a variety of donors down a potential gradient, via protein complexes, to a variety of electron acceptors. These electron donors and acceptors are dependant upon the type of bacterium and its physiological environment (Pettigrew and Moore, 1987). In plant cells, ATP is produced by a photoinitiated electron transfer from water to $NADP^+$, up a potential gradient, via the photosynthetic reaction complexes in the thylakoid membranes of chloroplasts (Campbell, 1996).

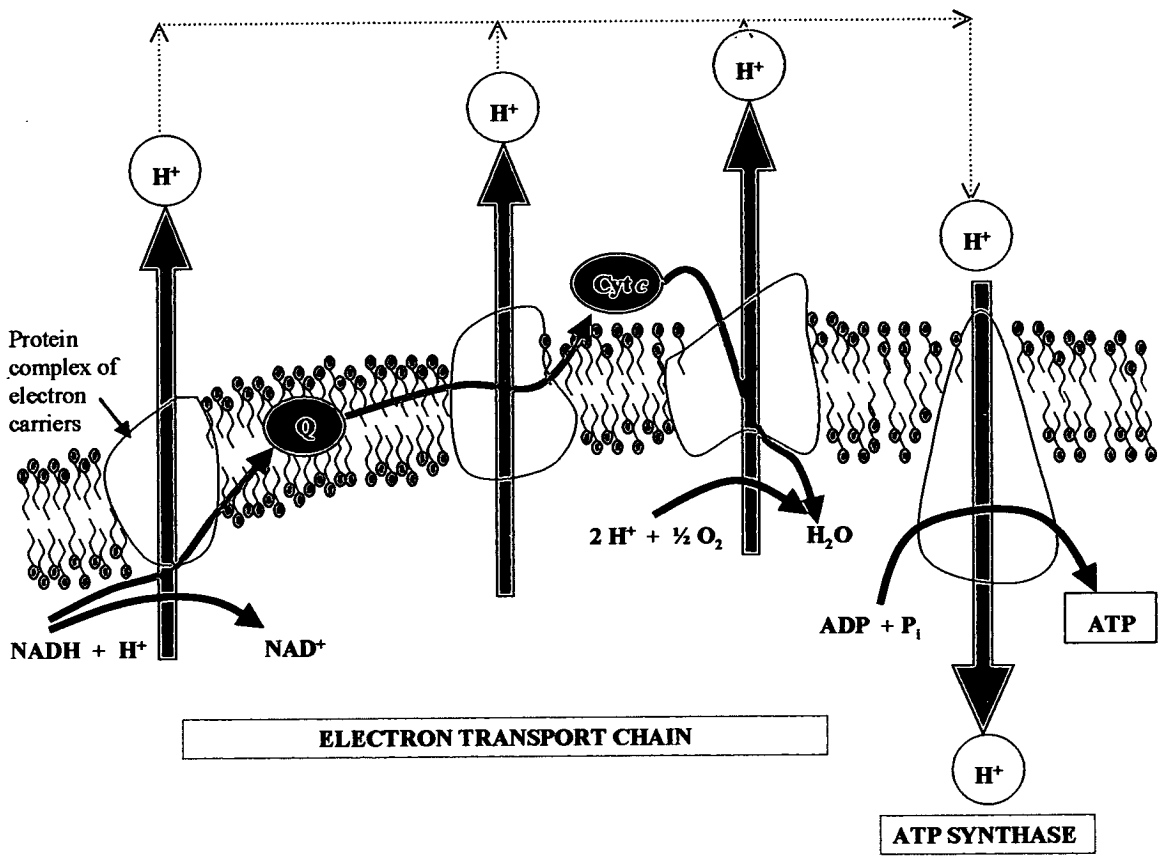

Figure 1.1: *Oxidative Phosphorylation: NADH transports electrons from an organic fuel to an electron transport chain which is built into the inner mitochondrial membrane. The pink arrow represents the transport of electrons, which pass to oxygen at the end of the chain to form water. Most of the cytochromes and redox centres are collected into complexes represented by the salmon coloured "blobs". Ubiquinone (Q) and cytochrome c (Cyt c) move rapidly along the membrane, carrying electrons between the complexes. As each complex accepts and donates electrons it pumps protons (H^+) from the mitochondrial matrix to the intermembrane space, thus forming a proton motive force (an electrochemical gradient). The protons then flow back through a H^+ channel in ATP Synthase. This complex exploits the proton motive force to phosphorylate ADP, thus by forming ATP.*

1.2 Redox Centres

Biological electron-transfer reactions occur between redox centres in proteins, i.e. moieties that can donate and accept electrons to one another. The electron transfer proteins consist of a suitable redox centre enclosed by a tertiary structure of peptide helix and sheet. Common redox centres include organic molecules such as flavin mononucleotide (FMN); iron contained within a porphyrin ring or held within a sulphur cluster; or metal ions, such as copper and nickel. The proteins themselves can be membrane bound such as those found in the photosynthetic and respiratory complexes. Alternatively, they can be soluble as is the case for simpler redox proteins such as cytochromes *c* and blue copper proteins. Examples of these cofactors found within redox proteins are given below.

1.2.1 Heme Containing Proteins

As well as being renowned for their excellence in electron transfer (Moore, 1996), heme-containing proteins enjoy a diversity of other biological functions such as oxygen transport and storage via hemoglobin and myoglobin (Jameson and Ibers, 1994), oxygen reduction to the level of water by cytochrome oxidase (Malatesta *et al.*, 1995), the reduction of peroxides by catalases and peroxides (Frew & Jones, 1984) and oxygenations of organic substrates as facilitated by the cytochromes P-450 (Oritz de Montellano, 1995). The heme group itself consists of an iron atom coordinated in a square planar geometry by the four ring nitrogen atoms of a porhyrin macrocycle. It has a number of common representations that are illustrated in Figure 1.2.

Heme-*a* provides cofactors for the cytochrome aa_3 of cytochrome oxidase so that oxygen reduction can take place (Malatesta *et al.*, 1995). The structure of heme-*a* shows a hydroxyethylfarnesyl sidechain at position 2 of the protoporphyrin ring and a formyl group at position 8.

Heme-*b* is the type seen in hemoglobin, myoglobin, catalase, *b*-type cytochromes and the cytochromes P-450. It is also termed protoheme IX.

Heme-*c* is the prosthetic group for the family of *c*-type cytochromes that have been extensively studied (Chapman *et al.*, 1997). These are usually electron transfer proteins

and differ from heme-*b* because they are covalently linked to the protein via thioether linkages between cysteine residues on the protein and the 1'-carbons of the vinyl groups at positions 2 and 4 of the porphyrin ring.

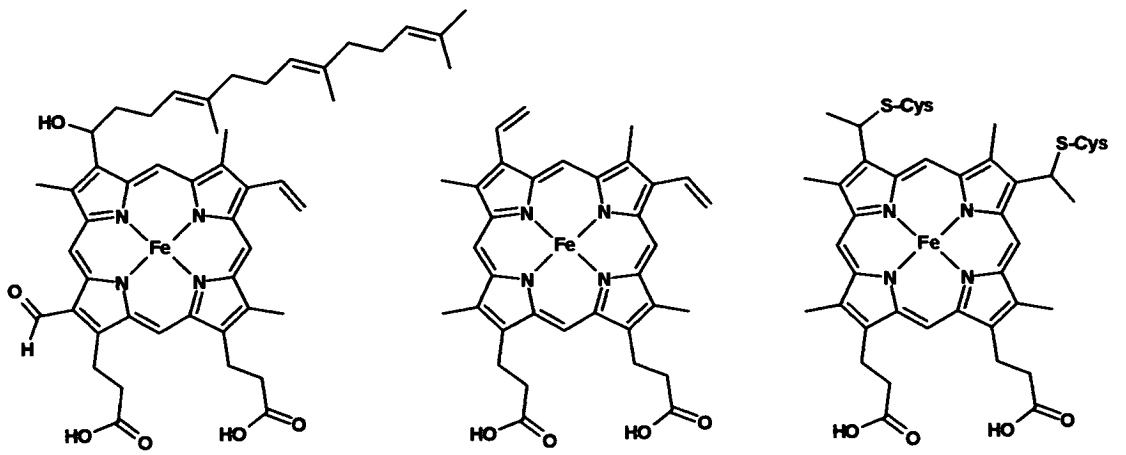

heme *a* heme *b* heme *c*

Figure 1.2: *Hemes commonly found in biological systems.*

The iron atom itself can form two additional bonds, one on either side of the heme plane. These sites are called the fifth and sixth coordination positions and depending upon the nature of the ligands that fill these sites, the hemoprotein will differ in reactivity. Simple electron transfer proteins, which require minimal structural change at the iron centre are invariably hexa-coordinate and low spin. In contrast, proteins that catalyse reactions at the heme face require an available coordination site and are therefore usually penta-coordinate and high spin.

The iron can adopt three oxidation states, these are the ferrous (+2) oxidation state, the ferric (+3) oxidation state, and Fe (+4) as postulated in the cytochromes P450. The oxidation state of the iron is an essential part of the role of the hemoprotein. An example includes hemeoglobin, where only ferrohemoglobin can bind oxygen to transport it around the body, while ferrihemoglobin cannot (Stryer, 1995).

1.2.2 Iron-Sulfur Centres

Iron-sulfur proteins, also known as non-heme iron proteins play a crucial role in a wide range of reduction reactions in biological systems. Several types of Fe-S clusters are known. The simplest type consists of a single iron atom tetrahedrally coordinated to the sulfhydryl groups of four cysteine resides of the protein. The second type, denoted by [2Fe-2S] and known as ferredoxins, contain two iron atoms and two inorganic sulfides, in addition to four cysteine residues. Ferredoxins carry out single electron transfers cycling between Fe(III) and Fe(II). When the iron is reduced it is paramagnetic and hence EPR active. The third type, denoted by [4Fe-4S], contain four iron atoms, four inorganic sulfides, and four cysteine residues. This type include the High Potential Iron-sulfur Proteins (HiPIP). These are a specific class of high-redox potential (+350 mV) 4Fe-4S ferredoxins that function in anaerobic electron transport. Figure 1.3 shows examples of these three different types of Fe-S clusters.

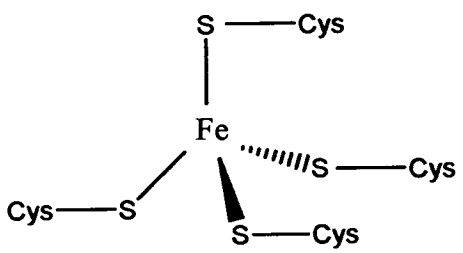

$Fe(S^{y}_{cys})_4$

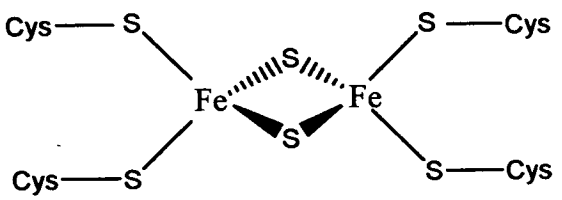

$[Fe_2S_2](S^{y}_{cys})_4$

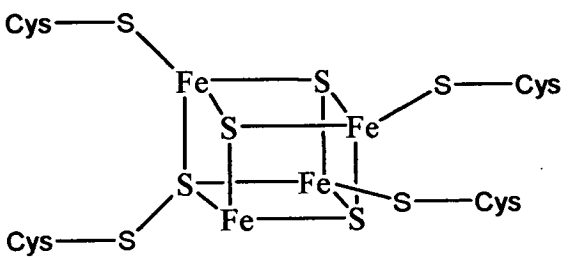

$[Fe_4S_4](S^{y}_{cys})_4$

Figure 1.3: *Examples of iron sulphur clusters. Iron is bound to the protein by the sulfur atoms of cysteine residues.*

1.2.3 Copper

There are three main types of biologically active copper centres found in the copper proteins. These depend on their optical and magnetic properties. The first are the small blue copper proteins that show several charge-transfer bands, the most characteristic of which appears at approximately 600 nm. The single copper centre is bound to the nitrogen atom of two histidine residues and one cysteine thiolate, and either a second cysteine or a methionine sulfur giving a distorted tetrahedral geometry. One of the most well known members of this group of proteins is the bacterial azurins, that exchange electrons with cytochrome *c*551. Type II are the non-blue copper centres and are the most common in copper proteins. They are essentially planar, with the copper ion coordinated to the imidazole N-atom of two or three histidine residues and to O-ligands. They do not show any strong charge-transfer bands in the visible region and its $A\|$ value in EPR spectra is normal. This group includes the copper/zinc superoxide dismutase. Type III copper centres are not detectable by EPR, because they are strongly antiferromagnetically coupled in pairs. The best known example of an enzyme containing a single Type III centre is tyrosinase which catalyzes the production of melanin and other pigments from tyrosine by oxidation.

1.2.4 Nickel

Nickel is a rare element and is found in the environment at only nanomolar concentrations. It is both essential and toxic and as such its detection and transport within a large number of organisms is very highly regulated. It is an integral component of a number of microbial enzymes, such as NiFe hydrogenases, ureases, acetyl coenzyme A synthases and carbon monoxide dehydrogenases (Lancaster, 1988). A recent example of a nickel containing protein is that of the periplasmic nickel transporter NikA, a 56 kDa protein of known structure that binds a single Ni(II) ion (Heddle *et al.*, 2003). A 1.8 Å resolution structure of NikA has shown it to bind $FeEDTA(H_2O)^-$ with high affinity (Cherrier *et al.*, 2005). These results suggest that nickel transport in *E. coli* requires the binding of this metal ion to a natural metallophore that resembles EDTA. These results are significant in that it may find applications in environmental bioremediation of toxic transition metals and the design of artificial metalloenzymes.

1.2.5 Flavin

Flavins are coenzymes based on riboflavin or vitamin B_2. They occur as flavin adenine dinucleotide (FAD) or flavin mononucleotide (FMN) and consist of an isoalloxasine ring system attached at the N-10 position to a phosphorylated ribityl chain (Figure 1.4). The isoaloxasine ring functions as a redox cofactor and can exist in three redox states; fully oxidized, one electron reduced (a stable semiquinone radical) and two electron reduced (hydroquinone). Flavins are able to take part in single electron transfer reactions due to their stable semiquinone state. This is useful in processes such as respiration that require the transfer of electrons to molecular oxygen. O_2 possesses degenerate π^* orbitals which are both singly occupied and are thus unable to accommodate an electron pair without first undergoing a spin-forbidden triplet to singlet electronic transition. This, however, does not apply to single electron transfers.

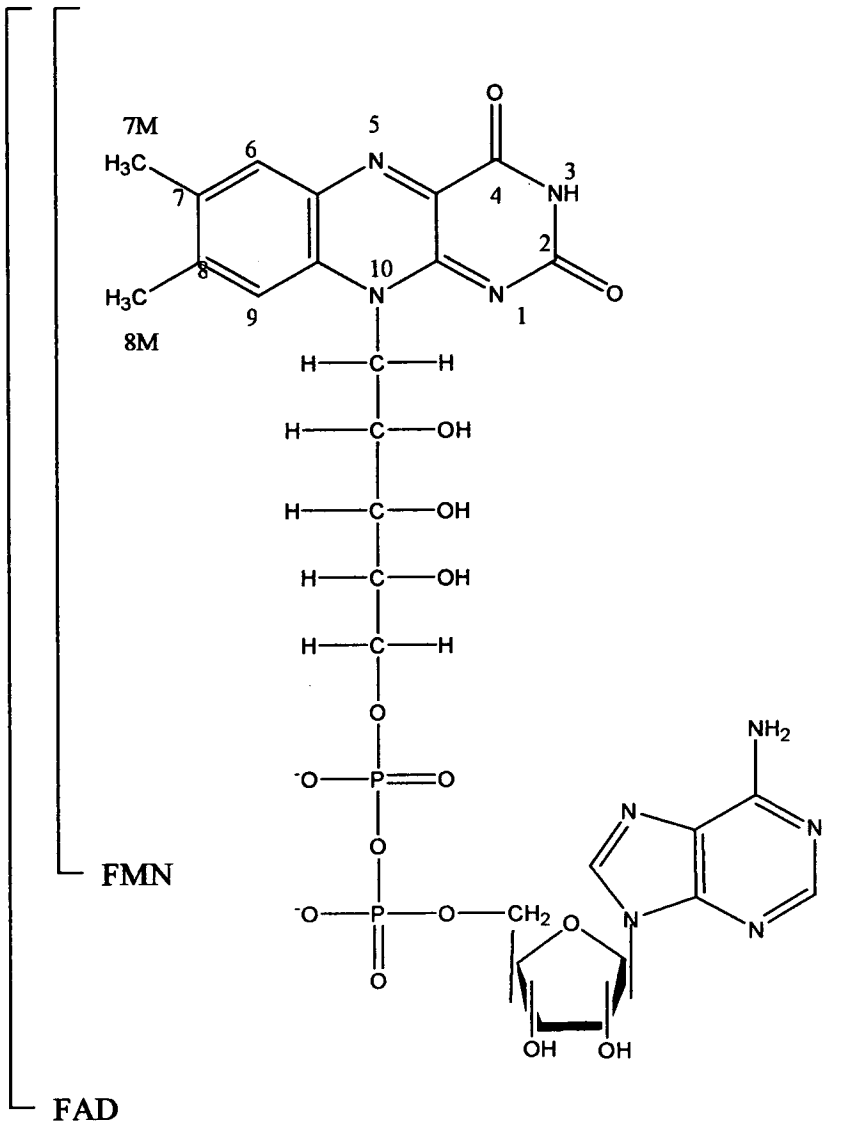

Figure 1.4: *The structures of the oxidized forms of the coenzymes FAD and FMN with the atom nomenclature of the isoalloxasine ring is shown. The electronic structures of the reduced and semiquinone flavin is shown in Figure 1.14.*

1.3 Electron Transfer Theory

The understanding of electron transfer in proteins originates from the work of Marcus (Marcus, 1956; Marcus and Sutin, 1985). For a reaction to occur, the reactants, i.e. those that can donate (D) and accept (A) electrons, must approach each other to enhance the coupling of their electronic orbitals. At the same time there has to be fluctuations in many other coordinates (configurations), such as vibrational configurations and the orientation of the surrounding solvent molecules. The potential energy of the reactants (R) and their surroundings is a function of very many nuclear coordinates, and defines a many-dimensional potential energy surface. A simpler, one-dimensional surface profile is illustrated in Figure 1.5. The profile for the products and their surroundings is labelled P.

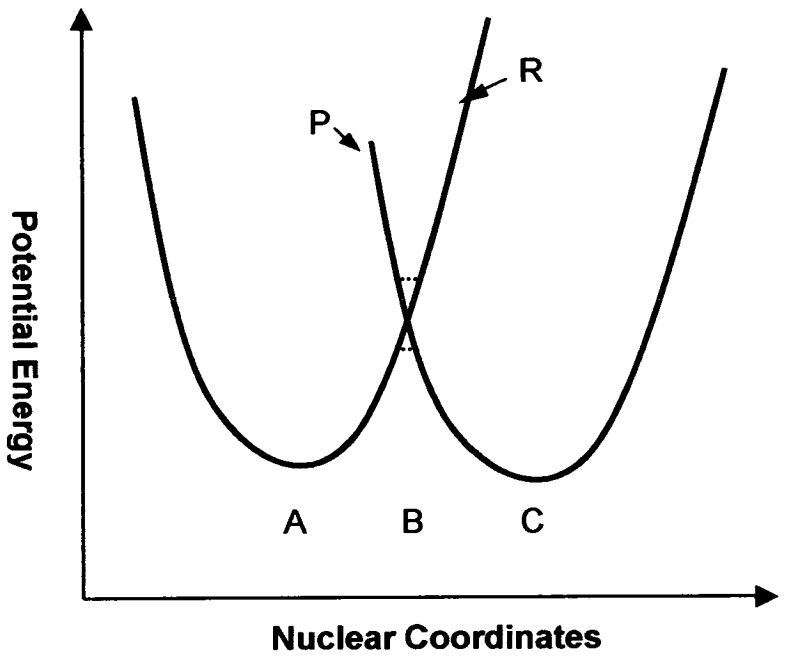

Figure 1.5: *Plot of the potential energy vs nuclear coordinates. This illustrates a many-dimensional potential surface of the reactants plus surrounding medium (R) and that of products plus medium (P). The splitting due to electronic interaction of reactants is shown by the dotted lines. A and C denote nuclear coordinates for equilibrium positions for the reactants and products respectively. B is the nuclear configuration at the intersecting position of the two potential energy surfaces.*

Due to the almost instantaneous electron transfer event between reactant and product, the Franck-Condon principle must be taken into consideration. This states that since electron transfer occurs instantaneously, the nuclei of the reacting species do not have time to change either their position or momenta. In this case, electron transfer must take place at positions at or near to the intersection region in Figure 1.5. In other words, the potential energy of the nuclear configurations for the reactants and products must be equal. For this to happen, the reactants and products must undergo reorganisational energy (λ). This is the amount of energy that must be added to the reactant at its potential minimum to bring the nuclei into the geometry resembling the product at its potential minimum without transferring an electron. In many cases an activation energy is required (ΔG^*), and this is related to the overall driving force (ΔG) and reorganisation energy (λ) by the following equation:

$$\Delta G^* = (\Delta G + \lambda)^2 / 4\lambda$$

Taking the Gaussian dependence on the free energy of electron transfer into account:

$$k_{ET} = k_{max} \exp-(\Delta G + \lambda)^2 / 4\lambda k_B T$$

where k_{ET} is the rate of electron transfer when ΔG^* is zero and k_B is the Boltzmann constant.

By varying ΔG, the rate of electron transfer can be changed because the position of the potential energy curve will move. This leads to three different cases that are shown in Figure 1.6. These are termed *normal* ($\lambda > -\Delta G$); *activationless* ($\lambda = -\Delta G$); and *inverted* ($\lambda < -\Delta G$). When the reorganisational energy is equalled by the free energy, the activation barrier to electron transfer will be zero (Figure 1.6(a)). At this point, $k_{ET} = k_{max}$. If the free energy is not as great as the required reorganisational energy then an activation energy will be required (Figure 1.6(b)). Where the driving force is greater than the reorganisational energy, the *inverted* region takes precedence (Figure 1.6(c)). Any increase in driving force will only act to increase the activation energy more.

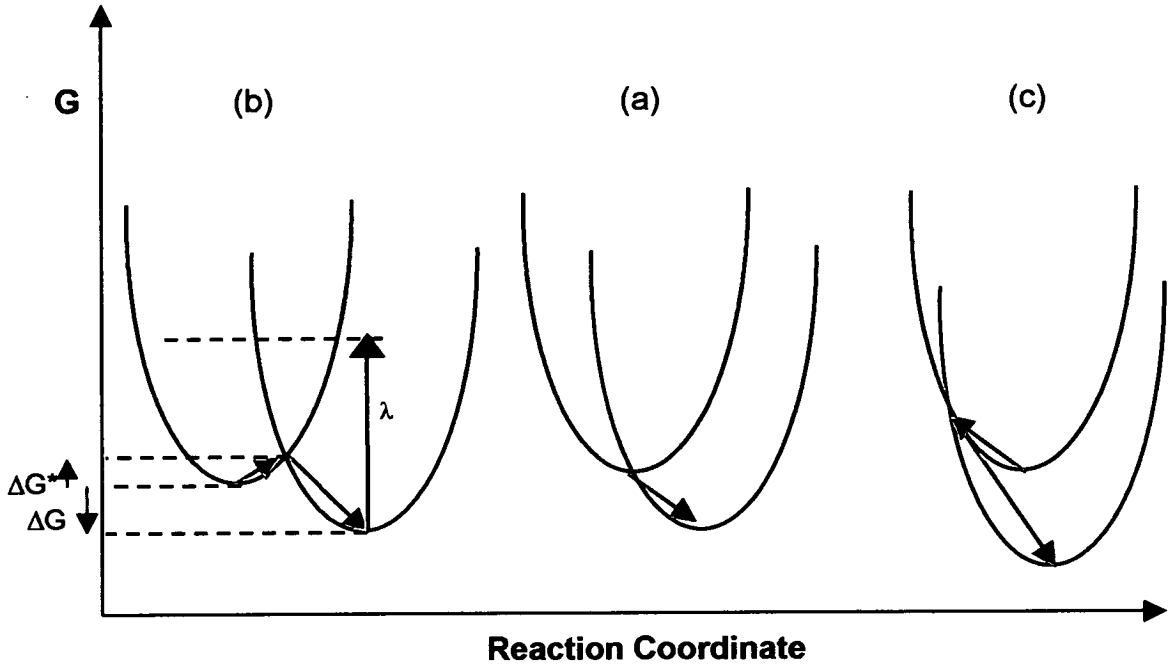

Figure 1.6: *A diagram of the nuclear potential energy (free energy) vs nuclear configuration. The potential well of the reactants is shown in black and that of the products is shown in blue. ΔG* is the activation energy, ΔG is the difference in potential between the reactants and products, and λ is the reorganization energy. Case (b) is the 'normal' region for electron transfer, (a) is 'activationless' electron transfer and (c) electron transfer in the 'inverted' region.*

These situations are depicted as a scheme of electron transfer rate *vs* free energy (-ΔG) in Figure 1.7.

Electron transfer in a biological system must involve the movement of an electron from a donor to an acceptor orbital. This requires the electron to tunnel through the intervening medium, which is of higher energy. The rate of decay of the electron transfer rate due to this medium is given by β. The extent of the tunneling necessary is dependant upon the amount of overlap of the electronic wavefunctions of the orbitals involved. Large overlaps will result in fast electron transfer. Quantum mechanics states that the energy of electronic wavefunctions decreases exponentially with edge-to-edge distance (d), and therefore the rate of electron transfer will also decrease exponentially with this distance.

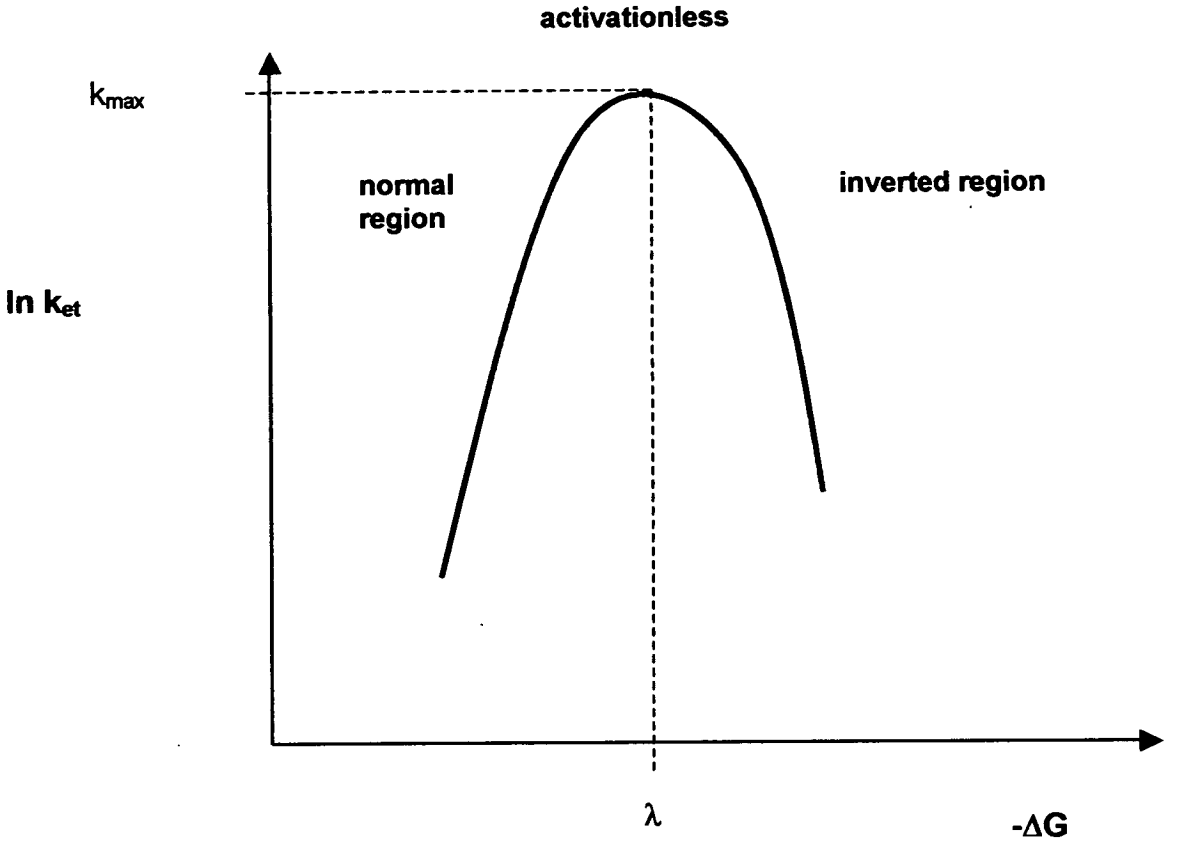

Figure 1.7: *A plot of the logarithm of the electron transfer rate constant (k_{ET}) vs the change in free energy between reactants and products. (ΔG).*

Thus,

$$k_{max} \propto \exp(-\tfrac{1}{2}\beta(d-d_0))$$

The maximal rate of electron transfer at van der Waals distance (3.6 Å) for two redox cofactors is 10^{13} s^{-1} as given by this relationship.

The rate of decay, β, (in $Å^{-1}$) is dependant on the nature of the intervening medium. Does the electron travel directly through space, or does it travel through the bonds in the protein, with a defined tunneling pathway? These different options provide various distances the electron must travel and consequently, different β values, both of which

affect k_{et}. In vacuo, $\beta = 2.8$ Å^{-1} (Moser *et al.*, 1992) and for covalently bridged redox centres in synthetic systems $\beta = 0.9$ Å^{-1} (Smalley *et al.*, 1995). A fully conjugated system has a β value of 0 Å^{-1}. This is a complicated consideration of electron transfer in biological systems where redox centres are normally surrounded by a protein medium. A β value for a protein matrix has been the subject of much discussion. There may be many possible routes for electron movement but the main areas of interest lie with the *through space* and *through bond* models.

The *through space* model gives a single β value, averaged over the entire electron transfer pathway. Moser *et al.* (1992) suggest a β value of 1.4 Å^{-1}, which is equivalent to a 10-fold change in rate for a 1.7 Å change of distance. This value is intermediate between that found for a covalent system and a vacuum and can be understood in terms of structural continuity between the donor and acceptor, a little like a frozen organic glass. Much of this research has been conducted on the photosynthetic reaction centre. One reason being that the X-ray structure solved from the bacterial source *Rhodopseudomonas viridis* (Deisenhofer *et al.*, 1985), allowed distances between redox centres to be measured. Page *et al.* (1999) have studied oxidoreductase proteins with a defined function and with multiple cofactors for intra-molecular electron transfer to take place. Electrons were found to be able to travel up to 14 Å between redox centres through the protein medium. Transfer over greater distances involved a chain of cofactors. It appeared there had been little necessity for proteins to evolve specific routes between cofactors since their proximity alone was sufficient to allow rapid tunneling of electrons at rates greater than the initial reaction with substrate. This, of course, simplifies the need for complicated electron transfer mechanisms.

The *through bond* model as described by Beratan *et al.* (1991, 1992) considers proteins with a more heterogeneous intervening medium. In this case, long-range electron transfer takes place by a tunneling process whereby the physical tunneling pathway is defined as a combination of interacting bonds that link the donor species with the acceptor species. Different portions of the pathway are characterized as being covalent, hydrogen-bonded or through-space, depending on whether they share a common atom, are linked by

hydrogen bonds, or are within Van der Waals contact. Each link is assigned a coupling decay, and a structure algorithm is used to identify the optimum coupling pathway between redox sites. Workers in this field have developed ruthenated derivatives of cytochrome *c* (Wuttke *et al.*, 1992, Karpishin *et al.*, 1994) to study this model. By chemically modifying certain histidine residues in the protein by addition of an atom of ruthenium, the electron transfer rate from heme *c* to the ruthenium atom can be measured. Ruthenating histidine residues at differing distances from the heme-*c* indicates that the rate and coupling correlate with the length of the tunneling pathways that are comprised of covalent bonds, hydrogen-bonds and through-space jumps. It is found however, that the space-jumps greatly decrease these couplings.

Despite these differing theories, it is certain that electron transfer from donor to acceptor does take place. There may be many possible routes by which this event takes place, possibly using both the *through space* and *through bond* models. This will remain an interesting field of study for some time to come.

1.4 Disulfide Bonds

1.4.1 Disulfide Bond Formation in Proteins

The chemistry of disulfide bond formation is well understood. For a long time, it has been known that the information for the correct folding of a protein is encoded in its amino-acid sequence (Anfinsen, 1973). Proteins are synthesized biologically as linear polypeptides, with free cysteine residues and no disulfides. Disulfide bonds form between the thiol groups (-SH) of two cysteine residues through a two-electron reaction that requires an oxidant or electron acceptor. *In vitro*, they are formed spontaneously by the loss of electrons from two cysteine thiols coupled with the gain of electrons by an available acceptor, such as O_2. Using O_2 requires the use of an intermediary such as a flavin to overcome the kinetically slow, yet thermodynamically favourable association of oxygen with protein thiols. *In vivo*, the ultimate electron acceptor for thiol oxidation is normally O_2, except in the case of anaerobic conditions where an electron acceptor such

as fumarate can be used. The general redox scheme below (Figure 1.8) describes the overall reactions that create (oxidize) or destroy (reduce) disulfide bonds:

$$\text{R-SH} + \text{R'-SH} \rightleftharpoons \text{R-S-S-R'} + 2\text{H}^+ + 2\text{e}^-$$

Figure 1.8: *Oxidation and reduction of a disulfide bond.*

Disulfide bonds differ from other types of interactions within folded proteins, such as hydrogen bonds and electrostatic and Van der Waals interactions because they are covalent, with their stability being almost entirely dependent upon the environment. The participating cysteine residues must obey stereochemical requirements for their position and orientation (Steudel, 1975). The optimal stereochemistry of a disulfide bond is shown in Figure 1.9, where the sulfur-sulfur distance lies at 2.05 ± 0.03 Å, with the angle between the disulfide bond and the β–carbon of each cysteine residue close to 103° (Creighton, 1988). Natural disulfide bonds can adopt either a right-handed or left-handed conformation, with approximately equal numbers being observed crystallographically.

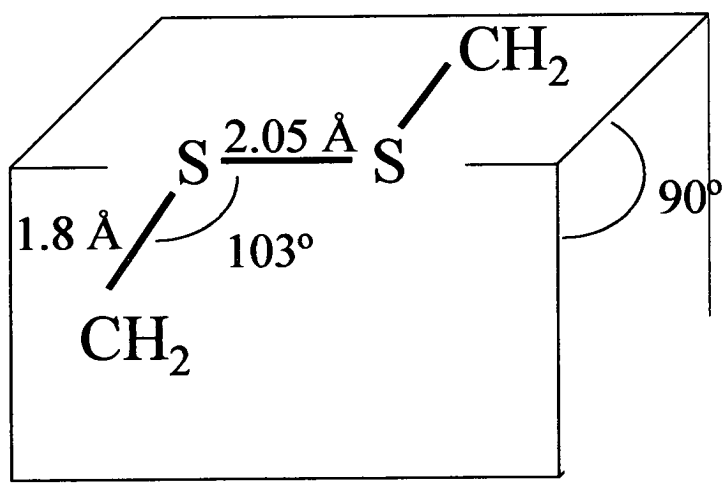

Figure 1.9: *Optimal Stereochemistry of a disulfide bond highlighting two possible torsion angles about the disulfide bond of + 90° and – 90°. Both are equally favourable.*

The reduction potential of the environment is important in determining whether or not a disulfide will form or if an existing disulfide will break (Gilbert, 1990). For example, in the cytoplasm where the reduction potential is low at - 230 mV, (Hwang *et al.*, 1992) it is rare that many disulfides are found. In contrast, they are widespread in the endoplasmic reticulum (ER) where the reduction potential is high (between –172 and –188 mV).

1.4.2 Disulfide Bond Formation *In Vivo*

Protein disulfide bonds are formed in the ER of eukaryotic cells and the periplasmic space of prokaryotic cells. Both share a similar catalytic pathway with shared mechanistic features. Despite the information for the final fold of a protein being encoded in its primary sequence other proteins are also implicated in the folding process *in vivo* (Gething & Sambrook, 1992). Some of these proteins catalyse disulfide bond formation as discussed below.

1.4.2.1 Eukaryotic Pathways for Protein Oxidation

The ER of eukaryotic cells is maintained under suitable redox conditions to enable folding catalysts to facilitate the formation and isomerisation of disulfide bonds. A family of proteins known as the ER oxidoreductases is responsible for this catalysis, and includes Protein Disulfide Isomerase (PDI) (Golberger *et al.*, 1963). The oxidoreductases are characterized by active sites which are homologous to the active site found in thioredoxin, which contains a pair of cysteines that are arranged in a Cys-X-X-Cys motif (where X can be any amino acid) and that shuttle electrons between the oxidized disulfide bond and reduced dithiol form (Ferrari & Soling, 1999).

PDI is an extremely versatile enzyme and depending on the redox conditions and the characteristics of the substrate proteins, it can catalyse the formation, isomerisation and reduction of disulfide bonds (Gilbert, 1994). The cysteine residues within the active site of PDI form an intra-chain disulfide bond that accepts two electrons from the polypeptide chain substrate. This electron transfer results in the oxidation of the substrate and the reduction of the PDI active site. It was previously believed that glutathione was involved in the oxidation of the PDI active site. However, studies carried out in the case of yeast,

suggest this not necessarily to be the case (Cuozzo & Kaiser, 1999). Reducing the levels of glutathione in the intracellular space does not effect disulfide bond formation. Instead, this leads to the suppression of a gene called ERO1 (for ER oxidase). The resultant protein, called Ero1p is responsible for the oxidation of PDI (Frand & Kaiser, 1998, Tu *et al.*, 2000) with a defect in this protein leading to a lack of disulfide bond formation. A disulfide exchange mechanism takes place which is illustrated in Figure 1.10.

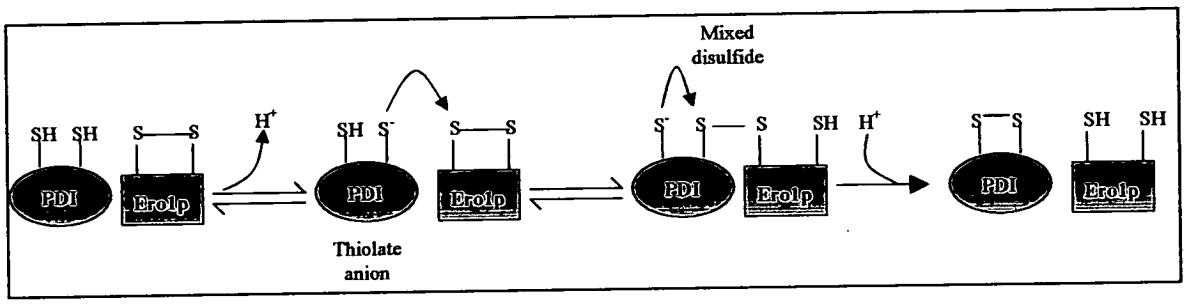

Figure 1.10: *Disulfide bond exchange between PDI and Ero1p. Deprotonation of a free thiol on PDI results in a thiolate anion that displaces one sulfur of the disulfide bond in Ero1p. A second exchange reaction follows where the remaining thiolate anion from PDI attacks the mixed disulfide bond. Finally, the originally reduced PDI is now oxidized.*

1.4.2.2 Prokaryotic Pathways for Protein Oxidation

The first protein shown to be involved in the formation of disulfide bonds within the bacterial periplasm was termed DsbA (for disulfide bond)(Bardwell *et al.*, 1991). It has a *Mr* of 21 kDa and possesses two active site cysteine residues present as a Cys-X-X-Cys motif. It is essential that these cysteine residues remain in their oxidized state for them to be active. However, oxidized DsbA is unstable (Zapun *et al.*, 1993) and will react immediately with unfolded proteins entering the periplasm. The substrate protein and the first cysteine of the Cys-X-X-Cys motif in DsbA (Cys30) react quickly to form a mixed disulfide, before this disulfide bond is transferred onto the substrate protein and reduced DsbA is released.

The oxidizing power of DsbA originates from the extraordinarily low p*K*a of the N-terminal Cysteine of the Cys-X-X-Cys motif at the active site, in this case Cys30. Normally, cysteine residues tend to have p*K*a values of around 9. Cys30, however, has a p*K*a in the region of 3 (Nelson & Creighton, 1994). As such, this residue will be almost entirely in its thiolate anion state at a physiological pH. The three-dimensional structure of DsbA (Martin *et al.*, 1993) as well as site-directed-mutagenesis studies have shed light on why the active site Cys30 is so reactive. The residues located in between the active site cysteines, namely, Pro31 and His32, act to stabilize the thiolate anion of Cys30 through electrostatic interactions (Guddat *et al.*, 1997). In particular, His32 forms a hydrogen bond to Cys30 in the reduced, but not oxidized form (Guddat *et al.*, 1998).

In order for DsbA to function catalytically, it must be reoxidised after transferring its disulfide bond to the substrate protein. A 21 kDa inner membrane protein with four transmembrane segments called DsbB carries out this task (Collet *et al.*, 2002). It contains two pairs of essential cysteine residues, one pair located in each of its two periplasmic domains. The first pair is present in the now familiar Cys-X-X-Cys motif whilst the other pair is not. The actual mechanism by which DsbB functions is not known to any substantial degree although it is believed that a mixed disulfide between Cys30 of DsbA and Cys104 of DsbB arises. The reduced Cys33 of DsbA attacks this mixed disulfide. DsbA is released in its oxidized form while cysteines 104 and 130 of DsbB are reduced. These two residues are thought to be regenerated by cysteines 41 and 44 on the other periplasmic domain of DsbB (Kishigami & Ito, 1996).

So what reoxidises DsbB? Bader *et al.* (1999) verified the connection between disulfide bond formation and electron transport. DsbB shuttles its electrons on to oxidized ubiquinone which then donates them to cytochrome oxidases which then reduce O_2. In anaerobic situations, DsbB passes its electrons to menaquinone and then to fumarate reductase or nitrite reductase. The overall oxidation pathway for the formation of disulfide bonds within the *E. coli* periplasm is outlined in Figure 1.11 below.

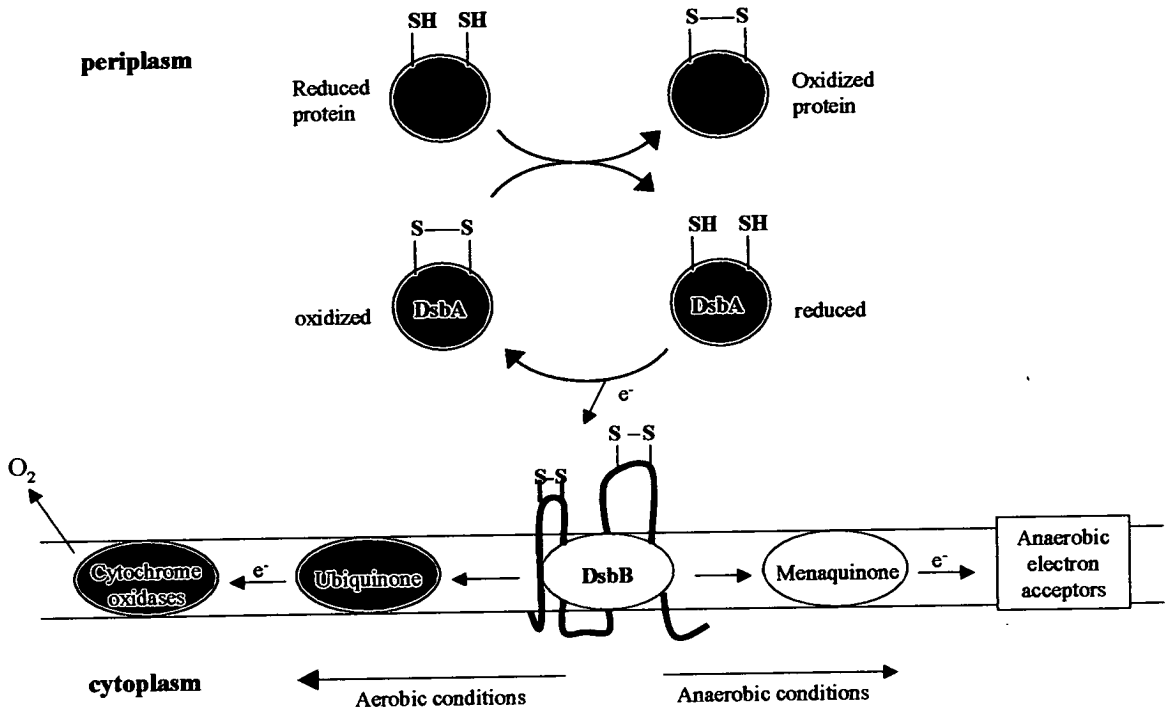

Figure 1.11: *Oxidative pathway in the E. coli periplasm. The reduced substrate protein is oxidized by the active site of the periplasmic DsbA protein. The inner membrane protein, DsbB, re-oxidizes DsbA and is re-oxidized itself by one of two different pathways. Under aerobic conditions, ubiquinone and cytochrome oxidase shuttle electrons from DsbB to molecular oxygen. Alternatively, anaerobic electron acceptors are used in a menaquinone-dependent reaction.*

1.4.3 Engineering Disulfide Bonds

The technology of site-directed mutagenesis has opened many possibilities into the realms of disulfide bonds in proteins. Naturally occurring cysteine residues can be replaced by another amino acid thus preventing the formation of a disulfide bond at a given position. However, it also possible to create a S-S bond in a position where it has not previously existed. One such example is the protease Subtilisin. This was a good model system to artificially engineer stability into the protein (Wells & Powers, 1986). Together with an available crystal structure and computer modeling studies, the authors were able to locate prime sites for the introduction of cysteine residues. The wild-type

protein contained no cysteine residues thus simplifying the analyses of disulfide formation. Two double-cysteine mutations were constructed, namely, Thr22Cys:Ser87Cys and Ser24Cys:Ser87Cys, as well as the corresponding single mutants, Thr22Cys, Ser24Cys and Ser87Cys. It was found that the autolytic properties of the wild-type and the Ser24Cys:Ser87Cys double mutant were similar while the Thr22Cys:Ser87Cys double mutant enzyme was less resistant to autolysis. Upon reduction of the disulfide bonds by dithiothreitol, both double mutant enzymes experienced an increased rate of autolysis. Both single mutants were less resistant to autolysis as compared to the wild-type enzyme. It was possible that a hydrogen bond from Thr22 to Ser87 could be important for stability in the wild-type structure and that the structure could be sensitive to minor changes in the amino acid sequence.

More recent work carried out by Hinck *et al* (1996) has studied the effect of disulfide bridges on the stability of the staphylococcal nuclease (V8 strain). Variants were studied, each containing one disulfide bridge created by changing two wild-type residues to cysteines by site-directed mutagenesis. Lengths of the amino acid sequence were restrained by these S-S bonds, but maintained at between 37 and 42 amino acids so as to minimize differences from chain entropy effects. Using NMR spectroscopy, it was found that the wild-type Staphylococcal nuclease favours the *cis* isomer about a lysine-proline or histidine-proline residue pair. It was expected this was because an increase in protein stability in the peptide chain adjacent to the proline would enhance the *cis* isomer present. The oxidation of the thiols to give a S-S bond tended to introduce strain into the folded state, as was noted by the increased proportion of *trans* proline.

Gokhale *et al* (1994) engineered two disulfide bridges across the dimer interface of the enzyme *Lactobacillus casei* thymidylate synthase. An examination of the 2.3 Å crystal structure revealed that stereochemically unstrained disulfide bridges could be constructed across positions Thr155 – Glu188', and the symmetry related positions (across the 2-fold axis of the dimer) Glu188 – Thr155'. An enhancement in the thermal stability of the covalently cross-linked double mutant enzyme was observed. It remained soluble and retained its secondary structure at 90 °C, in contrast to the wild-type enzyme which

precipitated at 52 °C. The mutant enzyme had a temperature optimum of 55 °C and still possessed significant enzymatic activity at 65 °C. These results suggested that inter-subunit crosslinks can impart substantial thermal stability in multimeric enzymes.

The design and construction of four different disulfide mutants of T4 lysozyme was carried out by Matsumara *et al* (1989a, 1989b). This was facilitated by the replacement of suitably positioned amino acids by cysteine residues. The mutations constructed were; Ile3Cys-Cys97, Ile9Cys-Leu164Cys, Thr21Cys-Thr142Cys, Ser90Cys-Gln122Cys, and Asn127Cys-Arg154Cys. In all cases the crosslinked lysozyme was more stable than the corresponding non-crosslinked enzyme towards thermal denaturation. Relative to wild-type lysozyme, the melting temperatures of the Ile9Cys-Leu164Cys and Thr21Cys-Thr142Cys mutants were increased by 6.4 °C and 11.0 °C, whereas the Ser90Cys-Gln122Cys and Asn127Cys-Arg154Cys mutants were either less stable or equally as stable. The Thr21Cys-Thr142Cys double mutant enzyme is also found to abolish activity because the engineered disulfide link forms across the active site cleft of the enzyme. The crosslink thus prevent substrate from binding to the active site leading to complete inactivation. In conclusion the authors suggested that the most influential S-S bond was formed in a position where there was backbone flexibility. More importantly, loop or hinge motion allowed the constrained geometry of the S-S bond to form more readily.

The aspartate receptor of *Escherichia coli* and *Salmonella typhimurium* is a cell surface sensor that binds extracellular aspartate and sends a transmembrane signal to the inside of the bacterium. The flexibility and allostery of this receptor was studied by Falke & Koshland (1987) by placing sulfhydryl groups as potential crosslinking sites at targeted locations in the protein. A series of seven cysteine mutants were constructed, each containing a single cysteine residue at a different position in the primary structure. Peptide backbone movements were estimated by the amount of intra- and inter-oligomer dimerisation caused by disulfide bond formation. This was carried out by use of a SDS-PAGE electrophoresis. Upon substrate binding, a large increase in the rate of S-S linkage was observed which indicated that, in this case, transmembrane signaling involved sizeable structure changes and an increase in flexibility in all sections of this protein.

1.5 Flavocytochrome b_2

1.5.1 Structure and Function

Flavocytochrome b_2 (L-lactate:cytochrome *c* oxidoreductase) from baker's yeast (*Saccharomyces cerevisiae*) was first identified by Bach *et al.* (1942). It is a homotetramer of subunit molecular weight 57 500 (Jacq & Lederer, 1974). The enzyme is a soluble component of the mitochondrial intermembrane space (Daum *et al.*, 1982) where it catalyses the oxidation of L-lactate to pyruvate, with subsequent electron transfer to cytochrome *c* (Appleby & Morton, 1954). It plays a dual role in respiration, as a supply of pyruvate for the Krebs cycle, and as a participant in a shorter respiratory chain which directs the energy gained from L-lactate dehydrogenation to oxygen, bypassing the Krebs cycle and gaining one molecule of ATP for every L-lactate consumed (Pajot & Claisse, 1974). The location and function of *S. cerevisiae* flavocytochrome b_2 are illustrated in Figure 1.12.

The complete amino acid sequence was determined (Lederer *et al.*, 1985) showing the enzyme to consist of a polypeptide of 511 amino acids (Appendix I). The *Saccharomyces cerevisiae* enzyme has been successfully expressed in *Escherichia coli* and it has been shown that the kinetic properties of flavocytochrome b_2 from both yeast and *E. coli* are identical (Black *et al.*, 1989a). Flavocytochrome b_2 has also been isolated from another yeast, *Hansenula anomola* (Labeyrie & Baudras, 1972) which shows 60 % sequence identity to that from *S. cerevisiae* (Haumont *et al.*, 1987).

The crystal structure of the native enzyme was solved to a resolution of 2.4 Å (Xia & Mathews, 1990) revealing it to exist as a tetramer. It contains two structurally and functionally distinct domains; the first being a N-terminal cytochrome domain (100 residues) containing protoheme IX, and the second, a C-terminal flavodehydrogenase domain (400 residues) containing FMN. The shortest distance between the flavin and b_2-heme groups lies at approximately 9.7 Å. Both domains are connected through a region of polypeptide proposed to function as a hinge (White *et al.*, 1993). The remainder of the protein makes up the much larger flavin-binding domain which has an extended C-

terminal tail region from residues 487-511. The intimate association of these C-terminal tails holds the four subunits together. The domain structure of flavocytochrome b_2 is illustrated in Figure 1.13.

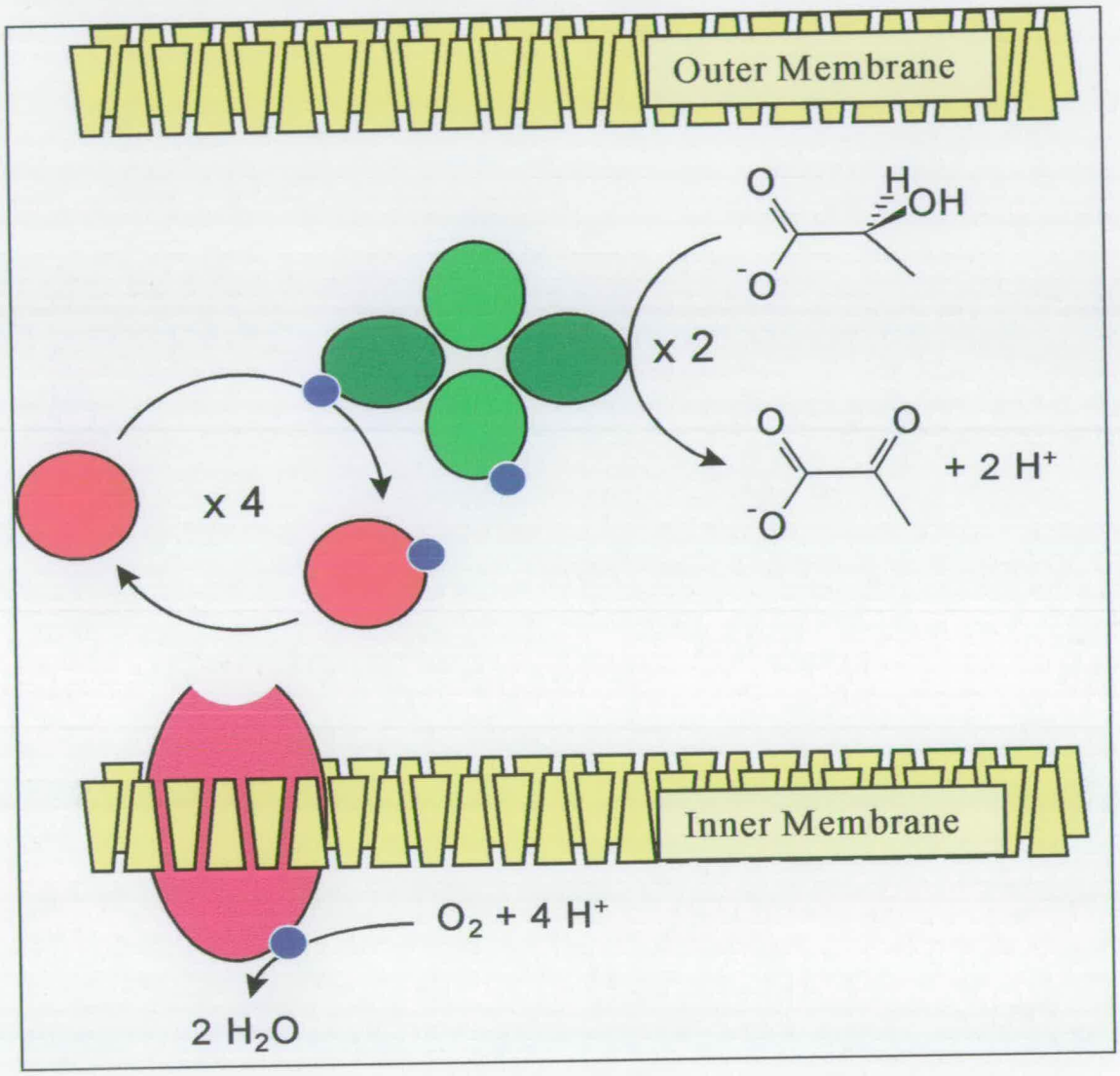

Figure 1.12: *The physiological role of flavocytochrome b_2 (green). The tetrameric enzyme is shown within the mitochondrial intermembrane space where it couples the dehydrogenation of L-lactate to reduction of cytochrome c (red). Electrons (blue) are passed onto cytochrome c oxidase (dark pink) and on to reduce oxygen to water.*

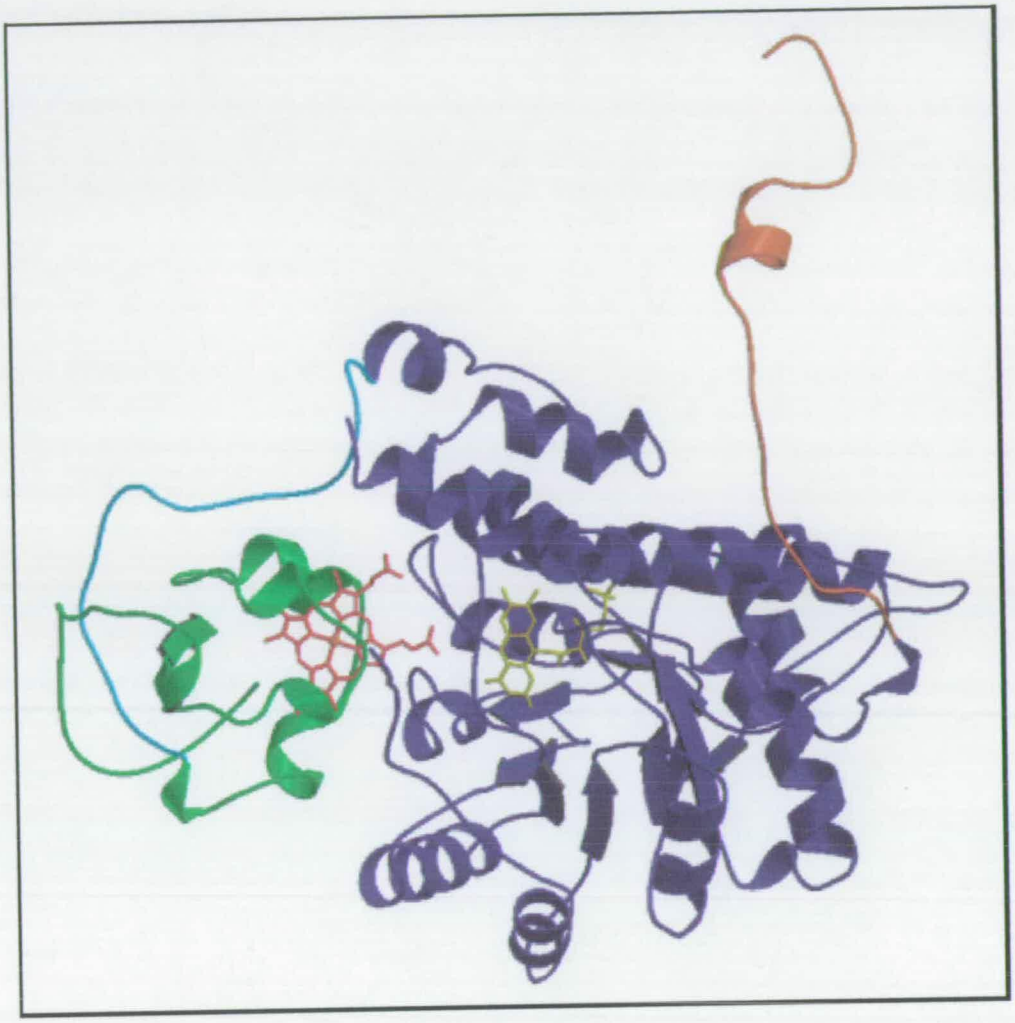

Figure 1.13: *An individual subunit of flavocytochrome b_2. The protein is shown as a ribbon diagram with the b_2-heme (red) and flavin (yellow) cofactors in a stick representation.*

The crystal data identified two distinct conformations of subunit structure in the asymmetric unit, termed subunits 1 and 2. In subunit 1, both the cytochrome and the flavin domains were clearly seen in the electron–density map whereas in subunit 2 the cytochrome domain was not resolved due to positional disorder. In addition, in this subunit there was a pyruvate molecule (the reaction product) bound to the active site of the flavin domain. Together with NMR evidence (Labeyrie *et al.*, 1988) that shows unusually sharp linewidths for b_2-heme resonances, there is implied flexibility about the hinge region and mobility of the cytochrome domain with respect to the flavin domain.

The two prosthetic groups of flavocytochrome b_2 are FMN (flavin mononucleotide) and protoheme IX. FMN is a cofactor based on riboflavin (vitamin B_2) and consists of an isoalloxazine ring attached to a phosphorylated ribityl chain. As shown in Figure 1.14, it can exist in three redox states, fully oxidized (quinone), one-electron reduced (semiquinone), and two-electron reduced (hydroquinone). With flavocytochrome b_2, the role of the FMN is to couple the transfer of electrons from a two-electron process as in the case of L-lactate dehydrogenation to the reduction of the b_2-heme and cytochrome *c* which are one-electron transfer events.

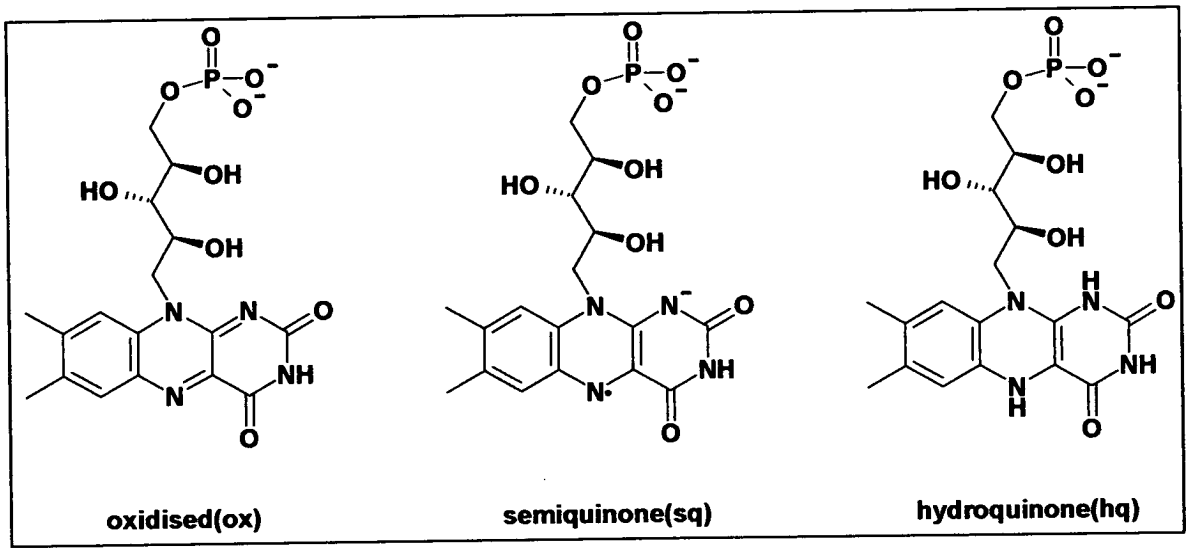

Figure 1.14: *The three different redox states of FMN; fully oxidized (quinone), one-electron reduced (semiquinone), and two-electron reduced (hydroquinone).*

In addition, the midpoint potential of the protein-bound FMN is -64 mV (Walker & Tollin, 1991) compared to the more negative midpoint potential of the lactate/pyruvate couple (-185 mV)(Short *et al.*, 1998) ensuring that a rapid transfer of electrons from L-lactate to FMN occurs. The specific interactions between the protein and the FMN moiety are largely made up of a hydrogen-bonding network. The interaction of Lys349

with atoms N-1 and O-2 of the flavin ring is thought to be responsible for stabilization of the anionic form of the flavin semiquinone and hydroquinone.

The b_2-heme is located in the cytochrome domain, in a pocket formed between two hydrophobic sections comprising of β–sheet and α–helix. It is coordinated to the nitrogen atoms of two histidine residues at positions 43 and 66. The propionate groups are directed towards the flavin domain and interact with three side chains that are located on the flavin domain and with three water molecules. One propionate group hydrogen bonds to Tyr97 and Lys296 as well as with two water molecules. The second propionate interacts with Tyr143 and with a third water molecule. Physioco-chemical studies of the b_2-core (Labeyrie *et al.*, 1966) highlighted similarities with cytochrome b_5. The sequence of the b_2-core was also found to be approximately 30 % identical to that of bovine cytochrome b_5 (Guiard *et al.*, 1974). As such, it was thought that the structures of the cytochrome b_2 core could be very similar to microsomal cytochrome b_5 (Mathews *et al.*, 1972). The role of the b_2-heme and the cytochrome domain is to mediate electron transfer between the FMN and cytochrome *c*. Studies carried out by Brunt (1993) confirmed this by illustrating the absence of direct reduction of cytochrome *c* by fully reduced FMN.

1.5.2 The Catalytic Cycle

The catalytic cycle of flavocytochrome b_2 consists of five steps, and is illustrated in Figure 1.15. The cycle couples the dehydrogenation of L-lactate to the reduction of cytochrome *c*, and although the enzyme is tetrameric, electron transfer between subunits is slow (Capeillère-Blandin, 1975) and thus each subunit can be considered to be acting individually. The first step comprises of the two-electron reduction of FMN by L-lactate dehydrogenation to produce the product molecule, pyruvate. Reduction of the flavin is followed by intra-molecular electron transfer between flavin and b_2-heme generating flavin semiquinone and reduced b_2-heme. At this point the first of two inter-molecular one-electron transfers from the b_2-heme to cytochrome *c* occurs. The b_2-heme is subsequently reduced again by the flavin semiquinone and finally, the second electron is transferred from the heme to cytochrome *c*. It was demonstrated (Miles *et al.*, 1992) that

steady-state reduction of cytochrome *c* by flavocytochrome b_2 proceeds at a rate of 207 ± 10 s^{-1}, and since two molecules of cytochrome *c* are reduced per molecule of L-lactate, the rate of turnover occurs at about 100 s^{-1}.

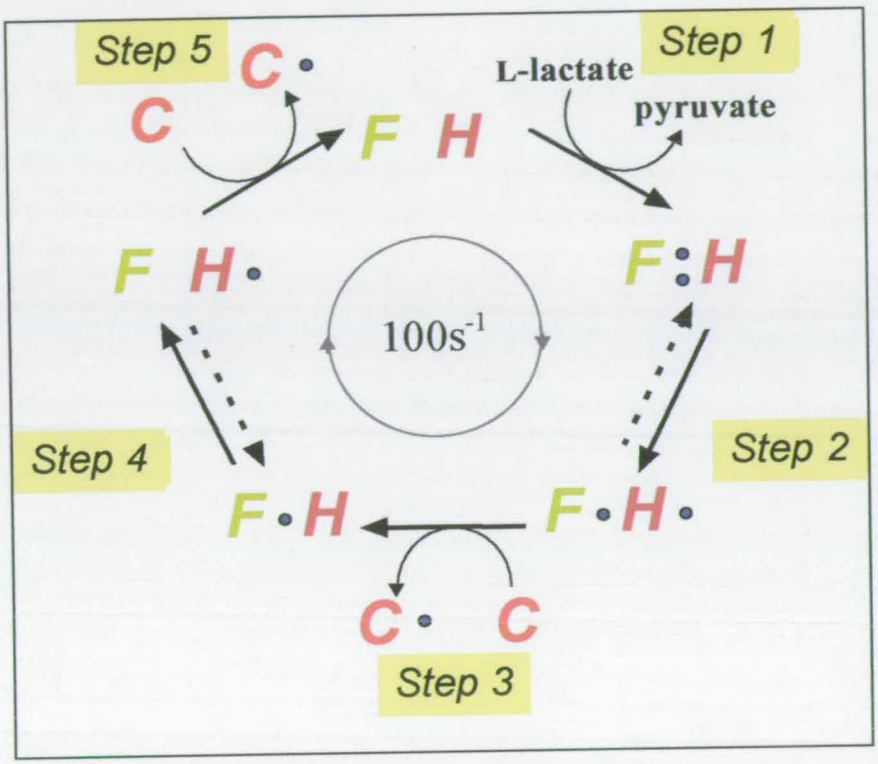

Figure 1.15: *The electron transfer steps in the catalytic cycle of a single subunit of flavocytochrome b_2. F = FMN; H = b_2-heme; C = cytochrome c. Electrons are represented by blue dots.*

1.5.2.1 Step 1: L-lactate dehydrogenation

The first part of this process to consider is the active site, and more importantly, which amino acid residues are chemically significant for substrate binding and catalysis to occur. The active site was identified from the crystal structure (Xia & Mathews, 1990) by locating the product of L-lactate dehydrogenation, pyruvate. As mentioned in section 1.5.1, two types of subunit within the tetramer were crystallographically distinct, with

pyruvate only being present in two out of four of the subunits. The residues involved with making contact to the pyruvate and/or the FMN molecule were readily identified and are shown in Figure 1.16.

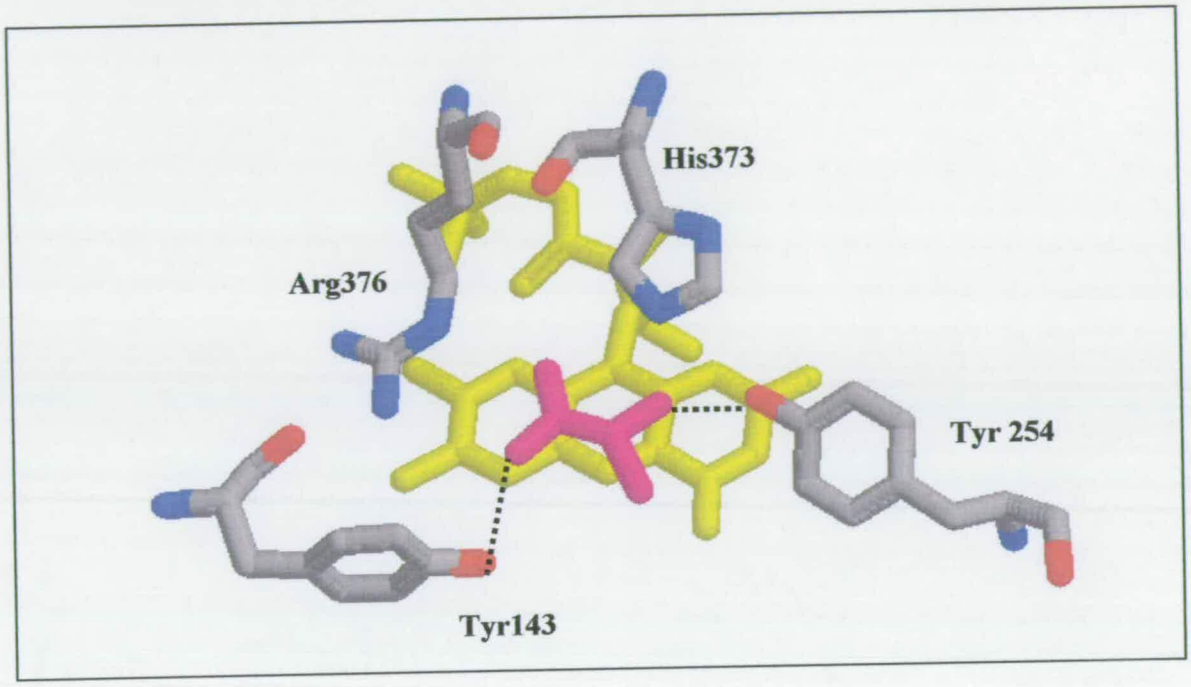

Figure 1.16: *The active site of flavocytochrome b_2 with pyruvate bound (shown in magenta). FMN shown in yellow. The important residues for substrate binding and L-lactate dehydrogenation are shown.*

Arg376 is proposed to ion-pair and hydrogen-bond its guanidinium group to the carboxylate group of pyruvate. In addition, the hydroxyl group of Tyr143 hydrogen-bonds to the other carboxyl group of the pyruvate. Thus, these two residues are proposed to orient the substrate, L-lactate, when it enters into the active site. Two additional hydrogen-bonds are formed between the ketone oxygen of the pyruvate, namely the N-2 atom of His373 and the hydroxyl group of Tyr254. His373 is proposed to be the active site base, abstracting either the α-carbon hydrogen as a proton resulting in carbanion formation (Urban & Lederer, 1985), or the deprotonation of the lactate α-hydroxyl group with subsequent transfer of the α-hydrogen to FMN as a hydride (Mowat *et al.*, 2000).

It was originally thought that Tyr254 could act as a general base and deprotonate the substrate hydroxyl thus facilitating electron transfer to the flavin. However, Dubois *et al.* (1990) studied the properties of the Y254F mutant flavocytochrome b_2 which clearly showed that Tyr254 does not function as a base, but contributes to transition state stabilization, possibly by locking the rotation around the C1-C2 bond of L-lactate, thereby orienting C-2 hydrogen favourably with respect to His373. Although not shown in Figure 1.16, the methyl group of the pyruvate is within van der Waals contact with Leu230 and is responsible for controlling substrate specificity in flavocytochrome b_2 (Daff *et al.*, 1994). Indeed, producing a L230A mutation caused the selectivity for 2-hydroxyoctanoate over L-lactate to increase by a factor of 80. Leu230 is not well conserved within the related flavoenzyme family and this idea is supported by the fact that L-mandelate dehydrogenase which utilizes a bulky aromatic substrate, the equivalent residue is alanine.

Having now considered the important amino acid residues involved with substrate binding, it is an opportune time to consider the mechanism of catalysis. There are two possible mechanistic routes by which this takes place and both will be considered here. These are the carbanion mechanism and hydride transfer.

Carbanion Mechanism

The basis of the carbanion mechanism came from studies conducted on the related enzymes D-amino acid oxidase (Walsh *et al.*, 1972, 1971), lactate oxidase (Walsh *et al.*, 1973) and flavocytochrome b_2 (Urban & Lederer, 1985). In the case of flavocytochrome b_2, the active site base (His373) must abstract the α-carbon hydrogen of L-lactate as a proton before forming a carbanion intermediate which is proposed to form a covalent adduct with N-5 of the flavin (Figure 1.17). The resultant imidazolium ion at His373 is stabilized by Asp282. Electron transfer to the flavin is facilitated by removal of the substrate hydroxyl proton to Tyr254 and by stabilization of the anionic form of the reduced flavin by electrostatic interaction with Lys349, as illustrated in Figure 1.18 below (Lederer & Mathews, 1987).

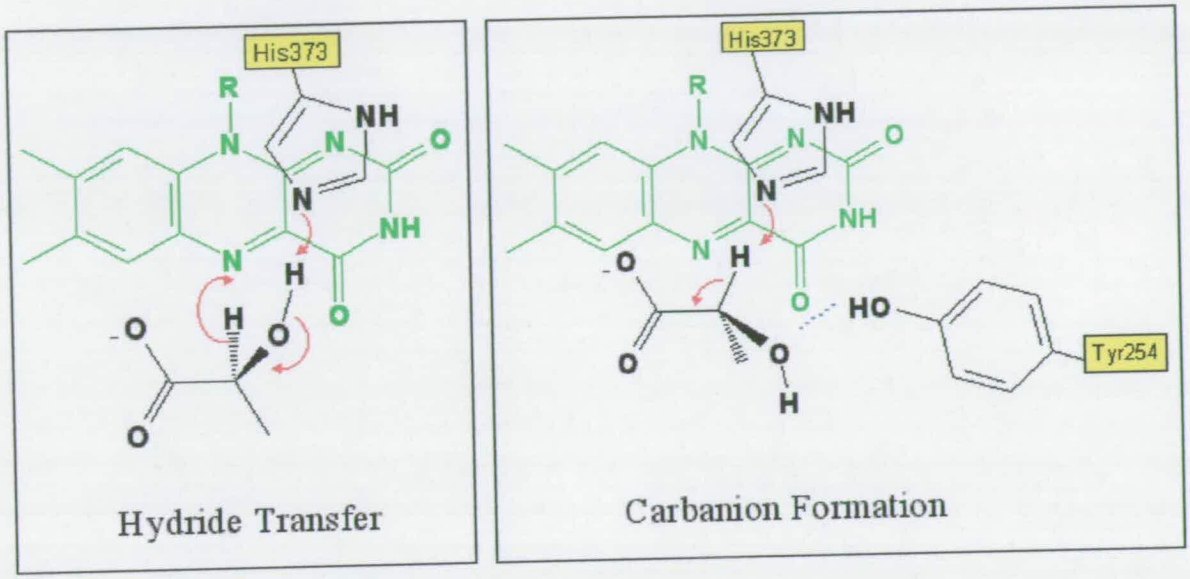

Figure 1.17: *The two possible catalytic mechanisms of flavocytochrome b_2.*

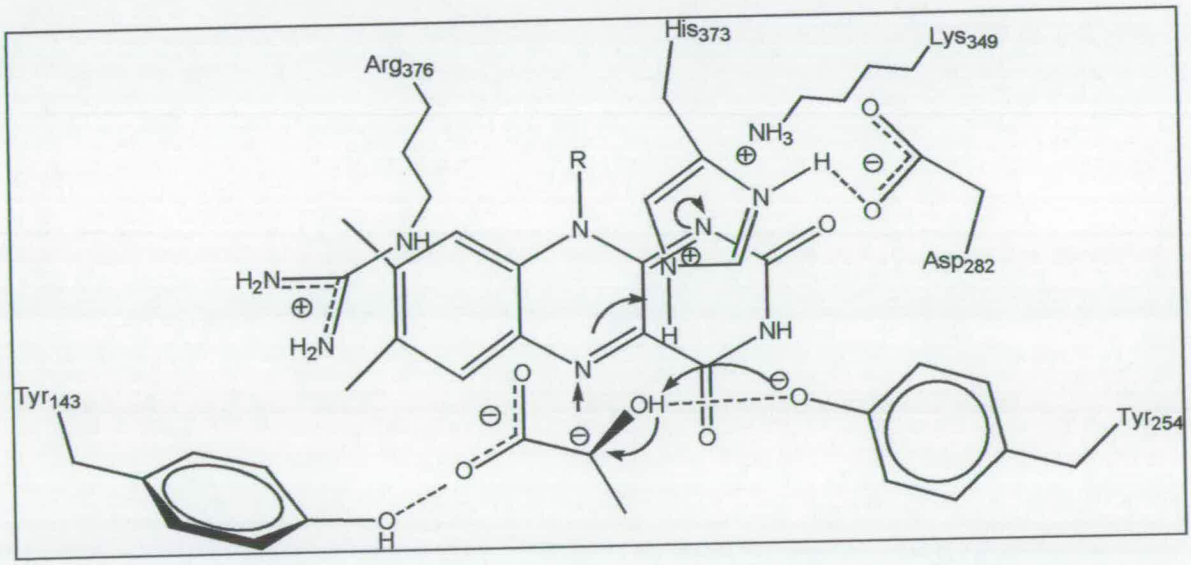

Figure 1.18: *The imidazolium ion is stabilized by Asp282. Removal of the hydroxyl proton by Tyr254 facilitates electron transfer from the carbanion to the flavin.*

However, much of this work was carried out prior to the availability of any crystal structures for the enzymes involved. When the structure of D-amino acid oxidase was solved by Mattevi *et al.* (1996) it called into question many aspects of the mechanism. For example, in order for this mechanism to occur, the α-H of L-lactate must be abstracted to form the carbanion intermediate (Lederer, 1991), however, in the crystal structure of D-amino acid oxidase, there is no residue correctly located to perform this abstraction (Mattevi *et al.*, 1996, Mizutani *et al.*, 1996).

Hydride Transfer

Consider now the mechanism of hydride transfer. The crystal structure of flavocytochrome b_2 (Xia & Mathews, 1990) showed the presence of pyruvate at the active site. This molecule, however, is a keto-acid with the α-carbon in a sp^2 configuration. Since L-lactate has a sp^3 α-carbon, the crystal structure cannot provide any significant idea as to the relative orientation of the three constituents on the α-carbon (-H, -OH, $-CH_3$). However, for hydride transfer to take place, the hydroxyl group of the α-carbon must be oriented towards the active site base (His373). In addition, the methyl group would then be in such a position to favourably interact with the hydrophobic residues Leu230 and Leu286. This leaves the α-H oriented towards flavin N-5 in a position favourable for hydride transfer to take place (Figure 1.17). Contrastingly, the carbanion mechanism requires the α-H of L-lactate to be oriented towards His373, with the result that the methyl group points towards flavin N-5 and Ala198, while the α-hydroxyl group lies in the hydrophobic environment of Leu230 and Leu286. Also, in the carbanion mechanism, Tyr254 is proposed to form a hydrogen-bond with the α-hydroxyl group of L-lactate. As mentioned in section 1.5.2.1, the Y254F mutation (Dubois *et al.*, 1990, Reid *et al.*, 1988) and Y254L (Gondry *et al.*, 1995) were found to have little effect on K_m, but found to decrease the catalytic rate. As such, it is unlikely that Tyr254 would be involved in the Michaelis complex but instead stabilizes the transition state through hydrogen-bonding, and thus orients the α-hydroxyl group towards His373 for proton abstraction.

Clearly there exists a wealth of structural and mutagenic evidence in favour of both the carbanion mechanism and hydride transfer with no one argument stronger than any other, therefore, an open-minded approach should be taken towards this subject. Whichever mechanism prevails, the rate limiting step of L-lactate dehydrogenation has been shown to be the cleavage of the α-carbon hydrogen bond. Miles *et al.*, (1992) found the deuterium kinetic isotope effect of this step to be about 8. However, it is clear from steady-state and pre-steady-state data that L-lactate dehydrogenation contributes little to rate limitation of the overall catalytic cycle. Electron transfer from L-lactate to FMN has been found to occur with a rate constant of 604 ± 60 s^{-1}, some 6-fold faster than the overall steady-state turnover rate found in flavocytochrome b_2 (Daff *et al.*, 1996a).

1.5.2.2 Steps 2 and 4: Inter-domain Electron Transfer

Inter-domain (or intra-molecular) electron transfer occurs in steps 2 and 4 of the catalytic cycle. Step 2 constitutes electron transfer from fully-reduced flavin (flavohydroquinone) to the b_2-heme, leaving the flavin in its semiquinone form and the b_2-heme reduced. After the subsequent transfer of the electron from the b_2-heme to cytochrome *c* (as discussed below), the flavin semiquinone passes its electron onto the re-oxidised b_2-heme (step 4), leaving the flavin in its fully oxidized state.

Using stopped-flow spectrophotometry, an estimate of the rate constant for electron transfer from fully reduced flavin to the b_2-heme has been given as 1500 ± 500 s^{-1} (Chapman *et al.*, 1994). Furthermore, stopped-flow studies were carried out by Daff *et al.* (1996a) that exploited the rapid b_2-heme to cytochrome *c* electron transfer process. By inducing flavin to b_2-heme electron transfer in fully reduced enzyme using a substoichiometric amount of cytochrome *c* to first partially oxidize the b_2-heme, a "b_2-heme re-reduction" trace could be generated. It was found that electron transfer from fully reduced flavin to b_2-heme was happening much too fast to be observed using this method, indicating that the rate constant must have been in excess of 1000 s^{-1}. Laser-flash photolysis (Hazzard *et al.*, 1994) and temperature-jump and potentiometric experiments (Tegoni *et al.*, 1998) also confirmed that this electron transfer step takes place at a rate constant of between 1500 and 2000 s^{-1}. Thus, there is little evidence to

suggest that inter-domain electron transfer from fully reduced FMN to the b_2-heme is in any way contributing to the limitation of the overall turnover rate to 100 s^{-1}.

However, intra-molecular electron transfer from the flavin semiquinone to the b_2-heme (Step 4) is a different story. Pre-steady-state kinetic analyses and quenched flow electron paramagnetic resonance (EPR) spectroscopy (Daff *et al.*, 1996a) have put this electron transfer event as occurring with a rate constant of 120 s^{-1}, thus rate-limiting the overall catalytic cycle to 100 s^{-1}. Temperature jump experiments (Tegoni *et al.*, 1998) put this flavin semiquinone to b_2-heme electron transfer rate constant at 200 ± 50 s^{-1}, in good agreement with that obtained by Daff *et al.* (1996a). However, the reason as to why electron transfer from the flavin semiquinone to b_2-heme should be so much slower as compared to electron transfer from flavin hydroquinone to b_2-heme (~ 1500 s^{-1}) is not clear. Given the redox couples for these two one-electron transfers (Walker & Tollin, 1991), thermodynamically, it would be expected that flavin semiquinone to b_2-heme electron transfer would be faster than flavin hydroquinone to b_2-heme electron transfer. Tegoni *et al.* (1990) discussed the possibility that in the presence of pyruvate, the semiquinone may be stabilized thereby altering its redox potential and making electron transfer thermodynamically less favourable. Eight years later, however, Tegoni *et al.* (1998) published results indicating that the variation of the rate constant (ln k_{et}) for step 4 correlates well with variations in the driving force ($-\Delta G$), strongly suggesting that this inter-domain electron transfer step is indeed thermodynamically controlled.

Another aspect of inter-domain electron transfer of which to consider is the segment of polypeptide chain that connects the flavodehydrogenase and cytochrome domains. It has been proposed to function as a hinge since it imparts mobility to the cytochrome domain relative to the flavin binding domain. Evidence for this mobility is supported by crystallography (Xia & Mathews, 1990) and NMR data (Labeyrie *et al.*, 1988). Studies have been undertaken to probe the importance of the hinge (White *et al.*, 1993, Sharp *et al.*, 1994, 1996a, 1996b). The primary structure of flavocytochrome b_2 from another yeast, *Hansemula anomala*, has been determined (Black *et al.*, 1989b). It shows a 60 % amino acid sequence identity to flavocytochrome b_2 from *S. cerevisiae*. However, there

are obvious differences in the primary structure and net charge of the hinge segment; the hinge in the *H. anomala* enzyme is six residues shorter and considerably more acidic than in the *S. cerevisiae* enzyme. The known kinetic differences observed between these two enzymes may be accounted for by these differences seen in the hinge region (Black *et al.*, 1989b). To investigate the role of the hinge more broadly, an interspecies hybrid enzyme consisting of the bulk of the *Saacharomyces* enzyme but containing the hinge section from the *Hansenula* enzyme was constructed (White *et al.*, 1993). This "hinge-swap" enzyme remained a good L-lactate dehydrogenase as was evident from steady-state experiments using ferricyanide as the electron acceptor, only a 3-fold decrease in k_{cat} was observed. Flavin reduction using stopped-flow spectrophotometry showed a 2.5-fold decrease in k_{cat}. The major effect of the hinge-swap mutation was to lower the enzymes effectiveness as a cytochrome c reductase. The k_{cat} observed for cytochrome *c* reduction fell 100-fold, from 207 ± 10 s^{-1} in the wild-type enzyme to 1.62 ± 0.41 s^{-1} in the hinge-swap enzyme. Since these k_{cat} values differ substantially depending on whether ferricyanide or cytochrome *c* are used as electron acceptor indicates that electron flow to each acceptor is affected in different ways by the mutation to the hinge region. Electron flow to cytochrome *c* is severely impaired, so while the hinge swap enzyme can function normally as a L-lactate dehydrogenase, thus indicating that the hinge is not important in FMN reduction, it is a poor cytochrome *c* reductase. In addition, the k_{cat} for b_2-heme reduction using stopped-flow methods in the hinge-swap enzyme is 300-fold lower than in the wild-type enzyme. This spectacular result indicates a major impairment of electron transfer between the FMN and b_2-heme (step 2 of the catalytic cycle). The hinge-swap mutant clearly disrupted inter-domain electron transfer. It is possible that since the hinge in the mutant enzyme is six residues shorter than that from the wild-type enzyme, this could be restricting hinge bending and preventing efficient recognition between the two domains. Deuterium kinetic isotope effect (KIE) studies carried out on the hinge-swap enzyme (White *et al.*,1993) also showed that FMN→b_2-heme electron transfer is the slowest step in the catalytic cycle of the hinge-swap enzyme. Only a slight erosion in the KIE value was observed for FMN reduction, 6.3 as opposed to 8.1 for wild-type enzyme. Therefore, proton abstraction at C-2 of L-lactate is still rate-limiting for FMN reduction. However, a KIE value for b_2-heme reduction of 1.6 was observed for the hinge-swap

enzyme, as opposed to 6.3 for the wild-type enzyme. This significant erosion of the KIE value indicates that in contrast to the wild-type, there is little or no rate-limitation to the b_2-heme arising from abstraction of the C-2 proton on L-lactate. Given that cytochrome *c* can only accept electrons from the b_2-heme (Ogura & Nakamura, 1966; Capeillère-Blandin *et al.*, 1980), it was not surprising that the KIE for cytochrome *c* reduction in the steady-state was identical with the value for b_2-heme reduction measured by stopped-flow spectrophotometry. Thus, the main conclusion drawn from the work carried out on the hinge-swap enzyme was that the hinge is critical in mediating electron transfer between the FMN and b_2-heme since the hinge-swap mutation resulted in FMN to b_2-heme electron transfer becoming the slowest step in the catalytic cycle.

More subtle mutations involving insertions and deletions in the hinge region have been studied to probe the importance of its structural integrity for efficient intra-protein electron transfer (Sharp *et al.*, 1994, 1996a, 1996b). Three mutant enzymes were constructed, namely HΔ3, HΔ6 and HΔ9 in which three, six and nine amino acids respectively were deleted from the hinge region (Figure 1.19). These were designed to start at the C-terminal end of the hinge and progress towards the cytochrome domain. In addition, these deletions were not expected to have any effect upon the net charge. Two further mutant enzymes were constructed that contained elongated hinge regions, H*I*3 and H*I*6 in which three and six amino acids respectively were added to the hinge region (Figure 1.19). These insertions are positioned between residues 100 and 101 of the wild-type primary sequence, the site defined structurally as the junction between the two domains (Xia & Mathews, 1990). The inserted residues were repeats of the tripeptide motif Ala-Pro-Gly, because it occurs naturally in this portion of the hinge (Figure 1.19). In addition, these amino acids contain small side chains that will have no effect upon the net charge and are commonly found in flexible regions of proteins.

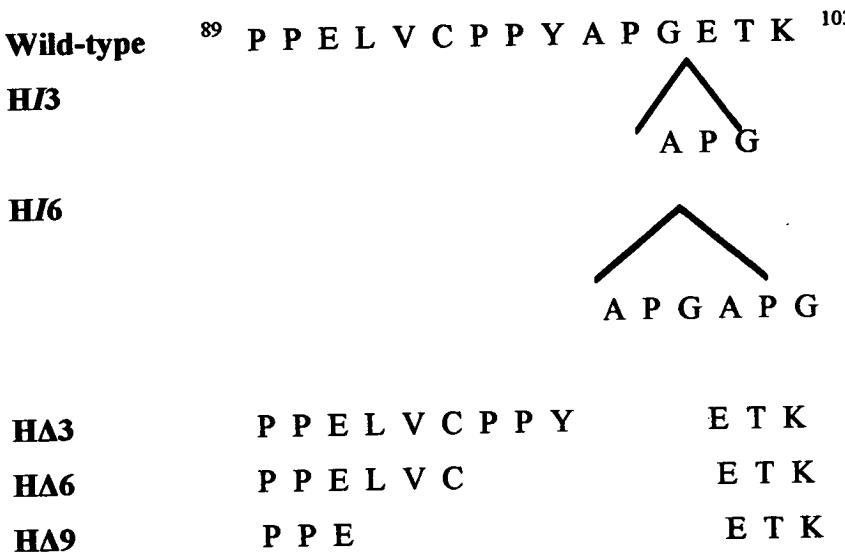

Figure 1.19: *The amino acid sequence for the inter-domain hinge is shown, from Pro89 to Lys103 of the wild-type enzyme. The HI3 and HI6 enzymes have three and six amino acids inserted at the indicated positions in the primary structure. The gaps in the sequence indicate the amino acid residues deleted from the hinge sequence in the HΔ3, HΔ6 and HΔ9 enzymes.*

A linear representation of the catalytic cycle of flavocytochrome b_2 together with rate constants from pre-steady-state kinetic analysis and steady-state cytochrome *c* turnover, for each of the hinge-modified enzymes is illustrated in Figure 1.20.

The steady-state results obtained using L-[2-^{1}H]lactate and L-[2-^{2}H]lactate as substrates with ferricyanide and cytochrome *c* as electron acceptors indicate that all three hinge deletion enzymes are good L-lactate dehydrogenases as judged by the k_{cat} value with ferricyanide as electron acceptor. Only a 40 % decrease was seen for HΔ3 and HΔ6 whereas in the case of HΔ9 the k_{cat} value was identical to that of the wild-type enzyme. However, when the physiological electron acceptor cytochrome *c* is used, the values of k_{cat} for HΔ3, HΔ6 and HΔ9 mutant enzymes are considerably decreased by factors of 5-, 6- and 26-fold respectively as compared to the value for the wild-type enzyme (207 ± 10 s^{-1}). With the exception of the HΔ6 enzyme, both HΔ3 and HΔ9 mutant enzymes have a deuterium KIE value significantly lower than those with wild-type enzyme for both electron acceptors.

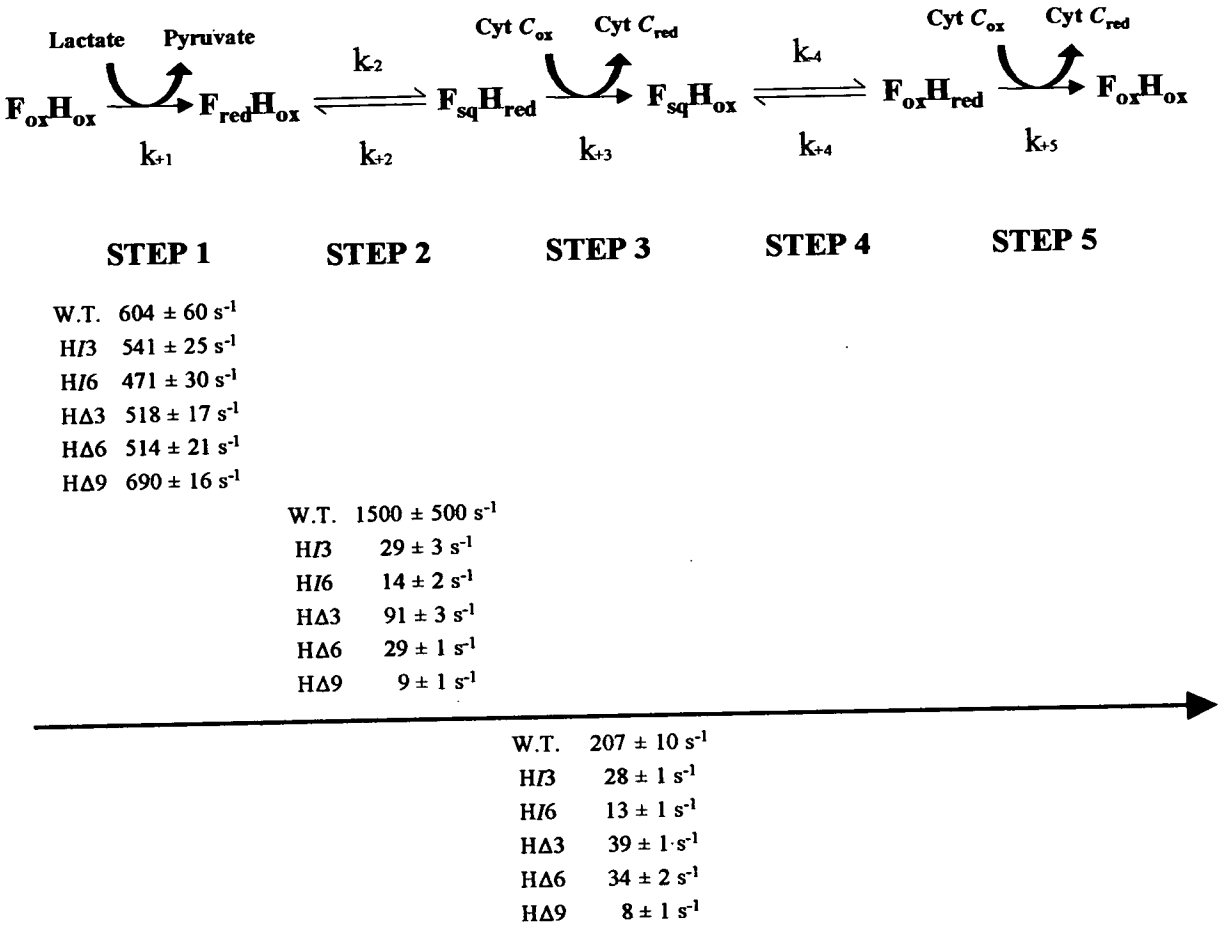

Figure 1.20: *Linear representation of the catalytic cycle of flavocytochrome b_2. The redox states of cytochrome c (cyt c) heme and flavocytochrome b_2 flavin (F) and b_2-heme (H) are indicated by the subscripts 'ox' and 'red' for the oxidized and reduced forms respectively. The flavin semiquinone is shown as F_{sq}. The pre-steady-state rate constants for FMN and b_2-heme reduction are shown for steps 1 and 2 in each of the wild-type (Miles et al., 1992) and hinge-modified enzymes (Sharp et al., 1994, 1996a, 1996b). The steady-state turnover rates for cytochrome c reduction are also shown.*

This implies that electron transfer events following α-H abstraction from the C-2 of L-lactate contribute to the overall rate limitation in these enzymes to a greater extent than in wild-type enzyme. It thus seems clear from steady-state experiments that electron transfer from FMN to b_2-heme is the most drastically effected. In addition, an interesting observation was made regarding substrate inhibition. The HΔ6 and HΔ9 mutant enzymes

and to a lesser extent the HΔ3 mutant enzyme showed evident substrate inhibition when cytochrome *c* was used as the electron acceptor. This was not observed with ferricyanide as the electron acceptor. This may be due to greater accessibility of L-lactate to the active site for these hinge-deletion enzymes compared to wild-type flavocytochrome b_2.

Pre-steady-state kinetic results were obtained by use of stopped-flow spectrophotometry. Rate constants for the reduction of FMN and b_2-heme prosthetic groups of the hinge-deletion enzymes using both L-[2-^{1}H]lactate and L-[2-^{2}H]lactate as substrates were acquired. As expected, the rate of FMN reduction by L-lactate was not significantly altered by the hinge deletions. In addition, the deuterium KIE values for all the hinge-deletion enzymes were the same as the value for wild-type enzyme, within experimental error. Therefore, the abstraction of the α-H from C-2 of L-lactate remains the rate-limiting step for L-lactate dehydrogenation. The rate constants obtained for b_2-heme reduction by L-lactate are more pronounced; some 5- 16- and 50-fold lower for each of the HΔ3, HΔ6 and HΔ9 mutant enzymes respectively compared to wild-type enzyme. As the value of the rate constant decreases further as the length of the hinge is truncated. Thus, maintaining the structural integrity of the hinge region is of vital importance for effective inter-domain (FMN→b_2-heme) electron transfer to take place. The deuterium KIE observed for b_2-heme reduction with all three hinge-deletion enzymes is appreciably lower than the value for wild-type enzyme. This implies that for these mutants, α-H abstraction from C-2 of L-lactate does not contribute to rate-limitation to the same extent as in wild-type enzyme. Instead, subsequent electron transfer steps contribute more to rate-limitation in the hinge-deletion enzymes.

It was possible that the decreases seen in the b_2-heme reduction rate constants for the hinge-deletion enzymes were due to a change in the thermodynamic driving force caused by a shift in the heme group midpoint potential. To rule out this possibility the midpoints were measured and found to be the same within experimental error of the wild-type enzyme (Sharp *et al.*, 1996a).

The rate constants for FMN reduction and the deuterium KIE values in the hinge-insertion enzymes, H*I*3 and H*I*6 are the same within experimental error, as the value for wild-type enzyme (Sharp *et al.*, 1996b). This indicates that the rate-limiting step for L-lactate dehydrogenation is hydrogen abstraction from C-2 of L-lactate. The consistency in data for FMN reduction between the five hinge-modified enzymes and wild-type enzyme implies that the truncation or elongation of the hinge region plays no significant role upon the L-lactate dehydrogenase function of flavocytochrome b_2. Steady-state results for the hinge-insertion enzymes using ferricyanide as electron acceptor support this data. Since the k_{cat} values for the H*I*3 and H*I*6 enzymes are exactly the same as the k_{cat} value for wild-type flavocytochrome b_2 ($400 \pm 10\ s^{-1}$), it is clear that these mutated enzymes can function normally in L-lactate dehydrogenation.

Pre-steady-state b_2-heme reduction of the H*I*3 and H*I*6 enzymes by L-lactate were found to have rate constants some 15- and 30-fold lower respectively compared to the value of wild-type enzyme (Figure 1.20). Therefore, as the length of the hinge is progressively increased, the rate constant for b_2-heme reduction decreases in value. The possibility that the lowering of the b_2-heme reduction rate constants were caused by a change in the heme midpoint potential was investigated. The heme midpoint potentials for the HI3 and HI6 mutant enzymes were measured and found to be the same as wild-type enzyme within experimental error. Steady-state cytochrome *c* reduction by the H*I*3 and H*I*6 enzymes using L-lactate shows k_{cat} values some 7- and 16-fold lower respectively compared to the value of the wild-type enzyme (Figure 1.20). Evidently, increasing the length of the hinge region severely deteriorates the cytochrome *c* reductase activity. In addition, the deuterium KIE for both hinge-insertion enzymes are lower than that for the wild-type enzyme when using cytochrome *c* as the electron acceptor. This is also the case for the other hinge-modified enzymes and therefore it is the electron transfer steps following hydrogen abstraction from C-2 of L-lactate that contribute to the overall rate limitation to a greater extent than in wild-type flavocytochrome b_2. Both the hinge-insertion enzymes display very similar substrate inhibition constants, despite the different degree of hinge-lengthening. As with the hinge-deletion enzymes, this inhibition could be due to the greater accessibility of substrate to the active site.

A remarkable observation that was made for all the hinge-modified enzymes, with the exception of HΔ3, is that the rate constants for step 2, fully reduced FMN to b_2-heme electron transfer, are the same within experimental error as that for steady-state cytochrome *c* reduction (Figure 1.20). Thus, for the HΔ6, HΔ9, H*I*3 and H*I*6 enzymes, intra-protein electron transfer from flavohydroquinone to b_2-heme is totally rate-limiting for enzyme turnover. It is known that the rate-limiting step in wild-type flavocytochrome b_2 is flavin semiquinone to b_2-heme. This is also likely to contribute substantially to the rate-limitation in the HΔ3 enzyme.

In summary to the studies carried out on the hinge-modified enzymes (Sharp *et al.*, 1994, 1996a, 1996b) several conclusions can be drawn. Firstly, modifying the hinge region has little effect on L-lactate dehydrogenation. Secondly, maintaining the structural integrity of the hinge is crucial for efficient electron transfer between FMN and b_2-heme. Third, the HΔ6, HΔ9, H*I*3 and H*I*6 enzymes are totally rate-limited by electron transfer from flavin hydroquinone to b_2-heme, whereas wild-type enzyme and the HΔ3 enzyme are rate limited by electron transfer from flavin semiquinone to b_2-heme.

More recently, an immunological approach has been taken to probe inter-domain electron transfer within flavocytochrome b_2 (Miles *et al.*, 1998). In this work, a monoclonal antibody (mAb) was raised against the holoenzyme that only recognizes the b_2-heme domain, with a K_d lower than 10^{-7} M. Under steady-state conditions, the antibody inhibits cytochrome *c* reduction by the enzyme, but not turnover in the presence of ferricyanide. Stopped-flow experiments show that in the enzyme-antibody complex, the two domains are uncoupled; the FMN is reduced normally and can only be reoxidised by ferricyanide. However, the b_2-heme domain is not reduced. It was postulated at this time that the mAb must bind to some part of the b_2-heme domain close to or at the interface of the two domains thus acting as a wedge to prevent docking and subsequent electron transfer between the FMN and b_2-heme. Further studies were undertaken to map the epitope on the surface of the b_2-heme domain (Diêp Lê *et al.*, 2003). The effect of 14 mutations at 12 different positions was analysed. These mutations were located mostly in the domain interface or at its edge. In addition, the effect of replacing protohaem IX with

its dimethyl ester was analysed. A series of kinetic and binding experiments allowed a minimum area for the mAb epitope on the b_2-domain to be defined. It encompasses positions 63, 64, 65, 67, 69 and 70 as well as one or both heme carboxylates. This area is illustrated in Figure 1.21 for the isolated b_2-heme domain and capped with the flavin-binding domain. The mutations with the most spectacular effects at positions 63, 67 and 69 all introduced steric bulk in addition to the introduction of a charge (N69K) or a charge reversal (E63K). Figure 1.21(B) illustrates the b_2-heme domain capped with the flavin-binding domain, in the same orientation as the free b_2-heme domain in Figure 1.21(A). It is evident that residues 65, 67, 70 and the heme propionates are shielded from solvent upon docking of the flavin-binding domain. Therefore only residues 63, 64 and 69 are partly or fully solvent accessible. Clearly, the antibody can only bind during movement of the cytochrome domain away from the flavin-binding domain. It appears then that the antibody acts as a physical barrier towards functional coupling between the flavin-binding and cytochrome domains and has gone some way to providing direct proof for cytochrome domain mobility in flavocytochrome b_2.

Figure 1.21 (following page): *(A) The residues of the b_2-heme domain where mutations decreased the antibody affinity, including the b_2-heme propionates. (B) The b_2-heme domain capped with the flavin-binding domain. This image was taken from Diêp Lê et al. (2003).*

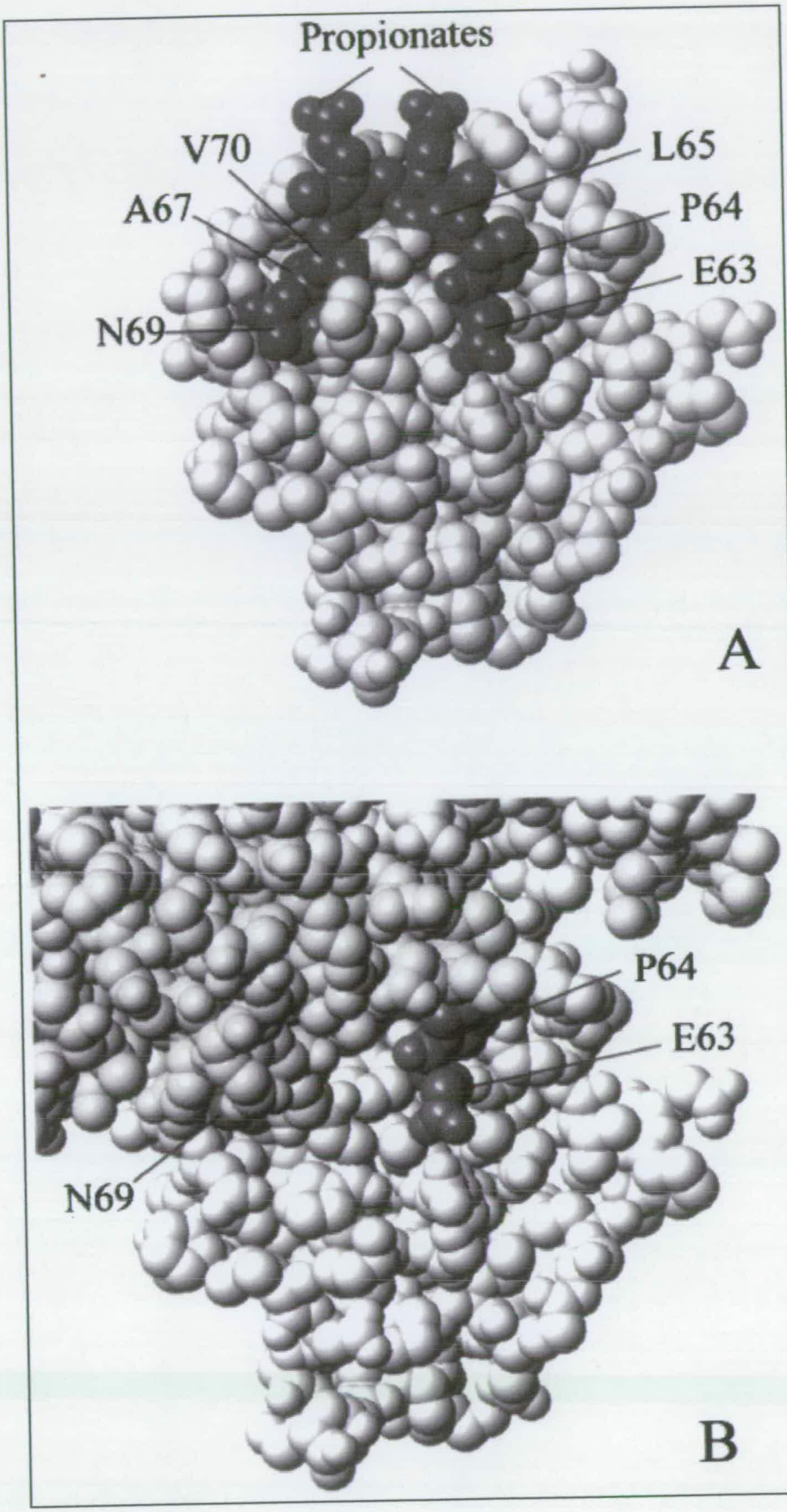
Propionates
V70
A67
N69
L65
P64
E63
A
P64
E63
N69
B

1.5.2.3 Steps 3 and 5: Reduction of Cytochrome *c*

Reduction of cytochrome *c* by reduced b_2-heme occurs at steps 3 and 5 of the catalytic cycle as shown in Figure 1.15. This is the only inter-protein electron transfer event that takes place with flavocytochrome b_2. The reaction between flavocytochrome b_2 and cytochrome *c* takes place as a two-step process, as illustrated in Figure 1.22. The reversible binding of the protein-protein complex has been found to be the rate-determining step of this reaction (Capeillère-Blandin, 1982; Daff *et al.*, 1996b). Electron transfer from the b_2-heme to heme *c* is irreversible due to the midpoint potentials of the two hemes (-17 mV for b_2-heme and +254 mV for heme *c*. This occurs at rates beyond the reliable range of the stopped-flow technique, in excess of 1000 s^{-1} (25 °C; Daff *et al.*, 1996b). The second-order rate constant for reduction of cytochrome *c* defines the rate of association of the two proteins, this being 34.8 ± 0.9 $\mu M^{-1}s^{-1}$ (Daff *et al.*, 1996b).

Cytochrome *c*, however, can donate and accept electrons to and from a number of soluble or membrane-bound enzymes. As such, it has been the subject of many studies devoted to the mechanisms that control the interaction and electron transfer between these enzymes. In particular, the association between cytochrome *c* and cytochrome b_5 has been postulated to involve a positively charged region from cytochrome *c* (Lys-13, 27, 72, 73) interacting with a cluster of negatively charged residues at or near to the heme group of cytochrome b_5 (Salemme, 1976). This is of particular interest since a high sequence homology exists between cytochrome b_5 and the cytochrome domain of flavocytochrome b_2 (Guiard *et al.*, 1974). Thus, the theory of electrostatic interaction is found to be applicable to the interaction between cytochrome *c* and flavocytochrome b_2. Indeed, such investigations performed using flavocytochrome b_2 from the yeast *Hansenula anomala* reported that the complex with cytochrome *c* was stabilized by electrostatic attraction (Capeillère-Blandin, 1982). Despite this, a lack of correlation between studies has made interpretation difficult. For instance, different values are reported in the literature for the stoichiometry of the complex between cytochrome *c* and flavocytochrome b_2. This varies from 1:1 (heme *c*:heme b_2) to 1:0.25 (heme *c*:heme b_2). However, other studies on flavocytochrome b_2 from *H. anomala* led to the conclusion that the site of binding of cytochrome *c* involves both the flavin and cytochrome domains of flavocytochrome b_2

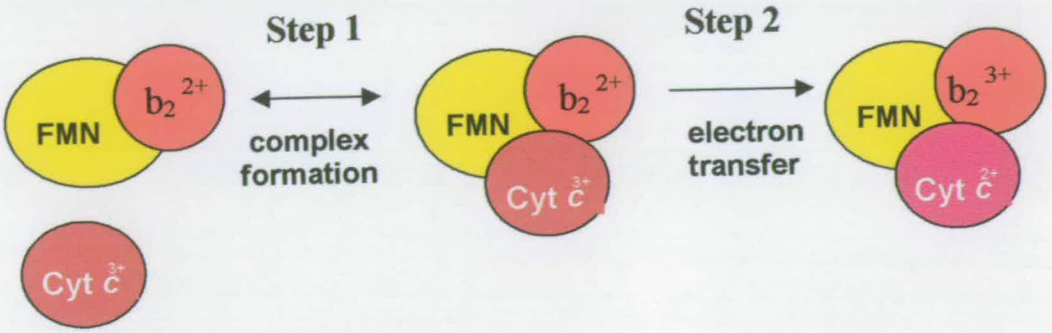

Figure 1.22: *The reaction between flavocytochrome b_2 and cytochrome c. The reversible formation of the protein-protein complex is shown in step 1. This is followed by fast electron transfer from the b_2-heme to heme c.*

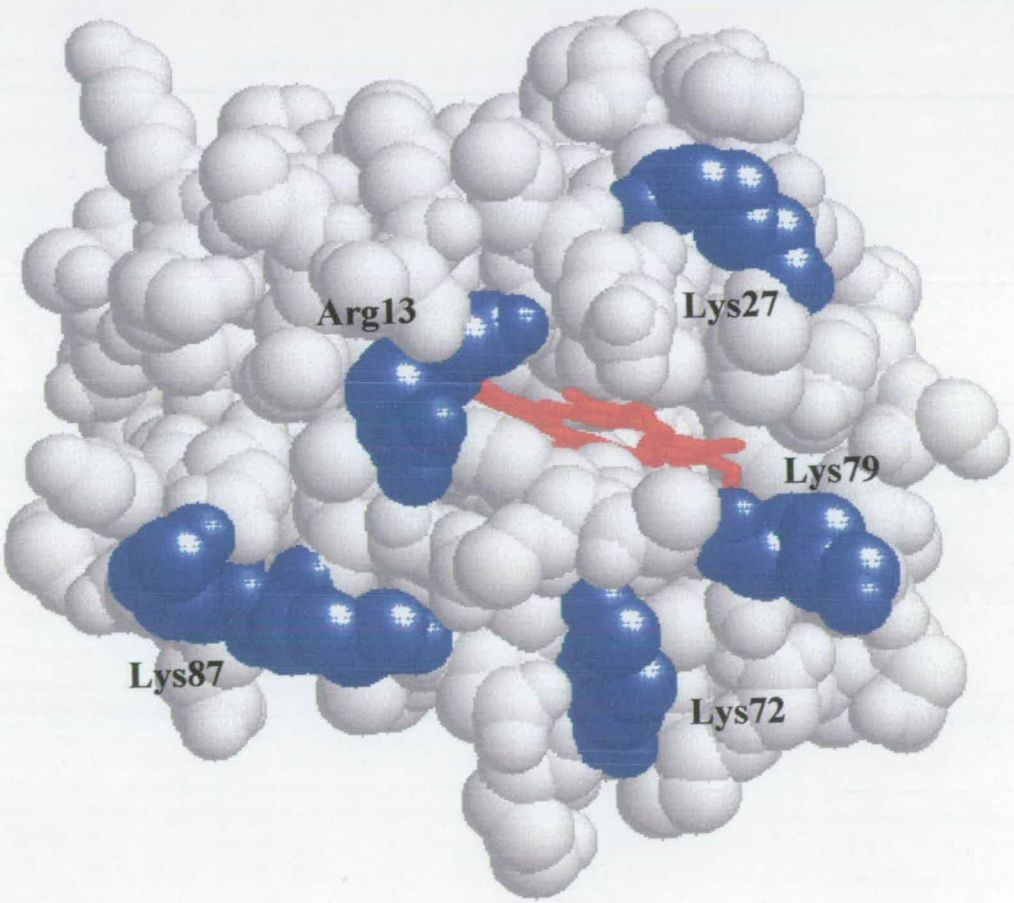

Figure 1.23: *The reacting surface of yeast cytochrome c. The heme is shown in red while the positively charged residues are shown in blue.*

(Thomas *et al.*, 1983a,b; Capeillère-Blandin & Albani, 1987). This conclusion was also reached for the *S. cerevisiae* enzyme since the isolated cytochrome domain (b_2-core) was found to have a second-order rate constant for cytochrome *c* reduction which is less than half the value for the intact enzyme, 16.2 ± 0.3 $\mu M^{-1}s^{-1}$ *vs* 34.8 ± 0.9 $\mu M^{-1}s^{-1}$ (Daff *et al.*, 1996b). In line with the above results, Tegoni *et al.* (1993) proposed a hypothetical model for the interaction of yeast cytochrome *c* and flavocytochrome b_2 in the crystal lattice. Their general criteria for the interaction included charge and surface complementarity, plausible orientation, and the distance separating the heme groups. In addition, the authors imposed a stoichiometry of four cytochrome *c* molecules interacting with a tetramer of flavocytochrome b_2 as well as the involvement of both the flavin and cytochrome domains. Central to the model is the involvement of four basic residues on the surface of cytochrome *c*, namely, Arg13, Arg38, Lys54 and Lys79 (Figure 1.23). It was proposed that these residues would be positioned near acidic residues on the surface of flavocytochrome b_2, and hydrogen bonds would help to stabilize the complex. Glu91 of flavocytochrome b_2 was postulated to be critical for electrostatic interaction with cytochrome *c*. Tegoni *et al.* also proposed a possible σ-tunneling pathway for electron transfer from the b_2-heme through the backbones of residues Ile50 and Lys51, and emerging on the surface of flavocytochrome b_2 at the sidechain of Phe52. To test this model, two mutant flavocytochromes b_2 were constructed (Daff *et al.*, 1996b); E91K reverses the charge of this supposedly important residue responsible for electrostatic interaction with cytochrome *c*, and F52A removes the phenyl ring suggested to be a crucial part of the electron transfer pathway between the two hemes. However, the E91K mutation did not show any significant deviation in the second-order rate constant for electron transfer between flavocytochrome b_2 and cytochrome *c* compared to that of the wild-type enzyme (37.7 ± 1.2 $\mu M^{-1}s^{-1}$ *vs* 34.8 ± 0.9 $\mu M^{-1}s^{-1}$ respectively). Similarly, no change was observed in the second-order rate constant for the F52A mutation (34.3 ± 1.4 $\mu M^{-1}s^{-1}$). In light of these result, neither of these residues were important for recognition and interaction between flavocytochrome b_2 and cytochrome *c*. Consequently, Short *et al.* (1998) undertook molecular modeling and kinetic studies on a possible new location for cytochrome *c* binding on the surface of flavocytochrome b_2. An examination of the crystal structure of flavocytochrome b_2 (Xia & Mathews, 1990) reveals a reasonably

uniform distribution of charge except for a few patches of surface acidity. However, the authors prime concern in locating a binding site was to allow the b_2-heme and heme *c* to be as close together as possible. In addition, the sequence similarity between flavocytochrome b_2 heme domain and cytochrome b_5 was considered in the context of the proposed cytochrome b_5:cytochrome *c* complex (Mauk *et al.*, 1995; Guillemette *et al.*, 1994). Superimposing the cytochrome domain of flavocytochrome b_2 on that of cytochrome b_5 in the cytochrome b_5:cytochrome *c* complex places the cytochrome *c* binding site on the surface of flavocytochrome b_2 near to the interface between the heme and flavin domains. In this case, two residues in flavocytochrome b_2 are implicated to be involved in the binding of cytochrome *c*, namely Glu63 and Asp72. The importance of these residues was tested by constructing three different mutant enzymes; E63K, D72K and E63K:D72K. Not surprisingly, all three mutant enzymes remained good L-lactate dehydogenases as judged by the pre-steady-state reduction of the flavin and b_2-heme. Values of the second-order rate constant (k_2) for the reduction of cytochrome *c* by the mutant enzymes were somewhat different to that of the wild-type enzyme. The k_2 values for the wild-type enzyme and the E63K, D72K and E63K:D72K mutant enzymes are $34.8 \pm 0.9\ \mu M^{-1}s^{-1}$, $13.0 \pm 1.0\ \mu M^{-1}s^{-1}$, $24.0 \pm 3.0\ \mu M^{-1}s^{-1}$ and $6.00 \pm 0.05\ \mu M^{-1}s^{-1}$ respectively. It is apparent that the mutations do have a significant effect on the reaction between the two proteins with the largest effect seen for the double mutation. To rule out the possibility that the driving force of the reaction was being affected by the mutations, the reduction potential of the b_2-heme in each mutant enzyme was measured. Small changes in the reduction potential as compared to wild-type enzyme were measured for each of the mutant enzymes. However, these differences were found to be insignificant compared to the changes for the rate constants for cytochrome *c* reduction. It thus appears that the effects seen on the rate of cytochrome *c* reduction arises from the kinetics of recognition and complex formation and not from changes in driving force.

Modelling studies were centered around the flavocytochrome b_2 residues D72 and E63 as well as maintaining a reasonably short heme-to-heme distance that would be compatible with fast electron transfer. While no one single best configuration was found for the complex between flavocytochrome b_2 and cytochrome *c*, it was found that in addition to

the residues from the b_2-heme domain (i.e. D72 and E63), residue Glu237 from the flavin-binding domain is important for binding. These three residues, Glu63, Asp72 and Glu237, form an acidic triangle that recognize and interact with the basic residues Lys13, Lys27 and Lys79 on cytochrome *c* (illustrated in Figure 1.22). It was proposed by Short *et al.* (1998) that through the middle of this triangle of interactions might run a σ-tunneling pathway for electron transfer. This pathway starts from the imidazole ring of His66 (a ligand to the b_2-heme iron) continuing up through the backbone of Ala67 and ending with the ring of Pro68 which is within van der Waals distance of the heme-*c*. The edge-to-edge "through-space" distance from the imidazole ring of His66 to the pyrrole ring of the heme-*c* is 13.1 Å, considerably shorter than the edge-to-edge distance of ≥ 20 Å reported in the Tegoni model (Tegoni *et al.*, 1993).

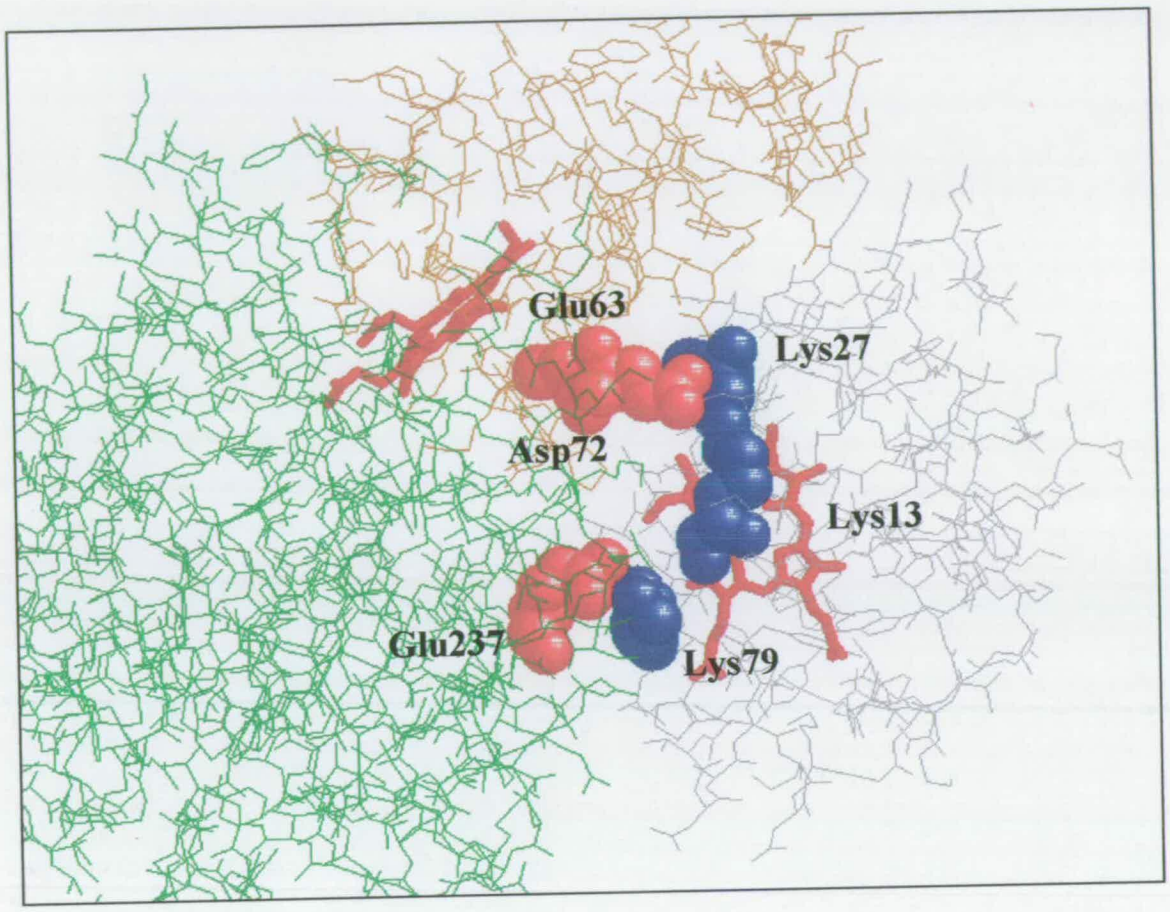

Figure 1.24: *The Short model for the interaction of flavocytochrome b_2 with cytochrome c (Short et al., 1998). Cytochrome c is shown in grey, with Lysines 13, 27 and 79 shown spacefilled in blue. The flavin and b_2-heme domains of flavocytochrome b_2 are coloured green and brown respectively, with Glu63, Asp72 and Glu237 spacefilled in red. Both the b_2-heme and heme-c are also shown spacefilled in red.*

1.6 Aim of this Thesis

The flavin-binding and cytochrome domains of flavocytochrome b_2 are connected by a hinge sequence, running from residues 89 to 103. It has been proposed that the most likely role of this hinge region is to confer inter-domain mobility, allowing movement of the cytochrome domain with respect to the flavin domain (White *et al.*, 1993). This proposal is supported by a number of observations from crystallography (Xia & Mathews,

1990) and NMR spectroscopy (Labeyrie *et al.*, 1988) as discussed in section 1.5.1. For example, in the three-dimensional structure of flavocytochrome b_2, two crystallographically distinct subunits are visible in the asymmetric unit (Xia & Mathews, 1990). In one subunit, neither product nor substrate is bound at the active site and the cytochrome domain is resolved. In the other, pyruvate is bound at the active site with no electron density observed for the cytochrome domain, implying that it is positionally disordered. In solution, NMR spectroscopy shows that the cytochrome domain is substantially more mobile that would be expected for a protein as large as the flavocytochrome b_2 tetramer; the observed linewidths for b_2-heme group resonances in the cytochrome domain are not broadened to the degree anticipated for such a large protein, again implying considerable flexibility of this domain (Labeyrie *et al.*, 1988).

In light of these observations, a key question arises – why is there inter-domain mobility in flavocytochrome b_2 and is it important for catalysis? There are three obvious reasons why inter-domain mobility may be important: The first is that the b_2-heme domain may have to move away from the flavin domain to allow substrate to enter the active site; the second is that domain movement may be essential to permit efficient flavin to b_2-heme electron transfer; and the third is that domain movement might be necessary to facilitate electron transfer from the b_2-heme domain to the electron acceptor, cytochrome *c*.

Previous experiments have been reported in which domain mobility was probed by alterations to the hinge region of flavocytochrome b_2 (see section 1.5.2.2 for a detailed discussion). The first of these involved a "hinge-swap" enzyme, in which the hinge region of *S. cerevisiae* flavocytochrome b_2 was replaced by the equivalent region of the *H. anomala* enzyme (White *et al.*, 1993). This study showed that the structural integrity of this hinge peptide was essential for efficient inter-domain electron transfer. More subtle mutations involving insertion and deletions in the hinge region again illustrated the importance of maintaining the structural integrity of the hinge for efficient inter-domain communication (Sharp *et al.*, 1994 1996a, 1996b).

An alternative approach to examine the importance of domain mobility is to try and restrict it. One way to do this is to introduce a disulfide bridge to link the two domains together. Such an approach has already been successful in the case of the soluble fumarate reductase from *Shewanella frigidimarina* (Rothery *et al*, 2004). Previous attempts to introduce a disulfide link between the two domains of flavocytochrome b_2 were carried out by Bell (1997). In this study, a Ala67→Cys mutation was made on the cytochrome domain of flavocytochrome b_2 in the hope that this imposed cysteine residue would form a disulfide bridge with the naturally occurring Cys233 of the flavin-binding domain. Ellman assays and kinetic experimentation suggested the formation of the desired disulfide bond between these two domains, although this was never proven since no crystal structure for this mutant enzyme was available. In this work, site-directed mutagenesis has been used to construct the N42C:K324C mutant flavocytochrome b_2. The α-carbon atoms of the cysteine residues introduced at position 42 of the b_2-heme domain and position 324 of the flavin-binding domain are within 6.1 Å of one another. Modelling these cysteine residues into the available three-dimensional structure of the native enzyme (Xia & Mathews, 1990) gives a S-S distance of 2.0 Å, an ideal distance in which to form a disulfide bridge. Figure 1.25(A) highlights the location of residues 42 and 324 at the interface of the flavin and cytochrome domains while Figure 1.25(B) illustrates the imposed disulfide bond between the two cysteine residues at these positions.

Other flavocytochrome b_2 mutations were constructed to introduce a disulfide bridge between the two domains. These were the A67C:S234C double mutation, A67C:S234C:C233A triple mutation. In addition, the single mutants, A67C, S234C, C233A, N42C and K324C were constructed as controls. However, due to restrictions of time, only the N42C:K324C mutant flavocytochrome b_2 was studied. In this thesis, the kinetic and crystallographic characterization of the N42C:K324C mutant enzyme is described.

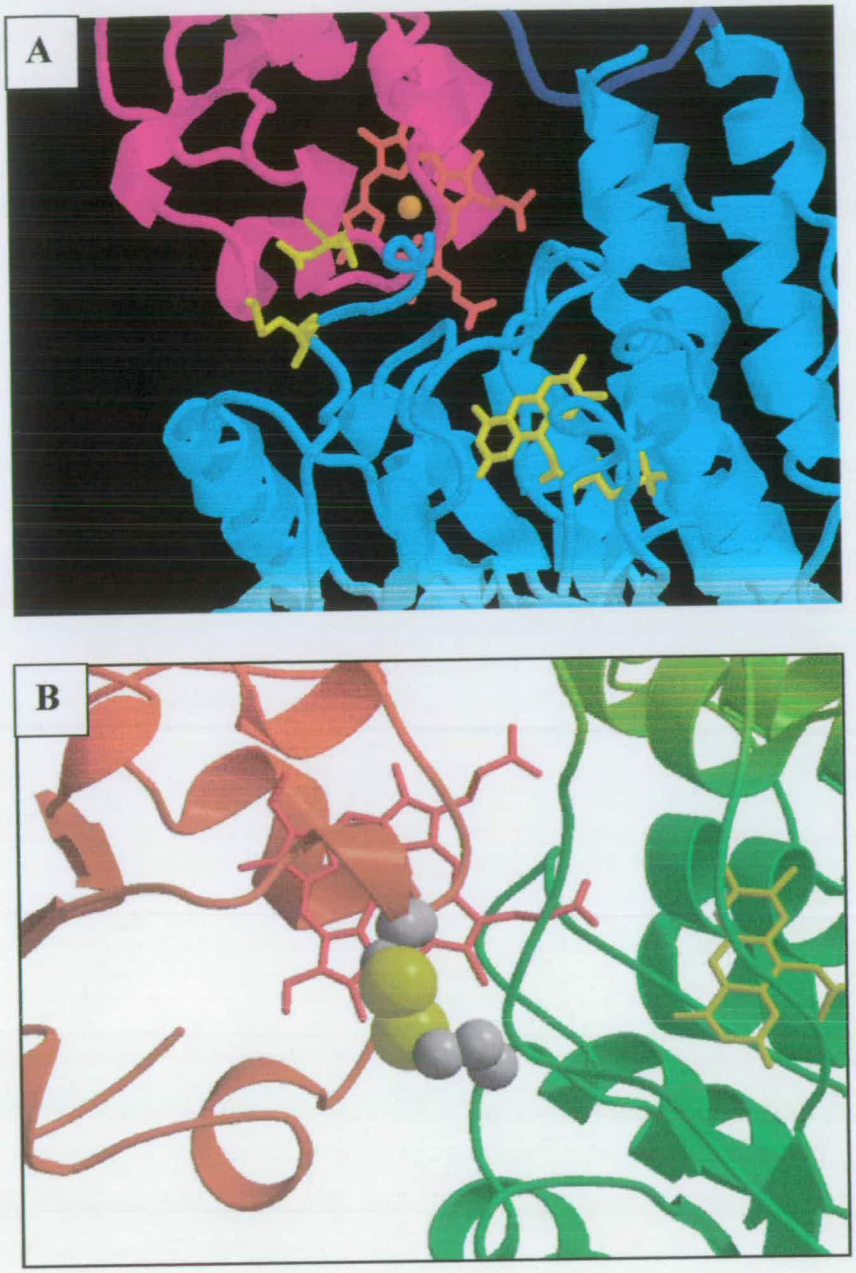

Figure 1.25: *(A) The interface of the flavin and cytochrome domains of flavocytochrome b_2. The cytochrome domain is shown in magenta, the flavin domain in light blue and the inter-domain hinge in dark blue. The heme is shown in red and FMN in yellow. Resides 42 and 324 are highlighted in yellow, to illustrate the positions of the imposed cysteine mutations. (B) The engineered disulphide bridge is shown space–filled linking the flavin (green) and heme (orange) domains.*

Chapter 2

Materials and Methods

Chapter 2

Materials and Methods

2.1 Growth and Maintenance of Strains

2.1.1 Bacterial Strains

Name	Genotype
E. coli AR120	λM99, (F⁻, *galK2*, *LAM*⁻, *prsL200*) derivative (cI, Δ-*gal*, *nad*A::Tn*10*)
E coli XL-10 Gold	Tet^{r}Δ(*mcrA*)*183*Δ(*mcrCB-hsdSMR-mrr*)*173 endA1 supE44 thi-1 recA1 gyrA96 relA1 lac* Hte [F' *proAB lacI*^{q}ZΔ*M15* Tn*10* (tet^r) Amy Cam^r]

2.1.2 Bacterial Plasmids

Name	Description
$pDSb_2$	contains the wild-type flavocytochrome b_2 coding sequence (Black *et al.*, 1989a), Figure 2.1.
pKD209	contains the N42C flavocytochrome b_2 coding sequence
pKD212	contains the K324C flavocytochrome b_2 coding sequence
pKD213	contains the N42C:K324C flavocytochrome b_2 coding sequence
pKD211	contains the S234C flavocytochrome b_2 coding sequence
pKD210	contains the C233A flavocytochrome b_2 coding sequence
pKD214	contains the C233A:S234C flavocytochrome b_2 coding sequence

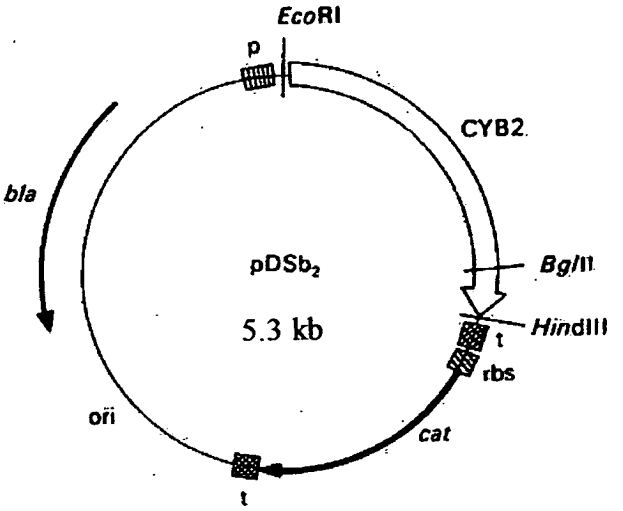

Figure 2.1: *$pDSb_2$ plasmid used for expression of flavocytochrome b_2 in E. coli.*

2.1.3 Growth Media

Luria-Bertani Broth (per litre)

Tryptone (Difco-Bacto)	10 g
Yeast extract (Merck)	5 g
NaCl (BDH)	5 g

Millipore water was added to 1 litre.

NZY^+ Broth (per litre)

NZ amine (casein hydrolysate)	10 g
Yeast extract	5 g
NaCl	5 g

Millipore water was added to 1 litre and the pH adjusted to 7.5 by addition of NaOH.

The following filter-sterilized supplements were added prior to use:

12.5 ml of 1 M $MgCl_2$

12.5 ml of 1 M $MgSO_4$

20 ml of 20 % (w/v) glucose (or 10 ml of 2 M glucose)

All growth media was sterilized by autoclaving at 121 °C for 20 minutes before use.

LB-Agar (per litre)	
Tryptone (Difco-Bacto)	10 g
Yeast extract (Merck)	5 g
NaCl (BDH)	10 g
Agar	20 g

Millipore water was added to 1 litre and the solution adjusted to pH 7.0 by addition of NaOH. The LB-agar was then autoclaved for 20 minutes at 121 °C. It was allowed to cool before addition of 50 mg l^{-1} carbenicillin (see section 2.1 6).

2.1.4 Growth of Bacteria

Liquid cultures of bacteria were grown in the appropriate broth by inoculating with a single colony using a sterile inoculating loop. Cultures of the bacterial strains were grown at 37 °C.

2.1.5 Storage of Bacterial Cultures

77 µl of sterile dimethyl sulfoxide was pipetted into an ice-cold sterile Eppendorf. 1ml of fresh overnight cell culture was added to the Eppendorf and the mixture inverted a few times to mix. The DMSO stock was placed directly into the – 80 °C freezer.

2.1.6 Antibiotics

A stock solution of carbenicillin (disodium salt, Duchefa) was prepared at 50 mg ml^{-1} in Millipore water, passed through a 0.22 µM filter and stored at -20 °C. Prior to inoculation, this was added to the growth medium to a concentration of 50 mg l^{-1}.

2.2 Preparation of Competent Cells ($CaCl_2$ method)

An overnight culture of an appropriate *E. coli* strain was subcultured (200 µl) into 5 ml of LB broth. This was grown until the optical density at 600 nm reached approximately 0.5.

The cells were harvested (5000 rpm / 3 minutes) and the supernatant disposed of. The pellet was placed on ice and resuspended in 2 ml of ice-cold 0.1 M $CaCl_2$. This was left on ice for 40 minutes. The resuspended cells were harvested (5000 rpm / 3 minutes). The supernatant was removed, and the pellet placed on ice. It was resuspended in 1 ml of ice-cold $CaCl_2$ and left on ice for 45 to 60 minutes. At this stage, the cells are competent.

2.3 Transformation of XL10-Gold® Ultracompetent Cells

The XL10-Gold ultracompetent cells were gently thawed on ice. 45 µl aliquots were added to a prechilled Falcon® 2059 polypropylene tube. 2 µl of the provided β-mercapto-ethanol mix was added. The tubes were swirled gently before being left to incubate on the ice for 10 minutes. During this incubation time, the cells were swirled gently every two minutes. 2 µl of *Dpn* I-treated SDM mix was transferred to the aliquot of ultracompetent cells. This transformation reaction was swirled gently and incubated on ice for 30 minutes. NZY^+ broth was now preheated in a water bath set to 42 °C. The Falcon® 2059 polypropylene tubes containing the reaction mixture were heat-pulsed in the 42 °C water bath for 30 seconds. It was important to ensure the water bath was maintained at exactly 42 °C since this temperature is critical for obtaining the highest efficiencies of transformation. Subsequent to the heat shock, the tubes were incubated on ice for 2 minutes. 0.5 ml of the preheated NZY^+ broth was now added to each tube, which were then incubated at 37 °C for 1 hour with shaking at 225-250 rpm. 250 µl of the transformation reaction mixture was plated onto each of two LB-agar plates supplemented with carbenicillin. These were incubated at 37 °C overnight.

2.4 Transformation of $CaCl_2$ competent AR120 Cells

1 to 2 µl of plasmid DNA was added to a pre-chilled Eppendorf. 200 µl of the competent cells were added and mixed on ice. This was left to stand on ice for 45 minutes. The Eppendorf tube and its contents were heat-shocked for 1 minute and 45 seconds at 42 °C. It was placed back on ice for a further 3 minutes. 0.8 ml of LB broth was added to the tube and incubated for an hour at 37 °C. The cells were then harvested by centrifugation

(13 000 rpm / 3 minutes). Most of the supernatant was discarded and the pellet resuspended in the remainder (~150 µl). The transformed cells were then plated out on LB-agar supplemented with carbenicillin.

2.5 Site-Directed Mutagenesis (carried out in conjunction with Dr C. S. Miles)

2.5.1 Preparation of Mutated DNA

Site-directed mutagenesis was performed using the Stratagene QuikChange® XL site-directed mutagenesis kit to generate all mutants mentioned in this report. The basic procedure utilized a plasmid DNA template ($pDSb_2$) containing the wild-type flavocytochrome b_2 coding sequence and two synthetic oligonucleotide primers which contained the desired mutation. The primers (obtained from Invitrogen) are shown in Table 2.1.

The oligonucleotide primers are each complementary to opposite strands of the template, and were extended during a temperature cycling period (shown in Table 2.2) by use of *PfuTurbo* DNA polymerase. The reaction mixture used for the N42C:K324C double mutant is detailed in Table 2.3.

Mutant	Forward primer sequence (5' to 3')	Reverse primer sequence (5' to 3')
N42C	CGC GAT TCC TAC CAT GTC ATC CAG GTG GGC AG	CTG CCC ACC TGG ATG ACA TGG TAG GAA TCG CG
K324C	GCT TCG AGA GCG TTA TCA TGC TTT ATT GAC CCC TCT TTG	CAA AGA GGG GTC AAT AAA GCA TGA TAA CGC TCT CGA AGC
S234C	CTA CTT TGG CTT CAT GTT GCC CCG AGG AAA TTA TTG	CAA TAA TTT CCT CGG GGC AAC ATG AAG CCA AAG TAG
C233A + S234C	GAT ATC TAC TTT GGC TTC AGC TTG CCC CGA GGA AAT TAT TG	CAA TAA TTT CCT CGG GGC AAG CTG AAG CCA AAG TAG ATA TC
C233A	CTA CTT TGG CTT CAG CTT CCC CCG AGG	CCT CGG GGG AAG CTG AAG CCA AAG TAG

Table 2.1: *Oligonucleotide primers used for site-directed mutagenesis of flavocytochrome* b_2. *Mismatches are underlined.*

Segment	Cycles	Temperature	Time
1	1	95 °C	1 minute
2	18	95 °C	50 seconds
		60 °C	50 seconds
		68 °C	5 minutes, 18 seconds*
3	1	68 °C	7 minutes

Table 2.2: *Cycling Parameters for the QuikChange®XL Method.*

* *The extension time here is based on 1 minute/kb of template DNA (pDSb$_2$ is a 5.3 kb plasmid and would thus require 5 minutes and 18 seconds at 68 °C per cycle).*

Reagent	Volume (µl)
ds DNA	2
Forward primer, N42C (125 ng)	1.25
Reverse primer, N42C (125 ng)	1.25
Forward primer, K324C (125 ng)	1.25
Reverse primer, K324C (125 ng)	1.25
dNTPs	0.5
Quik solution	3
10x reaction buffer	5
H_2O	33.5
PfuTurbo DNA polymerase (2.5 units/µl)	1

Table 2.3: *Reaction mixture used for the N42C:K324C double mutant.*

Incorporation of these primers generated a mutated plasmid containing staggered nicks (see Appendix II). Following temperature cycling, the product was treated with *Dpn* I endonuclease (target sequence: 5' –Gm^6ATC- 3'), which is specific for methylated and hemimethylated DNA and was used to digest the parental DNA template and to select for mutation-containing synthesized DNA. This was carried out by adding 1 µl of the *Dpn* I restriction enzyme (10 U/ µl) directly to the amplification reaction. This reaction was mixed thoroughly before being spun down in a microcentrifuge for 1 minute. It was then allowed to incubate at 37 °C for 1 hour to digest the parental (i.e., the non-mutated) supercoiled dsDNA. The nicked vector DNA incorporating the desired mutations was then transformed into *E. coli* XL 10-Gold® ultracompetent cells (see section 2.3).

The transformed *E. coli* XL 10-Gold® ultracompetent cells were plated on LB agar supplemented with carbenicillin and grown overnight. Only those cells which had taken up the plasmid containing the flavocytochrome b_2 coding sequence with carbenicillin resistance would grow. Transformants were picked and streaked for singles on LB agar supplemented with carbenicillin and incubated overnight. Single colonies from these

plates were then picked and grown in LB broth overnight. DMSO stocks of these cells were made.

2.5.2 Purification of Plasmid DNA

This was carried out by use of the QIAprep® Miniprep (Qiagen). The overnight culture of the transformed *E. coli* XL 10-Gold® cells were pelleted by centrifugation at 5000 rpm for 5 minutes. The cells were then resuspended in 250 µl of Buffer P1 ensuring that no clumps of pellet were visible, and transferred to a microfuge tube. 250 µl of Buffer P2 (NaOH/SDS) was then added to the tube to lyse the cells. SDS solubilises the phospholipid and protein components of the cell memebrane, leading to lysis and release of the cell contents. The alkaline conditions denature the chromosomal and plasmid DNAs, as well as proteins. The tube was then gently inverted between 4-6 times. 350 µl of Buffer N3 was added to neutralize the lysate and adjust it to a high salt concentration. This causes denatured proteins, chromosomal DNA, cellular debris and SDS to precipitate, while the smaller plasmid DNA renatures correctly and stays in solution. The tube was immediately inverted 4-6 times. This suspension was centrifuged for 10 minutes at 13000 rpm. The supernatant obtained was then transferred to a QIAprep spin column sitting on a 2 ml collection tube. This was centrifuged for 1 minute at 13000 rpm and the flow-through discarded. The QIAprep spin column was washed by addition of 0.75 ml of Buffer PE and centrifuging for 30 seconds at 13000 rpm. Again, the flow-through was discarded before the column was centrifuged for a further 1 minute to remove any residual wash buffer. The QIAprep column was then placed into a clean 1.5 ml microfuge tube. The DNA was eluted by addition of 50 µl of elution buffer (10 mM Tris.Cl, pH 8.5) to the centre of the QIAprep column. It was allowed to stand for one minute and then centrifuged for a further one minute at 13000 rpm. Samples were visualized on an agarose gel.

2.5.3 Agarose Gel Electrophoresis of DNA

DNA was visualised on 0.7 % agarose gels with ethidium bromide. This was prepared by dissolving 0.175 g of agarose in 25 ml of 1 x TAE buffer (diluted from a 1 litre 50 X stock prepared from 242 g Tris base, 57.1 ml glacial acetic acid and 100 ml of 0.5 M

EDTA at pH 8.0). 2.5 µl of a 10 mg/ml stock of ethidium bromide in H_2O was added to each 25 ml of gel solution. Prior to loading, each 2 µl DNA sample was mixed with 3 µl of loading buffer (15 % Ficoll (type 400) in water; 0.25 % xylene cyanol; 0.25 % bromophenol blue) and 9 µl of H_2O. A 1 kb marker (GIBCO) (4.5 µl of marker, 6.5 µl of H_2O and 3 µl of loading buffer) as well as the wild-type pDSb_2 plasmid (2 µl of plasmid, 3 µl of loading buffer and 9 µl H_2O) were run as a control. DNA was visualized by UV illumination and photographed as illustrated in Figure 2.2.

Figure 2.2: *UV illuminated agarose gel. Lanes 1,2,4,5; pDSb_2 containing DNA coding sequence for flavocytochrome b_2 containing the N42C:K324C mutation (samples 1-4), Lane 3; pDSb_2 containing DNA coding sequence for wild-type flavocytochrome b_2, Lane 6; 1 kb marker (GIBCO).*

2.5.4 Sequencing

The purified DNA was screened by sequencing (Institute of Cell and Molecular Biology's automated DNA sequencing service) to determine which plasmids contained the desired mutations. Once confirmed, the entire mutated flavocytochrome b_2 gene was sequenced to ensure there were no unwanted mutations. Table 2.4 shows the sequencing primers used. These are shown annealed to the flavocytochrome b_2 DNA coding sequence in Appendix III. The reagents and thermal cycling parameters used are detailed below.

Primer Name	Sequence (5' to 3')
B2SEQ1	CTT CGC ATA GGG TTT GAG TTA G
B2SEQ2	CGC CCG CTG AAG TTG CCA AGC
B2SEQ3	CCA AAG ATC CTT GTA GAT GTA C
B2SEQ4	CCA ATA CAA AGG CTG GTC C
B2SEQ5	GCC ATT GAA ATT TTA AGA GAT G

Table 2.4: *Primers used for sequencing the plasmids.*

Thermal Cycling Parameters: 96 °C for 30 seconds
50 °C for 15 seconds
60 °C for 4 minutes
Repeat for 25 cycles

Reagents:		
	dsDNA	3 µl (~ 150 – 300 ng)
	Primer	1 µl (~ 3.2 pmol)
	Big Dye reaction mix	2 µl
	Dilution Buffer	2 µl
	dH_2O	2 µl

The DNA sequence obtained was checked against that of the wild type flavocytochrome b_2 DNA sequence using the European Bioinformatics Institute (EBI) pairwise global and local alignment tool. An example is shown in Appendix IV.

Following sequencing, the plasmid DNA containing the desired mutations was transferred into the protease deficient expression strain *E. coli* AR120 by transformation (see section 2.4). The transformed *E. coli* AR120 cells were plated on LB-agar supplemented with carbenicillin and incubated overnight. Transformants were picked and streaked for singles as before. Single colonies were selected and grown overnight in

LB broth supplemented with carbenicillin. DMSO stocks of the cells were prepared for long term storage at -80 °C.

2.6 Buffers

2.6.1 Potassium Phosphate Buffer

100 mM potassium phosphate (KPi) was prepared by titrating 200 mM KH_2PO_4 (Fischer Scientific) with 200 mM K_2HPO_4 (Fischer Scientific), prepared in Millipore water to pH 7.0 and the volume doubled with Millipore water.

2.6.2 TrisHCl Buffer

10 mM TrisHCl buffer was prepared by titrating 10 mM HCl (1 N standard solution, Sigma) to pH 7.5 with a saturated solution of Trizma base (tris[hydroxymethyl]aminomethane, Sigma). Ionic strength was adjusted to *I* 0.10 by addition of NaCl (Fischer Scientific). All solutions were prepared in Millipore water.

2.7 Protein Purification

2.7.1 Large Scale Growth of Bacteria

Starter flasks (3 x 75 ml LB-broth) containing 50 mg/l carbenicillin were inoculated with a single colony from an LB-agar plate and grown overnight at 37 °C, 120 rpm. Approximately 20 flasks containing 500 ml of LB-broth and supplemented with 50 mg/l carbenicillin were then inoculated with 10 ml portions of starter culture and grown for 24 hours at 37 °C, 120 rpm.

2.7.2 Cell Harvesting and Lysis

After overnight growth, *E. coli* cells producing flavocytochrome b_2 were collected by centrifugation at 8000 rpm for 10 minutes (Sorvall RC5B refrigerated superspeed centrifuge). Cell pellets were suspended in 100 mM KPi, pH 7.0, 10 mM L-lactate

(lithium salt, Sigma), 10 mM DTT (Sigma). The presence of L-lactate ensures that the enzyme is maintained in its more stable reduced form on release from the cell. The DTT is thiol specific and will ensure any disulfide bridge is kept reduced. Any bridge formed too quickly could cause folding and structural problems within the enzyme. Cells were lysed by sonication on ice (MSE Soniprep 150) and cell debris removed by centrifugation (20000 rpm, 1 hour).

2.7.3 Ammonium Sulfate Precipitation and Dialysis

The supernatant retained after removal of cell debris was made up to 70 % saturation with $(NH_4)_2SO_4$ (BDH) and allowed to equilibrate by stirring for approximately 1 hour at 4 °C. The precipitated proteins (including flavocytochrome b_2) were then removed by centrifugation (20000 rpm, 15 minutes). The red pellet obtained was then resuspended in the minimum volume of 100 mM KPi, pH 7.0, 10 mM L-lactate, 1 mM DTT and dialysed (12000 Da pore size) against the same buffer overnight with multiple changes until all the $(NH_4)_2SO_4$ was removed. The solution was then centrifuged at 20000 rpm for 15 minutes to remove any denatured precipitated protein prior to column chromatography.

2.7.4 Column Chromatography

(i) DE52 Anion Exchange

The first step in the purification of flavocytochrome b_2 involves the use of a DE52 anion exchange column (diethyl-aminoethyl cellulose, Whatman). The diethyl-aminoethyl groups are covalently cross-linked to a cellulose matrix and when equilibrated to pH 7 it forms a positively charged binding surface for proteins that are negatively charged. The column material was prepared by suspending the appropriate amount in 100 mM KPi, pH 7.0, 10 mM L-lactate, 1 mM DTT, and the pH re-adjusted to pH 7.0 by the addition of concentrated HCl. The material was then poured into a glass column (15 cm x 2.5 cm) and allowed to equilibrate at the correct pH by washing with 100 mM KPi, pH 7.0, 10 mM L-lactate, 1 mM DTT. Post-dialysis supernatant was then loaded onto the column. The DE52 acts as a filter, hence the anionic contaminant proteins bind to the column whilst flavocytochrome b_2 passes straight through without binding.

(ii) Hydroxyapatite

The hydroxyapatite material (hydroxyapatite Bio-Gel® HTP Gel, BioRad) consists of crystalline $Ca_{10}(PO_4)_6OH_2$ and is often used as the basis for association columns since it is able to bind proteins tightly. The material is believed to interact with proteins via negatively charged phosphate groups and hence acts in the opposite way to the DE52 column. It will bind neutral and positively charged proteins that can then be eluted by use of an ionic strength gradient.

The material was prepared by suspension in 100 mM KPi, pH 7.0, 10 mM L-lactate, 1 mM DTT (6 parts buffer: 1 part hydroxyapatite). As the solid settled in the beaker, the smaller particles (finings) were removed by decanting to ensure a free-flowing column. The suspended material was poured into a glass column (10 cm x 4 cm) and allowed to settle. It was equilibrated with 100 mM KPi, pH 7.0, 10 mM L-lactate, 1 mM DTT. Post DE52 material was then loaded straight onto the hydroxyapatite where it bound as a tight red band. The bound flavocytochrome b_2 was washed with 100 mM KPi, pH 7.0, 10 mM L-lactate, 1 mM DTT, while the amount of contaminant protein washed off was monitored by regular checking of fractions for protein absorbance at 280 nm. Once A_{280} was found to be zero, a stepwise elution gradient was started. The column was washed with the same buffer, but with $(NH_4)_2SO_4$ added up to 10 % saturation in 2 % increments. The $(NH_4)_2SO_4$ concentration was only raised to the next increment when the A_{280} of the eluate was found to be zero. Flavocytochrome b_2 was generally found to be eluted from the column at between 8 % and 10 % saturation with $(NH_4)_2SO_4$ and was collected in 10 ml fractions. The purity of each fraction was determined by UV/vis spectrophotometry. Samples with spectra whose peaks at 423 nm and 269 nm had a ratio of $A_{423}/A_{269} \geq 2$ were deemed to be of sufficient purity for crystallography, while those with a ratio of $A_{423}/A_{269} \geq 1.5$ were deemed to be suitable for kinetic analysis. All others were discarded.

2.7.5 Precipitation and buffer Exchange

The pure fractions eluted from the hydroxyapatite column were pooled and made up to 70 % saturation with $(NH_4)_2SO_4$. After equilibration, precipitated flavocytochrome b_2 was removed by centrifugation (20000 rpm, 15 minutes) and the supernatant discarded. The pellet is then redissolved in the minimum volume of 10 mM TrisHCl, pH 7.5, I 0.10.

This solution was then loaded onto a Superdex 200 gel filtration column equilibrated with 10 mM TrisHCl, pH 7.5, *I* 0.10, and eluted with the same buffer. The nature of the size exclusion column causes flavocytochrome b_2 to migrate faster than small molecules such as $(NH_4)_2SO_4$ and L-lactate, in addition to effecting buffer exchange, and this was confirmed by observing the protein change colour as it became oxidized in the absence of substrate.

2.8 Protein Storage

2.8.1 Short Term Storage

For short term storage (up to one month) the enzyme was stored as the $(NH_4)_2SO_4$ precipitate obtained after the hydroxyapatite column and prior to buffer exchange. The pellet was stored at 4 °C under N_2.

2.8.2 Long Term Storage

For indefinite storage of flavocytochrome b_2, the purified enzyme was concentrated to between 0.5-1 mM and frozen as small aliquots (approximately 50 µl) in the -80 °C freezer.

2.9 Gel Electrophoresis

Electrophoresis exploits the fact that different proteins carry different masses and charges, and will move at different rates in an electric field. Small proteins move rapidly through the gel, whereas large ones stay at the top, near the point of application of the mixture.

In this case, pre-cast Invitrogen NuPAGE Novex 4-12% Bis-Tris gels were used to determine the purity of the protein throughout the purification procedure and also to ensure that protein with the correct molecular weight was obtained. Samples were prepared by adding 20 µl of NuPAGE LDS sample buffer (4x) to 60 µl of protein sample. They were then boiled for 5 minutes to denature the protein before being loaded onto the

gel. SeeBlue Plus 2 pre-stained protein standard was used as a marker system (illustrated in Figure 2.3).

The running buffer, NuPAGE MES SDS (20x), was prepared by diluting 50 ml of stock up to 1 litre in dH_2O. The gel took approximately 55 minutes to run at 150 V.

The gel was stained with a 1% coomasie blue solution in 40% MeOH, 10% AcOH for not less than 30 minutes. The stain was removed with 40% MeOH, 10% AcOH. This shows all proteins that are present in the sample. The gel was scanned and an example is shown below in Figure 2.3.

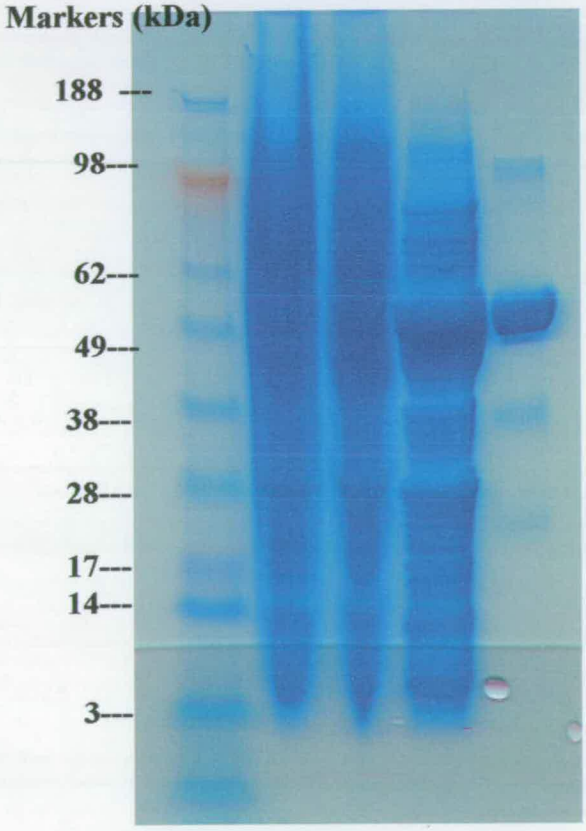

Figure 2.3: *Coomasie stained SDS-PAGE gel. Lane 1 shows molecular markers, with their weight indicated to the left hand side. Lane 2; Cell Free Extract (CFE), Lane 3; Post-$(NH_4)_2SO_4$ cut, Lane 4; Post-DE52, Lane 5; Post-gel filtration.*

2.10 UV/vis Spectrophotometry

UV/vis spectrophotometry was performed using a Shimadzu UV-1601 UV/vis scanning spectrophotometer with the UV-1601 software. The extinction coefficients for flavocytochrome b_2 in both its oxidized and reduced forms are shown below in Table 2.5. Example spectra of the mutant form of flavocytochrome b_2 (N42C:K324C) is shown in Figure 2.4

Oxidation State	Soret Maximum/ nm	ε^a/ M^{-1} cm^{-1}
Oxidised	413	129500
Reduced	423	183000

Table 2.5: *Extinction coefficients for flavocytochrome b_2*

[a] Pajot and Groudinsky, 1970

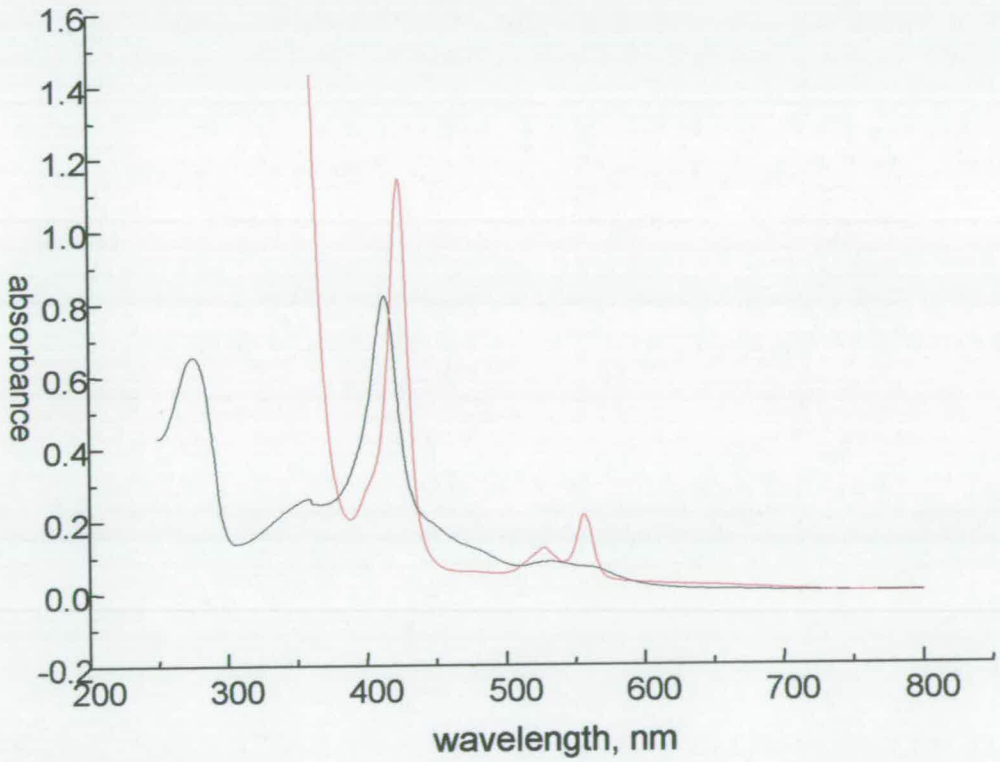

Figure 2.4: *UV/vis spectra of oxidized (black) and dithionite reduced (red) N42C:K324C mutant flavocytochrome b_2.*

2.11 FMN Determination

The FMN content of the mutant enzyme was determined as follows. 50 µl of enzyme at approximately 80 µM was added to 1 ml of 10 mM TrisHCl, pH 7.5, *I* 0.10 in an Eppendorf. 150 µl of 50 % trichloroacetic acid was added and the Eppendorf inverted a few times to ensure mixing. The protein matter should precipitate out of solution leaving the FMN in solution. Hence, the Eppendorfs were centrifuged for 5 minutes in a Spectrafuge 16M at full speed. The supernatant was then pipetted into a clean Eppendorf and the solution brought to pH 7 by the addition of sodium carbonate. A spectrum was taken of the solution with the peak at 450 nm corresponding to the FMN in solution. Knowing ε_{FMN} = 11100 M^{-1} cm^{-1}, the concentration of FMN in solution can be calculated and hence, the % FMN in the enzyme was calculated as follow:

$$\% \text{ FMN} = \frac{[\text{FMN}]}{[\text{enzyme}]} * 100\ \%$$

2.12 The Ellman Assay

The Ellman Assay allows the quantitative determination of the number of free cysteine residues within the protein. The Ellman reagent, 2, 2'-Dipyridyl disulfide (2-PDS) reacts with the sulfur of the cysteine and this results in the cleavage of the central S-S bond within the 2-PDS. This yields a protein-pyridyl product and a chromophore. The accumulation of the chromophore is monitored spectrophotometrically at 343 nm (ε_{343} = 8080 M^{-1} cm^{-1}) that gives quantification of the number of free cysteine groups within the protein. A schematic of the reaction occurring is shown in Figure 2.5.

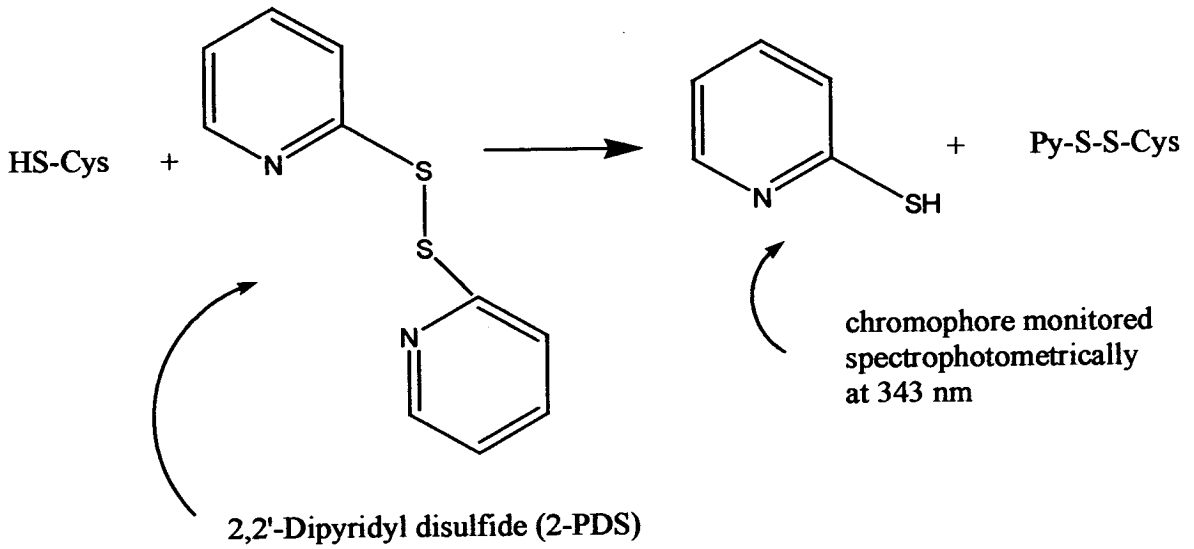

Figure 2.5: *2-PDS is reacted with a free cysteine within the protein. Cleavage of the central S-S bond occurs and results in the formation of a chromphore, whose presence can be monitored at 343 nm (ε_{343} = 8080 M^{-1} cm^{-1}) and a protein-pyridyl product.*

The initial part of the experiment was carried out in a nitrogen atmosphere (Belle Technologies glove box, with O_2 levels kept at less than 3 ppm) to prevent any air oxidation of free cysteinyl sulfur. The enzyme was prepared in 100 mM KPi, pH 7.0, 25 °C in the presence of 1 mM DTT. DTT ensures that any disulfide bridges and free cysteines within the enzyme are kept reduced. Excess DTT was then removed by use of gel filtration (Sephadex G-25). The eluted enzyme was diluted to 10 μM. The prepared enzyme sample was now brought out of the glove box and into the normal oxidative environment. 900 μl of the 10 μM enzyme sample was added to a 1 cm pathlength quartz cuvette. 100 μl of 1mM 2-PDS (prepared in EtOH) was added to the enzyme and hence diluted 10-fold. The change in absorbance at 343 nm was observed; the total absorbance change correlating with the quantity of free cysteine in the enzyme.

The Ellman Assay was repeated at approximately 2 hour intervals, to determine if the number of cysteine groups reacting was decreasing with respect to time, and hence the oxidative formation of any disulfides was occurring.

2.13 Electrospray Mass Spectrometry

Positive electrospray mass spectrometry was carried out on a Micromass platform electrospray mass spectrometer. The cone voltage was set to 50 V and the source temperature to 120 °C. Direct infusion was used to inject protein samples (~ 20 μM in 19:1 0.1 % formic acid in H_2O / 0.1 % formic acid in acetonitrile). For each sample, 10 spectra were accumulated and the average used to calculate the transformed mass using Mass Lynx software.

2.14 Sulfite Binding

980 μl of an approximately 5μM solution of flavocytochrome b_2 was pipetted into each of two 1 ml quartz cuvettes. Small aliquots (up to a total volume of 20 μl) of concentrated sulfite were added to the sample cell, with an equal volume of buffer being added to the reference cell. Spectra were recorded from 250 to 800 nm using a Shimadzu UV-PC 2101. Spectra were recorded after each addition of sulfite at 25 °C. Difference spectra were obtained and the dissociation constant (K_d) was determined by plotting the change in absorbance between 520 nm and 470 nm against the concentration of sulfite. Data were fitted to $\Delta A = A_{max}(((S+E+K_d) \pm \sqrt{((S+E+K_d)^2-4ES)}))/2$, see Appendix V.

2.15 Preparation of substrates

2.15.1 L-[2-^{1}H] lactate

This solution was made as a standard by the addition of buffer (10 mM TrisHCl, pH 7.5, *I* 0.10 for kinetic experiments) to the calculated amount of lithium salt of L-lactic acid.

2.15.2 L-α-2-Hydroxybutyrate

An appropriate amount of L-α-2-Hydroxybutyric acid was made up in buffer to the desired concentration. Due to the fact that this was the acid, the desired pH was achieved by titrating in a weak solution of NaOH.

2.15.3 Sulfite

This solution was made as a standard by the addition of buffer (10 mM TrisHCl, pH 7.5, *I* 0.10 for kinetic experiments) to the calculated amount of sodium sulfite.

2.16 Steady-State Kinetic Analysis

Steady-state kinetic analyses were carried out in 10 mM TrisHCl, pH 7.5, *I* 0.10 at 25 °C. The flavocytochrome b_2 used was thawed on ice directly prior to use, and incubated on ice throughout the whole experiment. The concentration of the enzyme was determined before use (see section 2.10) and a suitable concentration of enzyme was added to each assay to obtain a good trace. Assays were carried out using both ferricyanide ($K_3[Fe(CN)_6]$, Fisons) and cytochrome *c* (horse heart, type VI, Sigma) as electron acceptors. Ferricyanide is an artificial one-electron acceptor, and its reduction (Fe(III) to Fe(II)) was followed by monitoring the decrease in absorbance at 420 nm ($\varepsilon_{ox\text{-}red}$ = 1010 $M^{-1}cm^{-1}$). Saturating concentrations of between 1 and 5 mM ferricyanide were satisfactory depending on the mutant form, however, this resulted in the need to use 2 mm or 5 mm pathlength cuvettes and either smaller or larger assay volumes depending on which cuvette was being used. Such incidencies are indicated where relevant.

Cytochrome *c* was used freshly prepared in 10 mM TrisHCl, pH 7.5, *I* 0.10 and diluted to a suitable concentration. Cytochrome *c* reduction by flavocytochrome b_2 was monitored at 550 nm ($\varepsilon_{ox\text{-}red}$ = 22640 M^{-1} cm^{-1}) (Hazzard *et al.*, 1986). A saturating cytochrome *c* concentration of 100 μM was used.

Assays were carried out in both the closed (disulphide bridge formed) and open (disulphide bridge reduced on addition of dithiothreitol (DTT)) forms of the enzyme. Where DTT is used, a control assay was performed to assess for any background activity produced as a result of electrons provided by DTT. This was subtracted from the overall activity obtained in the presence of enzyme.

Analysis of data was carried out using non-linear least squares analysis on the program Microcal Origin to obtain values for k_{cat} and K_m. For an overview of Michaelis-Menten theory, please refer to Appendix V.

2.17 Pre-Steady State Kinetic Analysis

2.17.1 Theory

Pre-steady state kinetic analysis (also known as stopped-flow) allows experiments to be designed, where, by rapid mixing of equal volumes of the enzyme and its substrate, individual steps of the catalytic cycle can be studied and gives microscopic rate constants. In this situation, the flow of electrons is stopped before the catalytic cycle can be completed because of the absence of an external electron acceptor. Choosing the appropriate wavelength to monitor the reaction allows us to observe whichever cofactor we are interested in.

One problem associated with this stopped-flow technique is that of the dead time and mixing time of the apparatus. For the apparatus used, this time is approximately 1-2 ms, meaning that rates over 1000 s^{-1} could not be measured accurately.

2.17.2 Experimental

All stopped-flow experiments were carried out on an Applied Photophysics SF.17 Microvolume stopped-flow spectrophotometer. Enzyme dilutions were made in 10 mM TrisHCl, pH 7.5, I 0.10 at 25 °C and the reacting solutions were maintained at a temperature of 25.0 ± 0.1 °C throughout the course of the experiment. At least 3 runs were performed for each experiment and all data was analysed using both the instrument SF.17 software and Microcal Origin.

2.17.3 Flavocytochrome b_2 Reduction

The reduction of the enzyme was observed in two different experiments by recording FMN and b_2-heme reduction at the appropriate wavelengths. FMN reduction was observed at the b_2-heme isosbestic point of 438.3 nm. The reduction of b_2-heme was observed at 557 nm where FMN absorbance is essentially zero. Both FMN and b_2-heme reduction experiments were performed in the closed and open (addition of DTT) forms of the enzyme. Despite initial attempts to perform these experiments anaerobically, it was difficult to keep the b_2-heme oxidized after addition and removal (using a G-25 column) of the DTT. As such, they were performed aerobically and a control experiment was

performed to check the effect of FMN and b_2-heme reduction by electrons provided from the DTT.

2.17.4 Cytochrome *c* Reduction

Flavocytochrome b_2 was pre-reduced with 10 mM L-lactate (after mixing). Reduction was carried out over a range of flavocytochrome b_2 concentrations, typically 2-15 μM after mixing. To ensure that the reduction occurred under pseudo-first-order conditions, flavocytochrome b_2 was always present in excess and as such, the cytochrome *c* concentration was 1 μM after mixing. The reduction of cytochrome *c* by pre-reduced flavocytochrome b_2 was monitored at 416.5 nm, a flavocytochrome b_2-heme isosbestic point.

This series of experiments was carried out in both the closed and open forms of the enzyme. Excess DTT was removed from the enzyme by use of a G-25 column. To prevent re-oxidation of the disulphide bond, all experiments (both in the open and closed forms of the enzyme), were carried out under fully anaerobic conditions.

2.17.5 Sulfite Binding

Flavocytochrome b_2 (~ 4 μM after mixing) was reacted against a sulfite solution (0.1 – 10 mM after mixing). This was monitored at 450 nm, which allows direct observation of the flavin chromophore. The experiment was performed on both the open and closed forms of the enzyme and under aerobic conditions.

2.18 Protein Crystallization (with Dr Chris Mowat and Miss Chiara Bruckmann)

Crystallization of the N42C:K324C double mutant form of flavocytochrome b_2 was carried out by hanging drop vapour diffusion (Figure 2.6) in an air atmosphere at 18 °C in Linbro plates. Crystals were obtained with a well solution comprising 100 mM sodium citrate pH 4.5, 200 mM NaBr, 10-12 % PEG4000, and 50 mM sodium pyruvate. Hanging drops (4 μl volume) were prepared by adding 2 μl of 15 mg/ml protein (in 10 mM TrisHCl pH 7.5, *I* 0.1) to 2 μl of well solution. After 2-3 days long needle-like crystals were obtained. Prior to mounting in nylon loops for data collection crystals were

immersed in paraffin oil for cryoprotection and then flash-cooled in liquid nitrogen. A dataset was collected to 3.0 Å resolution at ESRF in Grenoble (beamline BM14; λ = 0.95373 Å) using a Mar Research CCD detector. Crystals were found to belong to space group $P2_1$ with cell dimensions a = 64.226 Å, b = 179.895 Å, c = 96.369 Å and β = 90.68 °. Data processing was carried out using MOSFLM and SCALA (Leslie, 1992) The structure was solved by molecular replacement using MOLREP and the wild-type flavocytochrome b_2 structure (PDB ID 1FCB (Xia & Mathews, 1990)), stripped of water, as a starting model. Electron density fitting was carried out using the program TURBO-FRODO (Roussel & Cambillau, 1991), and structure refinement was carried out using Refmac5 (Murshudov *et al.*, 1997).

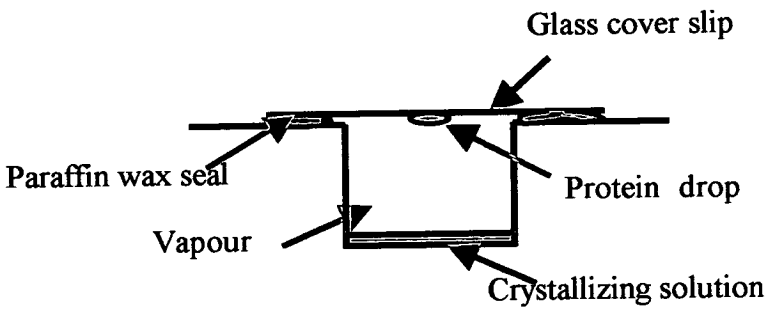

Figure 2.6: *The Hanging Drop Vapour Diffusion method. Over time, the crystallizing solution will pull water from the droplet in a vapour phase such that an equilibrium will exist between the drop and the reservoir. During this process the protein is concentrated, increasing the relative supersaturation of the protein in the drop and ultimately forming crystals.*

Chapter 3

Biochemical and Structural Characterisation of the N42C:K324C Mutant Flavocytochrome b_2

Chapter 3

Biochemical and Structural Characterisation of the N42C:K324C Mutant Flavocytochrome b_2

3.1 Introduction

The purification of wild-type and mutant forms of flavocytochrome b_2 has been a straightforward process since its over-expression in *E. coli* (Black *et al.*, 1989a). Many single and multiple site mutant forms of the enzyme have been produced, including the individual FMN and b_2-heme domains (Balme *et al.*, 1995; Brunt *et al.*, 1992).

The N42C:K324C mutant flavocytochrome b_2 has been constructed, overexpressed in *E. coli* and subsequently purified as detailed in Chapter 2. The biochemical and structural characterisation of this mutant enzyme are discussed in this chapter.

3.2 Results and Discussion

3.2.1 Molecular Weight of the N42C:K324C Mutant Enzyme

The molecular weight of the mutant enzyme was confirmed by electrospray mass spectrometry (Figure 3.1) and SDS PAGE (Figure 3.2). The difference between the predicted mass and the actual mass of the mutant enzyme was 12.1 Da (this does not include the cofactors FMN and heme since they are lost during the ionisation process). Wild-type enzyme was used as a comparison (Figure 3.1). In this case, the difference between the predicted mass and the actual mass was 6.6 Da. Both these mass differences lie within the error of the instrument.

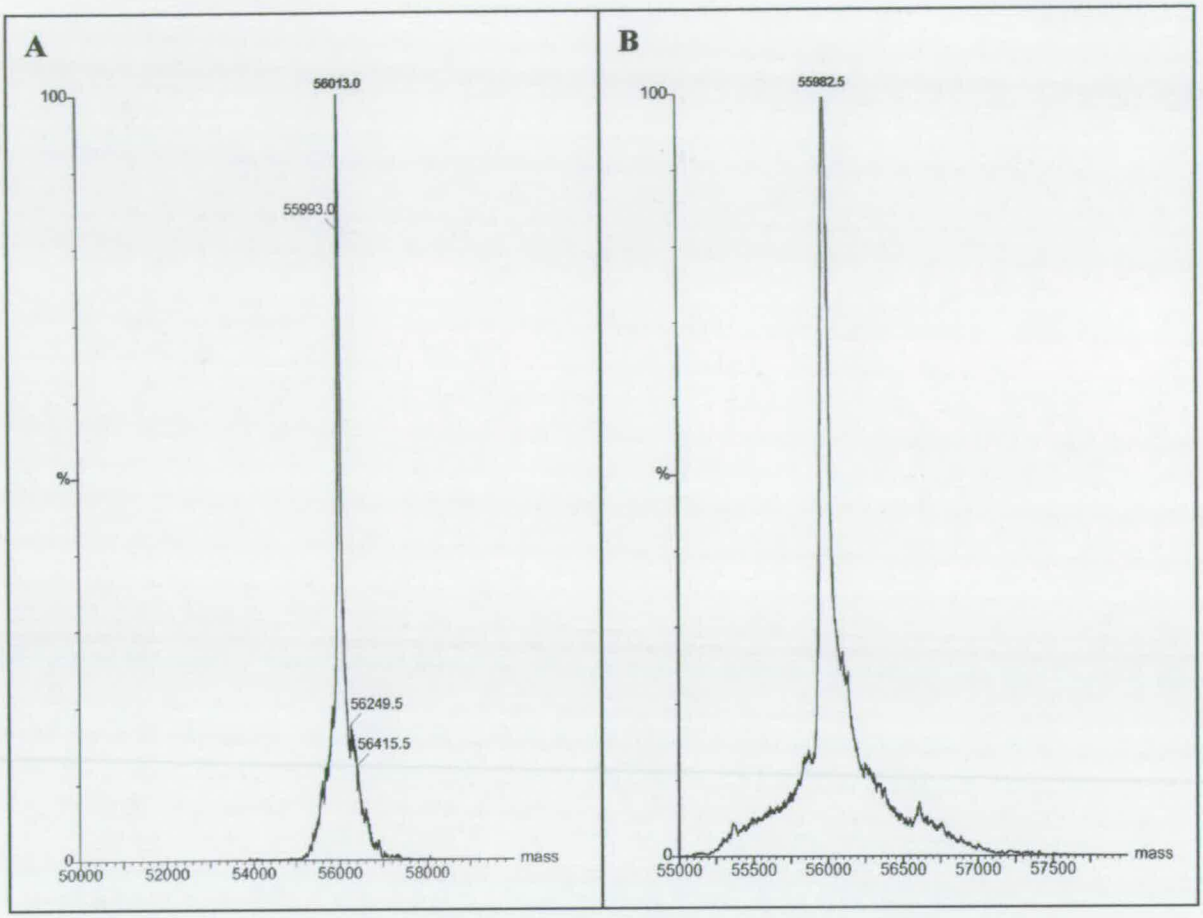

Figure 3.1: *Mass spectrum of Wild-Type and N42C:K324C flavocytochrome b_2. Panel A; Wild-type flavocytochrome b_2, actual mass 56013.0 ± 10.78 Da. The amino acid sequence in Appendix I gives a predicted mass of 56006.4 Da. Panel B; N42C:K324C flavocytochrome b_2, actual mass 55982.5 ± 4.19 Da. The predicted mass taken from the amino acid sequence and corrected for the substituted cysteine residues gave a mass of 55970.4 Da.*

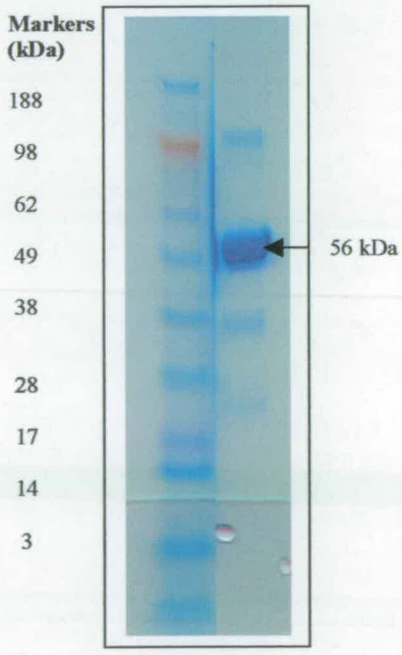

Figure 3.2: *Coomassie stained analysis of proteins. Lane 1 shows the molecular weight markers. Lane 2 shows purified N42C:K324C flavocytochrome b_2. The band runs at about 56 kDa.*

3.2.2 The Multimeric Nature of the N42C:K324C Mutant Enzyme

We have carried out many crystalisation trials on the N42C:K324C enzyme with little success. Despite setting up numerous different conditions, no crystals were obtained. Since purity could be a limiting factor in crystal growth, efforts were focussed on the purification procedure. However, from using SDS-PAGE, where a single band of flavocytochrome b_2 was observed on the overloaded gel, it seemed unlikely that purity was a real problem. However, instead of using a Sephadex G-25 column as the final purification step as would normally be the case when purifying flavocytochrome b_2 (desalting step), a Superdex 200 gel filtration column was used. The column material in this case has a larger pore size and is suitable for the separation of globular proteins between molecular weights of approximately 10^4 to 10^6 Da. In addition to this, the resolution should be high. When the protein was passed through this column it was noticed that three different peaks appeared on the chromatogram (Figure 3.3, A).

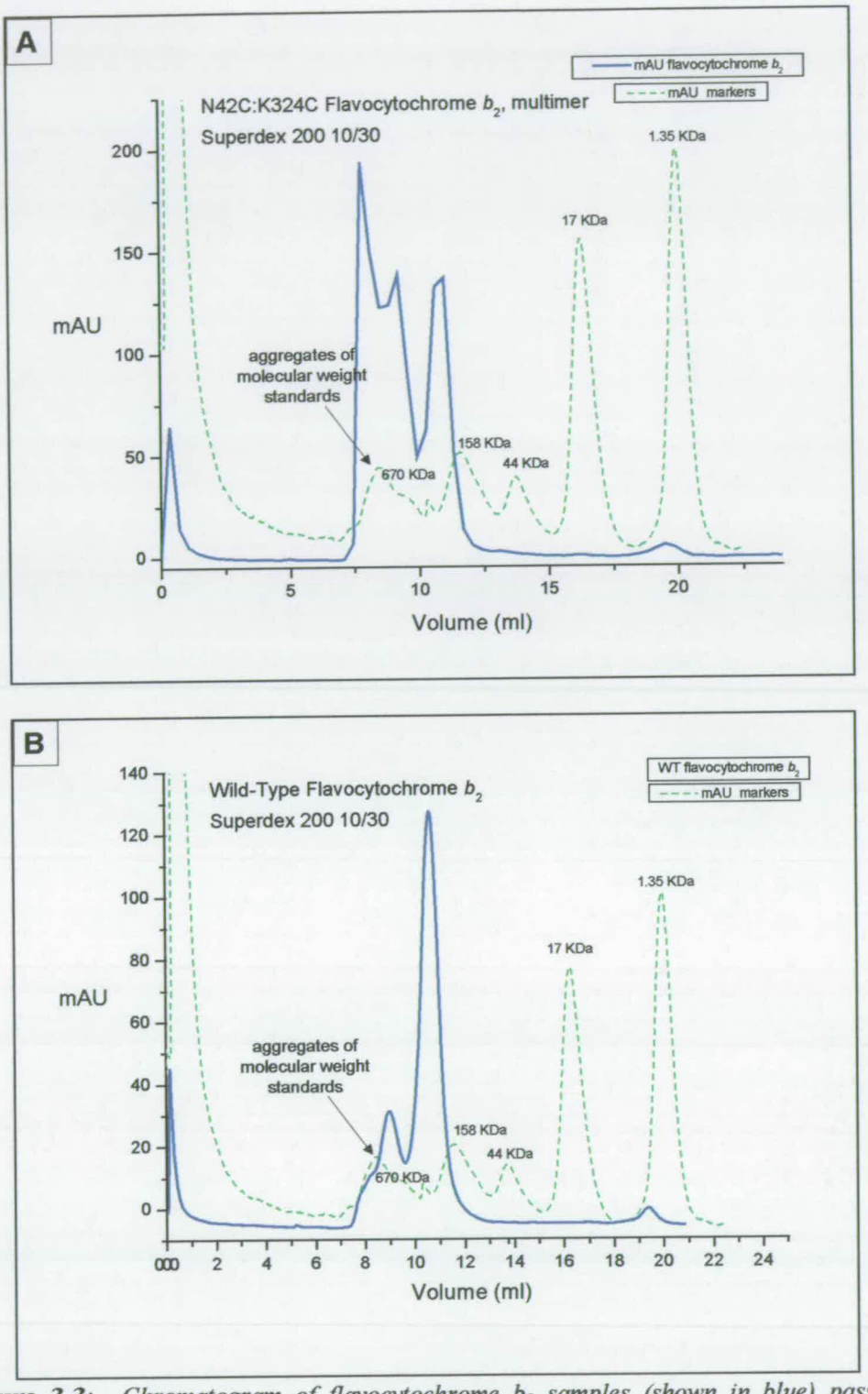

Figure 3.3: *Chromatogram of flavocytochrome b_2 samples (shown in blue) passed through the Superdex 200 gel filtration column. They are shown against molecular weight standards (shown in green). (A) multimeric enzyme, (B) wild-type enzyme.*

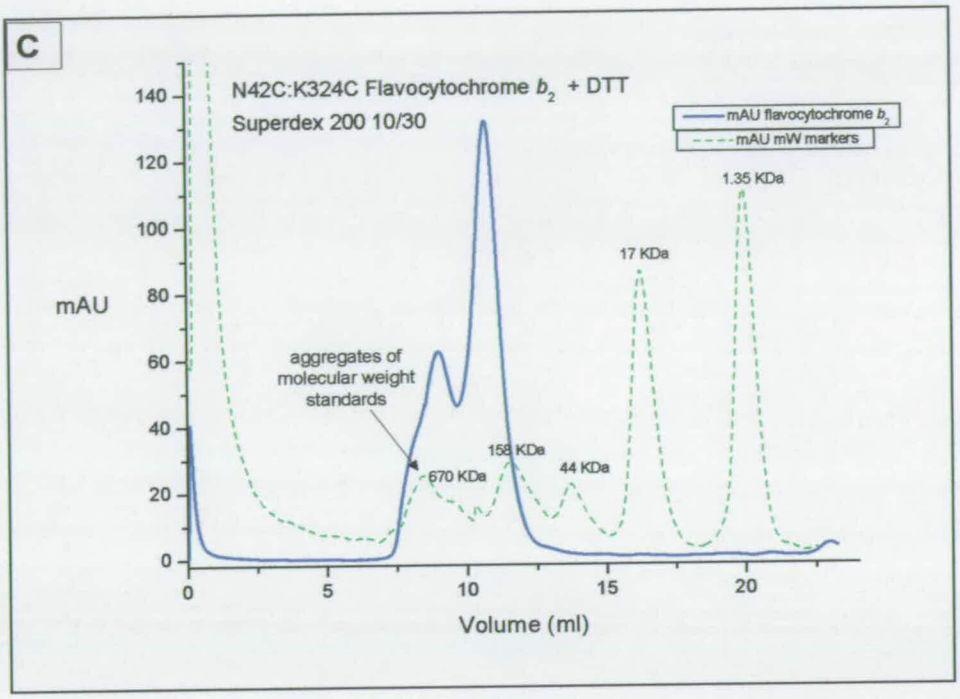

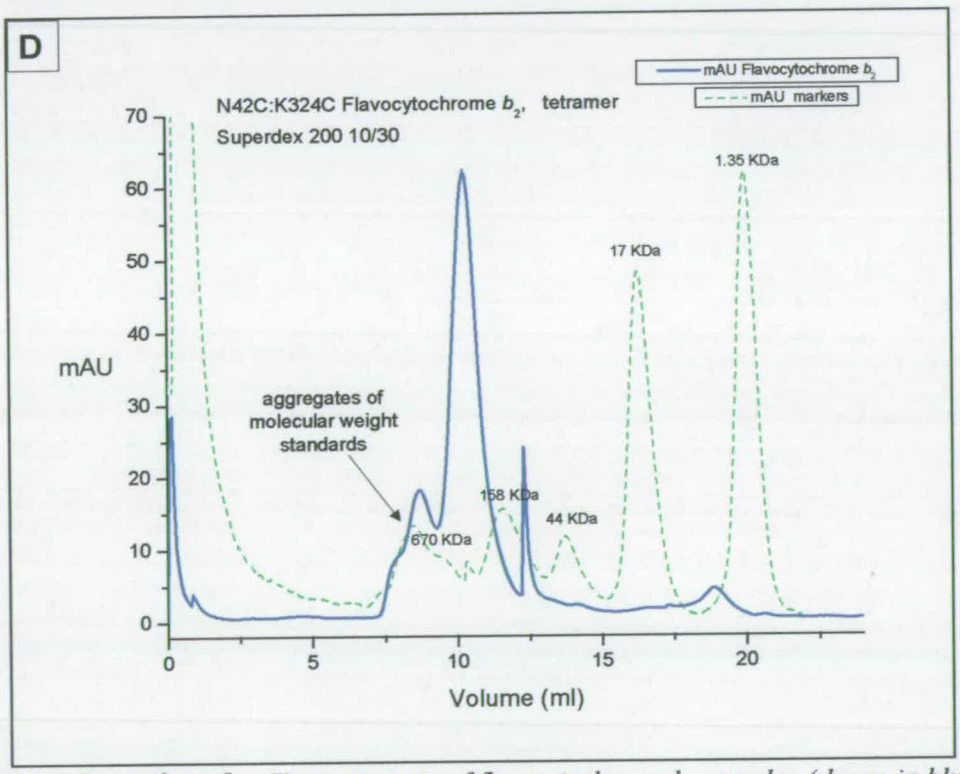

Figure 3.3 continued: *Chromatogram of flavocytochrome b_2 samples (shown in blue) passed through the Superdex 200 gel filtration column. They are shown against molecular weight standards (shown in green).(C) N42C:K324C mutant enzyme + DTT, (D) tetrameric N42C:K324C mutant enzyme .*

Appropriate molecular weight standards were passed through the column to calibrate it. Extrapolation from a plot of Log M_r *vs* V_v/V_e (Figure 3.4) allowed the determination of the molecular weight of the sample peaks.

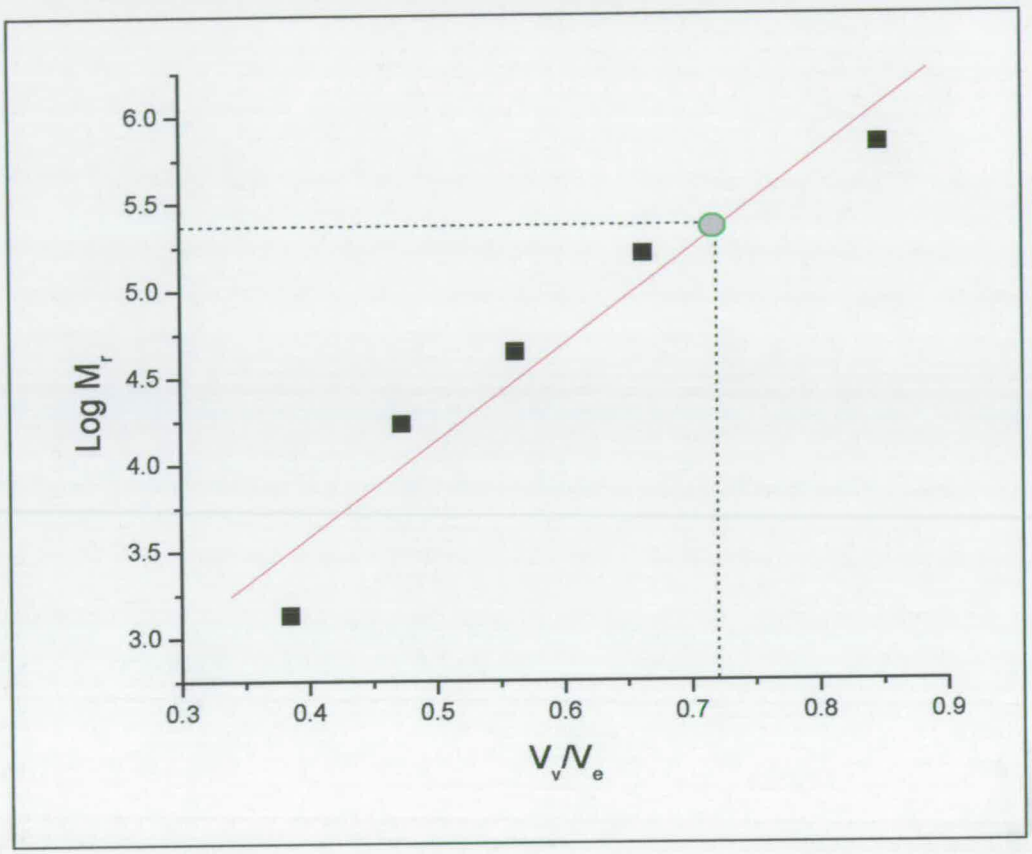

Figure 3.4: *Plot of Log Mr vs void volume (V_v)/elution volume (V_e) of the standards used for the Superdex 200 gel filtration column. These were bovine Thyroglobulin (670 kDa), bovine γ-globulin (158 kDa), chicken Ovalbumin (44 kDa), horse Myoglobin (17 kDa) and Vitamin B_{12} (1.35 kDa). The points were fitted to a linear gradient, ($y=mx + c$, where $m = 5.5 \pm 0.8$, $c = 1.4 \pm 0.5$). The corresponding V_v/V_e for the N42C:K324C tetramer is highlighted by the grey circle.*

The first peak eluted with the void volume of the column, since it was at a molecular weight in excess of the columns capability. The second peak eluted at a molecular weight of approximately 1000 kDa. The third peak eluted at a molecular weight of 200 kDa. It was immediately obvious that the peak at 200 kDa corresponded to the tetrameric enzyme. The peaks eluting at the void volume, plus the peak at 1000 kDa

are likely to be caused by the tetramer aggregating together, the latter case possibly existing as a tetramer of tetramers. This raised the question whether the engineered cysteine residues had possibly formed inter-subunit covalent bonds rather than the intended inter-domain disulfide bridge. In fact, aggregation exists as a problem for many proteins including Histone H1 from *Diptera* species. Cysteine is present in H1 and confers to it the ability to aggregate under oxidising conditions (Franco *et al.*, 1977), presumably through intermolecular disulfide bridges.

To investigate this possibility, wild-type enzyme was passed through the column as a control (Figure 3.3, B). A slight bump can be seen eluting at the leading edge of the void volume, followed by a peak at approximately 1200 kDa. The last peak corresponds to a molecular weight of 230 kDa. Since wild-type enzyme cannot form inter-subunit covalent bonds, the aggregated state must be a result of weak forces, such as hydrogen bonds, bringing the tetramers together. Dithiothreitol (DTT) was added to the mutant enzyme to test whether the aggregate was held together my inter-subunit covalent bonds due to the introduced cysteine residues. The DTT will chemically reduce the contacts between the cysteine residues and allow the protein to run in a similar fashion to wild-type enzyme through the gel filtration column (Figure 3.3, C). Indeed, the sample ran exactly like wild-type enzyme, with the first smaller peak eluting with the void volume, the second peak eluting at 1300 kDa and the third eluting at a molecular weight of 215 kDa. Thus, a portion of the tetrameric mutant enzyme aggregates together through weak bonding, whilst the remainder forms inter-subunit disulfide bonds.

To rule out the possibility that the separated tetramer fraction of the mutant sample may over time re-aggregate, DTT was added to the sample and removed through a small gel filtration column. The protein sample was then left for 30 minutes before being run through the Superdex 200 column. The chromatogram is shown in Figure 3.3, D. It is clear to see that it runs exactly like wild-type enzyme indicating that once in the tetrameric state it will stay as such.

The separated fractions of the mutant enzyme from the Superdex 200 gel filtration columns (i.e. the higher molecular weight aggregate, the lower molecular weight

aggregate and the tetramer) were taken forward for further analysis. This is detailed in the subsequent sections of this chapter.

3.2.3 The Ellman Assay - Is there a Disulfide Bond?

The Ellman assay is an ideal means by which to quantitively assess the presence of free cysteine within a protein. It involves the reaction of 2,2'-Dipyridyl disulfide (2-PDS) with the sulfur of the cysteine residue(s) resulting in cleavage of the central disulfide bond of the 2-PDS reagent. This yields a protein-pyridyl product and a chromophore (section 2.8). Accumulation of this chromophore was monitored spectrophotometrically at 343 nm over a 500-second time scale as shown in Figures 3.5, 3.6 and 3.7. The absorbance change is shown on the left hand axis while the right hand axis has been recalculated to show thiol equivalents. Data were collected for the mutant enzyme in both its disulfide reduced and bridged forms. In addition, this was carried out for each of the higher molecular weight aggregate (Figure 3.5), the lower molecular weight aggregate (Figure 3.6) and the tetrameric (Figure 3.7) mutant enzymes. In each case, the mutant enzyme shows a thiol count of two in the nonbridged form. Incubation of the mutant enzyme in an aerobic atmosphere allowed the oxidative formation of the disulfide bond, which is seen in the Ellman assay. This resulted in a trace that is identical to that of the mutant enzyme which did not have any treatment with DTT.

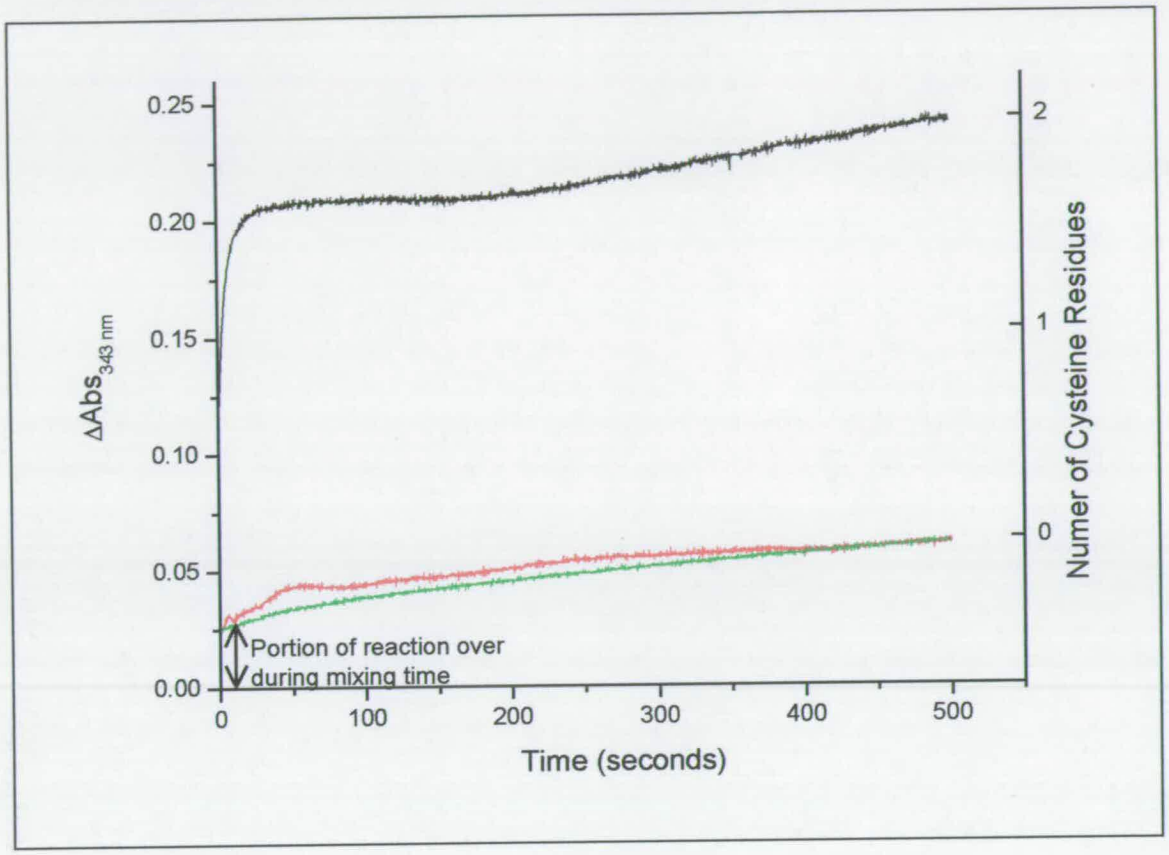

Figure 3.5: *Time-dependant traces of the accumulation of chromophore produced during the Ellman assay analysis of the higher molecular weight aggregate of the N42C:K324C mutant flavocytochrome b_2. Shown are traces for the mutant enzyme with the disulfide bridge intact (green), the disulfide bridge open (black) and re-bridged (after incubation in the aerobic atmosphere)(red). Data recorded at 25 °C, pH 7.0, I = 0.1 M., traces monitored at 343 nm, where $\varepsilon_{343} = 8.08\ mM^{-1}\ cm^{-1}$.*

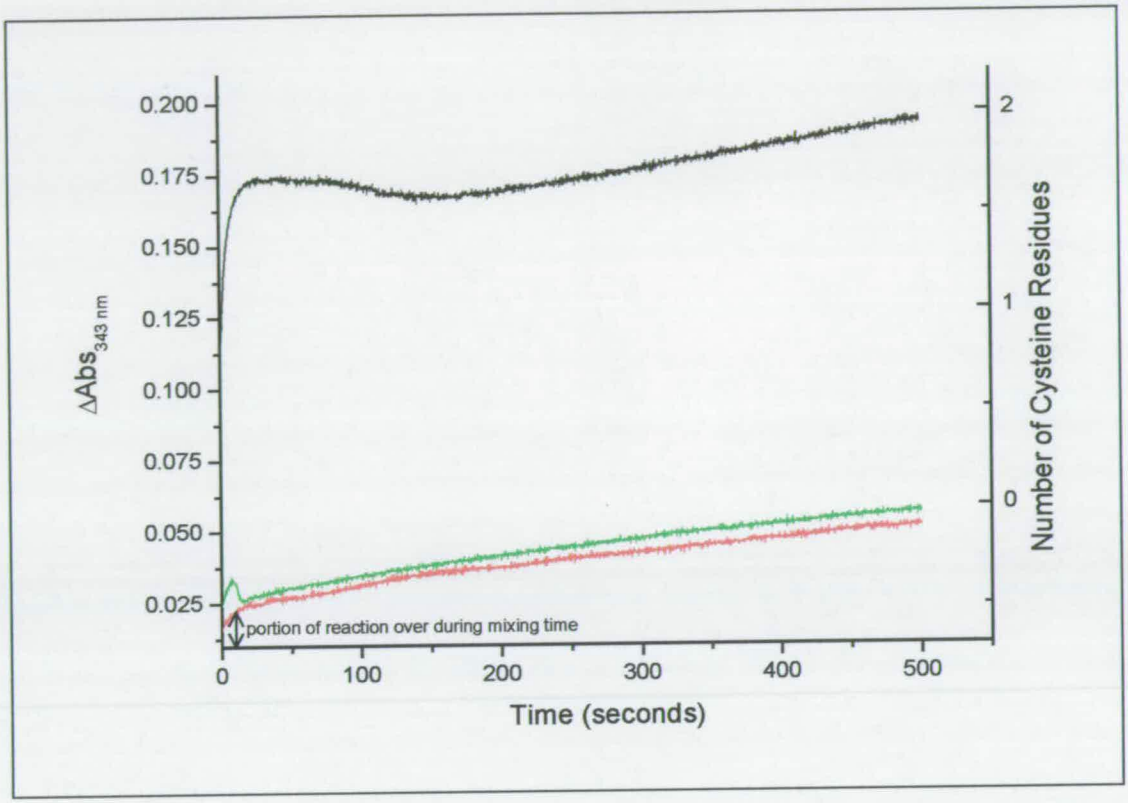

Figure 3.6: *Time-dependant traces of the accumulation of chromophore produced during the Ellman assay analysis of the lower molecular weight aggregate of the N42C:K324C mutant flavocytochrome b_2. Shown are traces for the mutant enzyme with the disulfide bridge intact (green), the disulfide bridge open (black) and re-bridged (after incubation in the aerobic atmosphere)(red). Data recorded at 25 °C, pH 7.0, I = 0.1 M., traces monitored at 343 nm, where $\varepsilon_{343} = 8.08\ mM^{-1}\ cm^{-1}$.*

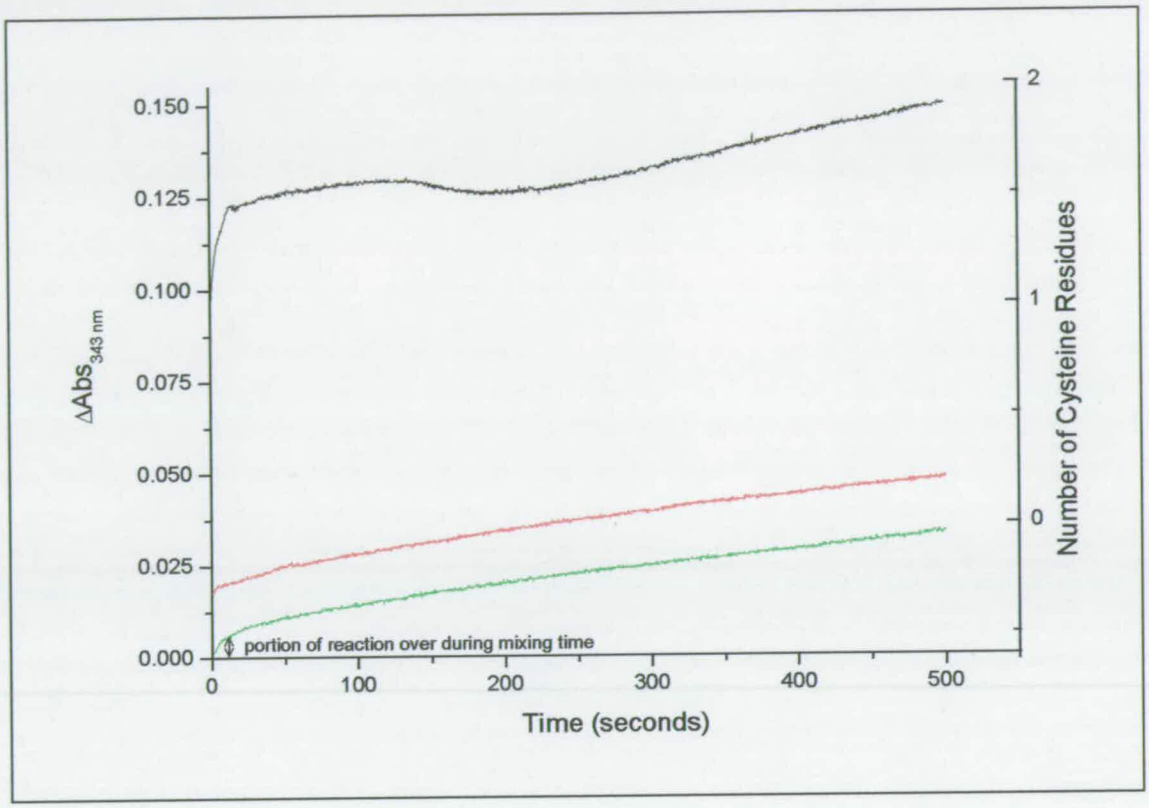

Figure 3.7: *Time-dependant traces of the accumulation of chromophore produced during the Ellman assay analysis of the tetramer of the N42C:K324C mutant flavocytochrome b_2. Shown are traces for the mutant enzyme with the disulfide bridge intact (green), the disulfide bridge open (black) and re-bridged (after incubation in the aerobic atmosphere)(red). Data recorded at 25 °C, pH 7.0, I = 0.1 M., traces monitored at 343 nm, where $\varepsilon_{343} = 8.08\ mM^{-1}\ cm^{-1}$.*

3.2.4 Steady-state and Pre-steady-state Kinetics of the Aggregated and Tetrameric N42C:K324C Mutant Enzyme

It was important to ascertain whether the kinetics of the aggregated and tetrameric forms of the mutant enzyme behaved in a similar fashion.

Steady-state experiments were carried out on the higher molecular weight aggregate, lower molecular weight aggregate and the tetrameric N42C:K324C mutant enzyme with the disulfide bond in both its reduced (open) and oxidised (closed) forms. Both the physiological electron acceptor, cytochrome *c*, and an artificial one-electron acceptor, $[Fe(CN)_6]^{3-}$ were used. A saturating concentration of L-lactate was used in each case to obtain the observed rate constant. It was found that the rate of turnover for each of the higher molecular weight aggregate, the lower molecular weight aggregate and the tetramer in the closed form of the mutant enzyme were similar. On addition of DTT to reduce the disulfide bridge, the increase in the rate of turnover of the enzyme was comparable in each case.

Stopped-flow experiments were also carried out on both the closed and open forms of the higher molecular weight aggregate, the lower molecular weight aggregate and tetrameric enzyme. 10 mM L-lactate was reacted with 15-25 μM enzyme and flavin and b_2-heme reduction was monitored at 438.3 nm, and 557 nm respectively. The difference in the rate constant obtained between the closed and open forms of the mutant enzyme for the higher molecular weight aggregate, the lower molecular weight aggregate and tetrameric enzyme were very similar.

Since each of the separated fractions obtained from the Superdex 200 gel filtration step were found to behave in a kinetically similar manner, they were pooled together to give a sufficient quantity of enzyme that could be further used for kinetic experimentation.

3.2.5 The Crystal Structure of N42C:K324C Flavocytochrome b_2 (with Dr Chris Mowat and Miss Chiara Bruckmann)

It was shown in section 3.2.2 that the N42C:K324C mutant enzyme could exist as three different forms; a tetramer, higher molecular weight aggregate of tetramers, and a lower molecular weight aggregate of tetramers. This would almost certainly be restricting the growth of any crystals. The unhomogeneity of the sample would distort the protein packing away from a uniform lattice and decrease the stability of the complex. Undoubtedly, this would have been the initial, underlying problem with obtaining crystals. Having solved this puzzle, only enzyme in the tetrameric form was taken forward for crystal trials. Crystals were obtained as detailed in section 2.18.

A dataset to 3.0 Å resolution was used to refine the structure of N42C:K324C flavocytochrome b_2 to a final R-factor of 18.03 % (R_{free} = 25.62 %; Table 3.1).

space group	$P\,2_1$
cell dimensions (Å)	a = 64.226, b = 179.895, c = 96.369, β = 90.68 °
resolution (Å)	2.7-3.0
total no. of reflections	160404 (22292)[a]
no. of unique reflections	42925 (6178)[a]
completeness (%)	98.3 (97.5)[a]
$I/[\sigma(I)]$	11.5 (3.0)[a]
R_{merge} (%)[b]	10.2 (35.3)[a]
R_{cryst} (%)[c, d]	18.03
R_{free} (%)[c]	25.62
rmsd from ideal values	
bond lengths (Å)	0.048
bond angles (deg)	4.162
Ramachandran analysis	
most favoured (%)	92.4
additionally allowed (%)	5.3
no. of waters included in refinement	213

Table 3.1: *Data collection and refinement statistics.*

[a]Values in parentheses represent statistics for the highest resolution shell, 3.16 – 3.00 Å. *[b]$R_{merge} = \Sigma_h\Sigma_i|I(h) - I_I(h)|/\Sigma_h\Sigma_i I_I(h)$, where $I_I(h)$ and $I(h)$ are the ith and mean measurement of reflection h, respectively.* *[c]$R_{cryst} = \Sigma_h|F_o - F_c|/\Sigma_h F_o$, where F_o and F_c are the observed and calculated structure factor amplitudes of reflection h, respectively. R_{free} is the test reflection data set, 5 % selected randomly for cross validation during crystallographic refinement.* *[d]Medium NCS restraints were used during refinement, with each subunit (A – D) being defined as a group.*

The final model consists of four protein molecules (subunits A-D) each comprising residues Glu1-Ala511, one b_2-heme and one FMN. The arrangement of the subunits to form the tetrameric enzyme in the asymmetric unit is shown in Figure 3.8. In all subunits there is a region of disordered polypeptide not observed in the density map, spanning residues Thr300 to Gln317, similar to that found in other structures of this

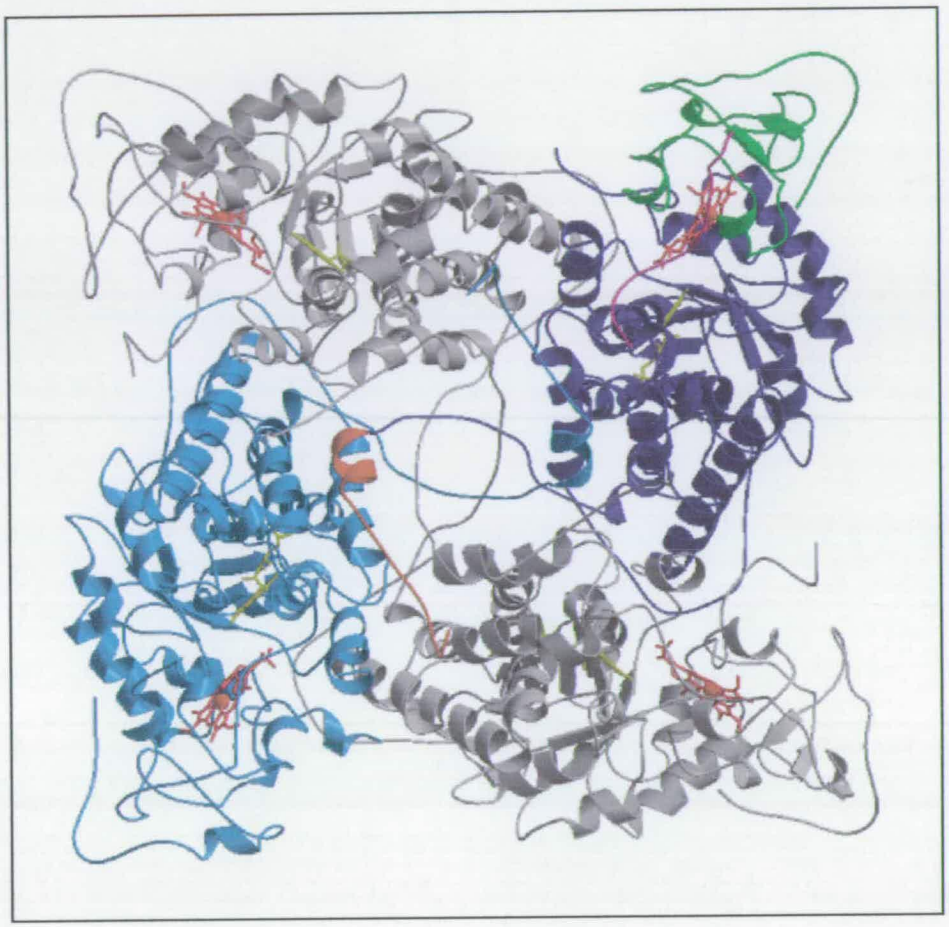

Figure 3.8: *Ribbon diagram showing the structure of N42C:K324C flavocytochrome b_2. Subunit A is shown with the cytochrome domain in green and the flavodehydrogenase domain in purple. Subunit C is shown in blue. In all subunits FMN is yellow and heme is red.*

and similar enzymes (Xia & Mathews, 1990). In addition the model contains 213 water molecules. The presence of the amino-acid substitutions (N42C and K324C) is seen in the electron density map, and this is shown in Figure 3.9. What is also apparent from the electron density is that in each subunit a disulfide bond has been formed between Cys42 and Cys324 (Figure 3.9). The major effect of this inter-

domain disulfide bond formation is the presence of an ordered heme domain in each of the four subunits. There are 9 other structures of holo-flavocytochrome b_2 deposited in the Protein Data Bank, all from crystals which belong to space group $P3_221$ (Xia & Mathews, 1990, Mowat *et al.*, 2000, 2004, Tegoni *et al.*, 1994, 1995, Cunane *et al.*, 2002)). In all cases the model consists of two subunits, at least one of which has a disordered cytochrome domain (as mentioned in the introduction). It is interesting to note that the conditions used to grow crystals of N42C:K324C flavocytochrome b_2 are almost identical to those used to grow crystals of other forms of the protein in the $P3_221$ space group. However, in the case of N42C:K324C flavocytochrome b_2, no crystals in the $P3_221$ space group were obtained. It is therefore presumed that the crystallisation of N42C:K324C flavocytochrome b_2 in the $P2_1$ space group is as a result of the structural changes imposed by the formation of the four disulfide bonds in the tetrameric enzyme. The presence of the disulfide bond has little effect on the overall structure of the protein, with the average rmsd fit for all backbone atoms of each subunit with those of subunit A of the wild-type enzyme structure (PDB ID 1FCB) being 0.95 Å. An overlay of subunit A of the N42C:K324C double mutant enzyme with subunit A of the wild-type enzyme is shown in Figure 3.10.

Figure 3.9 (following page): *(a) Stereoview of the electron density surrounding residues 41-43 and 323-325 of subunit A of N42C:K324C flavocytochrome b_2. The b_2-heme (red) and His66 are also shown. The disulfide bond is clearly visible in the electron density map. The electron density map was calculated using Fourier coefficients $2F_o - F_c$, where F_o and F_c are the observed and calculated structure factors, respectively, the latter based on the final model. The contour level is 1σ, where σ is the rms electron density.*

(b) Stereoview of the same region overlaid with that in subunit A of the wild-type enzyme (green; PDB 1FCB).

(c) Stereoview of subunit A of N42C:K324C flavocytochrome b_2. The position of the disulfide bond is indicated.

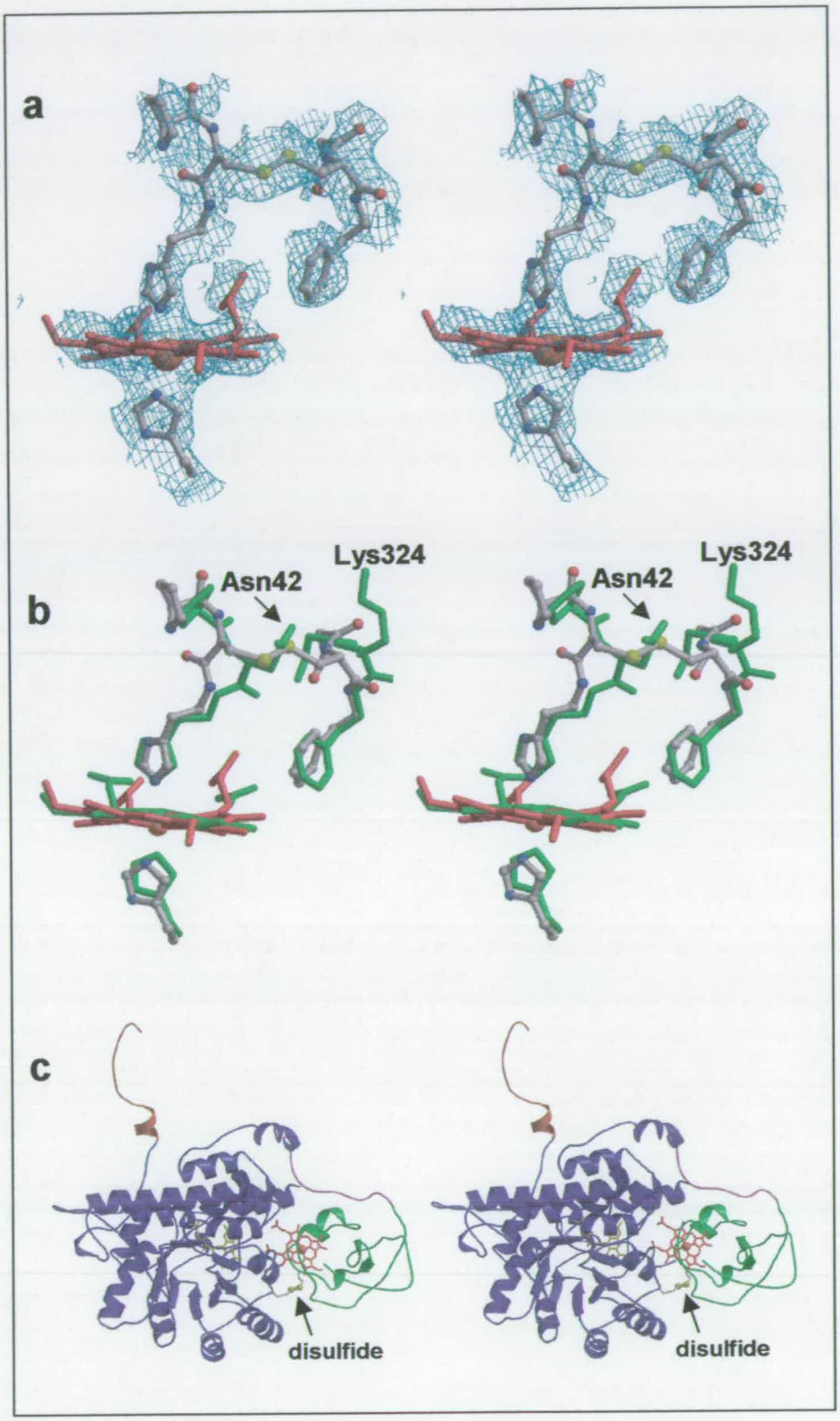
a
b
Asn42
Lys324
Asn42
Lys324
c
disulfide
disulfide

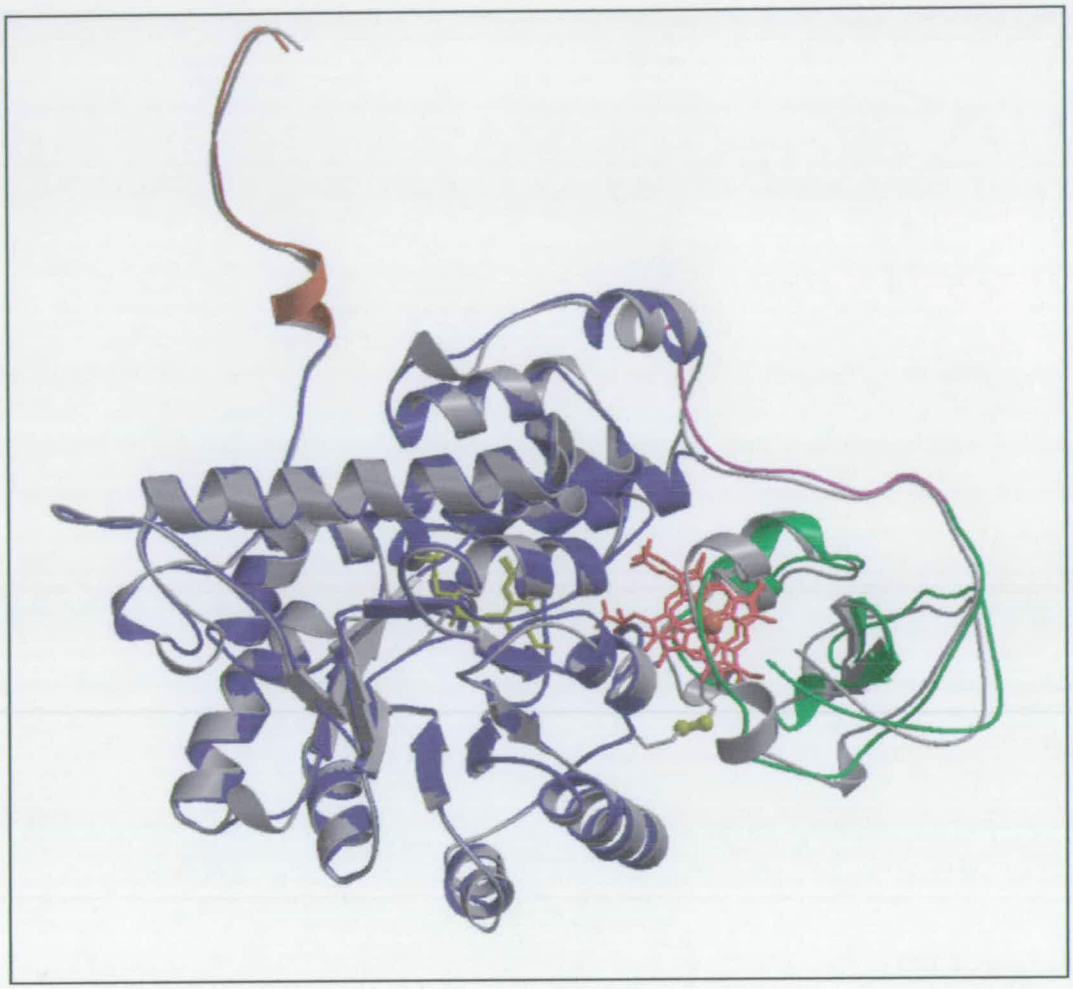

Figure 3.10: *An overlay of subunits A of the N42C:K324C (green and purple) and wild-type (grey) flavocytochromes b_2. It can be seen that there is little change in the position of the cytochrome domain as the result of the substitutions and resultant disulfide bond formation.*

Although the formation of the disulfide bond results in a second point of attachment between the cytochrome and flavodehydrogenase domains of the enzyme, the cytochrome domains remain relatively mobile, with B-factors considerably higher than the average over the whole protein (70-100 $Å^2$ compared to a mean B-value of ~49 $Å^2$ over the whole model). Consequently it is clear that although the formation of a disulfide bond results in the 'fixing' of the cytochrome domain to the flavodehydrogenase domain (leading to its crystallographic ordering), it does not prevent mobility within the domain itself.

The nature of the active site in the structure of the N42C:K324C flavocytochrome b_2 is also of great interest. In the structure of wild-type enzyme, pyruvate is only seen at the active site in subunit B (when the b_2-heme domain is disordered)(Xia & Mathews, 1990). In the case of N42C:K324C flavocytochrome b_2, even though the enzyme is crystallised in the presence of 50 mM pyruvate, none is observed in the structure. This is an interesting observation since it suggests that the 'fixing' of the two domains by the disulfide-bridge is having the effect to prevent access of this molecule to the active site. Figure 3.11 shows an overlay of the active site of subunit A of the double mutant enzyme with (a) subunit A and (b) subunit B of the wild-type enzyme. It can be seen that in the N42C:K324C flavocytochrome b_2 there are water molecules present at the active site. The number of water molecules varies from 1 to 3 between subunits, but for illustrative purposes subunit A has been chosen. In subunit A Wat25 is adjacent to the FMN (3.1 Å from N-5), 3.2 Å from His373 and 3.7 Å from Tyr143. The second water molecule, Wat146, is 3.3 Å from Wat25, and is also hydrogen bonding to one of the heme propionate groups at a distance of 2.7 Å. A third water, Wat194, is 3.1 Å from Wat146. The b_2-heme propionate is found to lie between 2.5 Å and 3.9 Å from Tyr143 (the mean distance over all subunits is 3.2 Å), and around 4.2 Å from where pyruvate would be bound if it was present in the same position as observed in the wild-type enzyme structure.

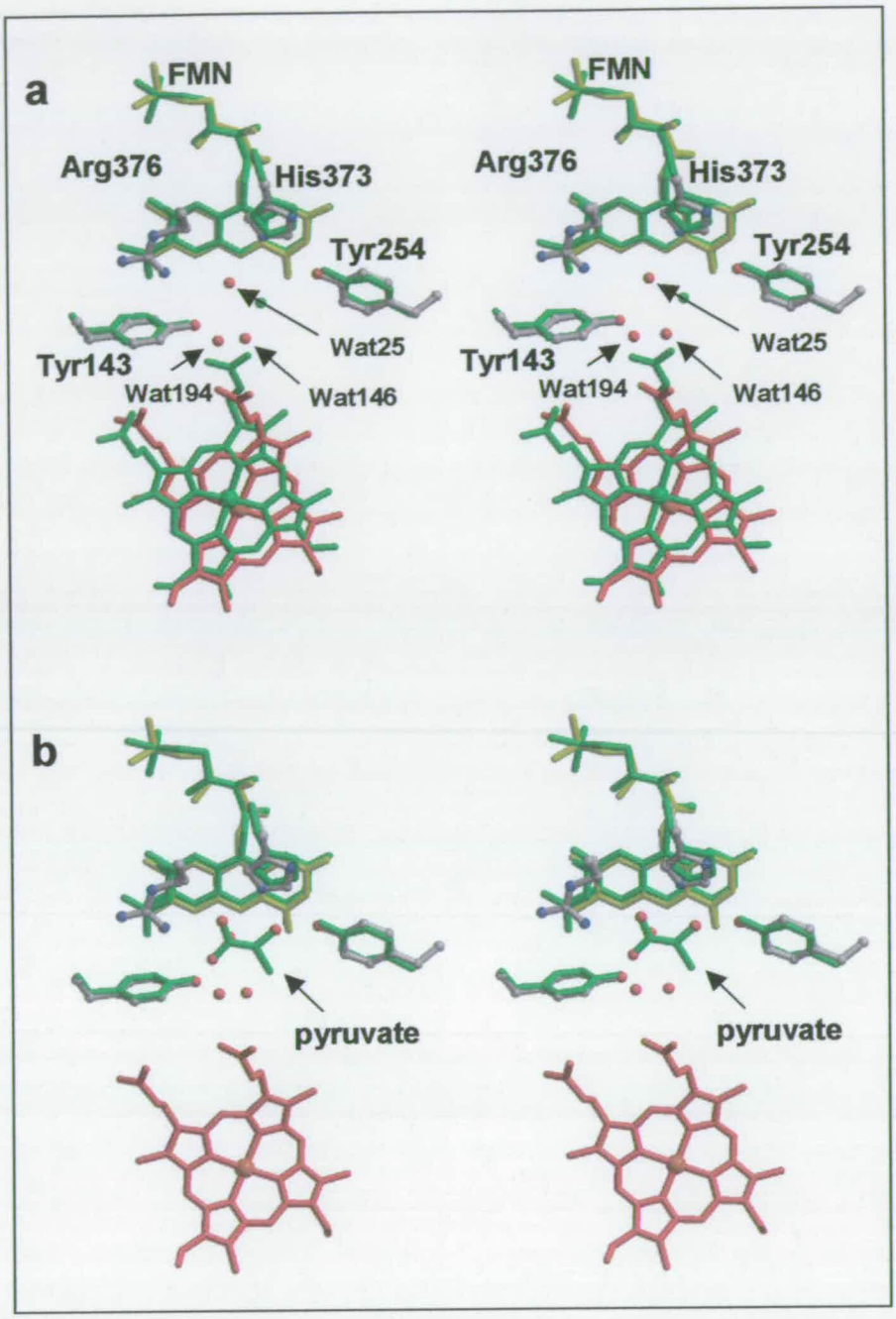

Figure 3.11: *(a) Stereoview of the overlaid active sites of N42C:K324C (subunit A) and wild-type (subunit A, green) flavocytochromes b_2. (b) Stereoview of the same region in the N42C:K324C enzyme overlaid with that in subunit B of the wild-type enzyme (green). The positions of the water molecules in the double mutant enzyme are indicated, as is the pyruvate in subunit B of the wild-type enzyme. Heme groups are also shown, illustrating the proximity of the propionate group to the substrate binding site.*

3.3 Conclusions

In this chapter, the biochemical and structural characterisation of the N42C:K324C mutant flavocytochrome b_2 has been described.. Ellman assays were used to chemically confirm the existence of the imposed disulfide-bridge between residues 42 of the b_2-heme domain and 324 of the flavodehydrogenase domain. Gel filtration experiments show that the engineered cysteine residues could be forming inter-subunit disulfide-bridges, rather than forming the desired bond between the cytochrome and flavin-binding domains. However, steady-state and pre-steady-state kinetic analyses have shown that each of the higher molecular weight aggregate, the lower molecular weight aggregate and tetrameric enzyme behave in a kinetically similar fashion: the difference in rate constant between the closed (disulfide-bridged) and the open (disulfide-bridge cleaved) mutant enzymes is comparable in each case.

The crystal structure of the N42C:K324C mutant flavocytochrome b_2 has been solved to 3.0 Å. Whilst this resolution is limiting and over analysis of the structure should be avoided it is apparent that the structure has confirmed the existence of the disulfide-bridge across the b_2-heme and flavin-binding domains. The major effect of 'fixing' these two domains is the presence of an ordered b_2-heme domain in each of the four subunits of the tetramer. Despite this ordering there is still a certain amount of mobility within the cytochrome domain itself. However, despite the crystallisation conditions containing 50 mM pyruvate, none was observed in the structure of the active site. It is possible that cross-linking the b_2-heme and flavodehydrogenase domains could be restricting access of this molecule to the active site.

Chapter 4

Using Sulfite as an Investigative Tool for Accessibility to the Active Site in N42C:K324C Flavocytochrome b_2

Chapter 4

Using Sulfite as an Investigative Tool for Accessibility to the Active Site in N42C:K324C Flavocytochrome b_2

4.1 Introduction

4.1.1 Aim of this Chapter

It was proven in Chapter 3 that a disulfide bridge exists between the introduced cysteine residues at position 42 of the b_2-heme domain and position 324 of the FMN-binding domain of flavocytochrome b_2. The major effect of this disulfide bridge has been to restrict the movement of the cytochrome domain with respect to the FMN-binding domain by 'fixing' these two domains together. Despite this, mobility within the cytochrome domain itself still remains as judged by relatively high B-factors. It is interesting that pyruvate is not found to be bound at the active site of either subunit in the N42C:K324C mutant flavocytochrome b_2, despite this molecule being present in the precipitation buffer. Pyruvate is observed at the active site of the wild-type structure (Xia & Mathews, 1990) and the Y143F mutant flavocytochrome b_2 (Tegoni *et al.*, 1995). This raises a fundamental question – does cross-linking these two domains at their interface restrict the access of substrate to the active site?

A detailed study of the literature has shown (as discussed below) that sulfite forms a reversible, covalent adduct at the N-5 position of the FMN. As such, this small molecule seemed an ideal tool to investigate the accessibility of the active site within the disulfide-bridged form of the enzyme. This chapter reports the second-order rate constant (k_{on}) for the binding of sulfite to the FMN for each of the closed (disulfide oxidised), open (disulfide reduced on addition of DTT) and wild-type enzymes. Also reported are the dissociation constants for sulfite with each of the closed, open and wild-type enzymes through use of difference spectroscopy.

4.1.2 A Historic Background to Sulfite Reactivity in Flavoproteins

Sulfite ions possess the ability to form an adduct with the flavin prosthetic group of a large number of flavoproteins. These include glucose oxidase (Sworoda & Massey, 1966), D- and L-amino acid oxidases, oxynitrilase, lactate oxidase, and glycolate oxidase (Massey *et al.*, 1969). It has been shown that the reaction of glucose oxidase from *Aspergillus niger* with sulfite is independent of the presence of O_2 as well as other electron acceptors such as ferricyanide or sulfate. The reaction was characterised by a bleaching of the visible absorption spectrum of the enzyme, and resulted in the production of a new absorption band in the region of 330 nm. This visible absorption spectrum was similar to, but not identical to that of the fully reduced flavoprotein ($FADH_2$). The proportion of combined to uncombined enzyme being found to be dependent on the absolute concentration of the reactants, the temperature and the pH. Stopped-flow studies have shown the complex to be enzymatically inactive. It seemed likely that in light of the spectroscopic shift on reaction with sulfite that a weak covalent interaction was occurring at the N-5 position of the isoalloxazine ring of the FAD. Indeed, experiments carried out with model flavins (Müller & Massey, 1969) presented evidence to this effect. Flavin in the oxidised state is electron deficient while sulfite is a powerful nucleophile. As such, only when flavin is oxidised can it interact with SO_3^{2-} or HSO_3^-. Müller & Massey showed that the interaction of free flavin as well as protein-bound flavin with sulfite led to a new compound which had a visible absorption spectrum similar to, but not identical with, that of the fully reduced (1,5-dihydro-) flavin. Elemental analysis and the hydrolysis of the crystalline flavin-sulfite complex show that one SO_3^{2-} is bound per flavin. The proposed structure is shown in Figure 4.1.

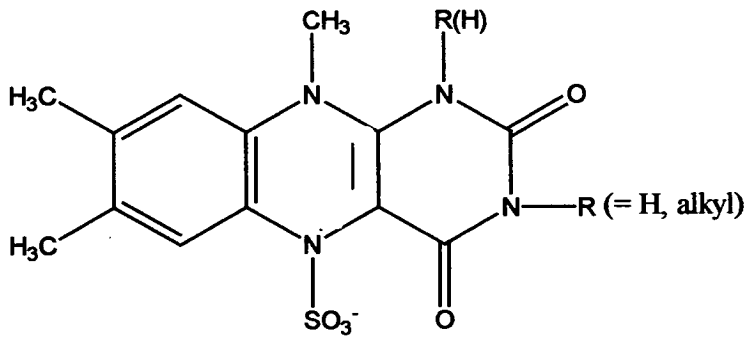

Figure 4.1: *The proposed flavin-sulfite complex*

As a result of the work carried out by Massey *et al.*, on D- and L-amino acid oxidases, oxynitrilase, lactate oxidase, and glycollate oxidase, a correlation was made between sulfite reactivity and oxygen reactivity of flavoproteins, where only flavoprotein oxidases formed addition complexes with sulfite. While free reduced coenzyme is rapidly reoxidised by molecular O_2, this property is retained only by the aforementioned flavoproteins, the flavoprotein oxidases. No explanation had ever been offered for this phenomenon until this point. It appeared the correlation was absolute with the exception of oxynitrilase and old yellow enzyme isolated from bakers yeast (Matthews & Massey, 1969). Oxynitrilase catalyses the condensation of cyanide and aldehydes (Becker and Pfeil, 1966). It does react with sulfite suggesting it may have some other function involving reaction with O_2 and it reacts readily with O_2 after reduction with dithionite. Old yellow enzyme does not react with sulfite but does react with oxygen.

In addition to this, a further correlation was postulated between oxygen reactivity of flavoproteins and the semiquinoid form of the enzyme. With only few exceptions, the semiquinoid form of the enzyme was found to be the red, anionic form in the oxidases. The dehydrogenases formed the blue, neutral semiquinone. The tautomeric forms of the neutral and anion radicals are shown in Figure 4.2.

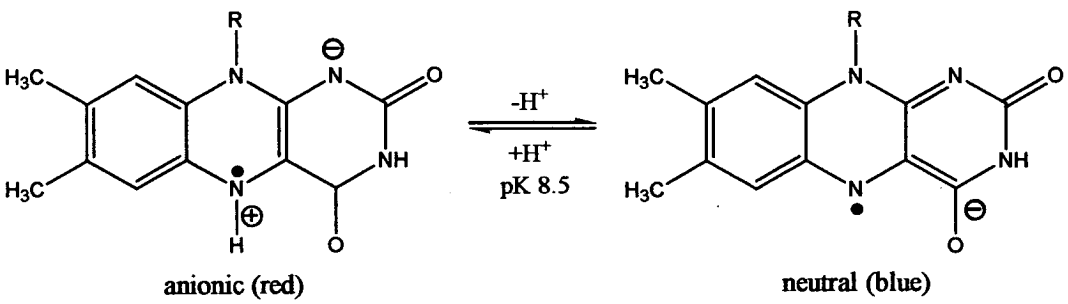

Figure 4.2: *The preferred tautomeric forms of the neutral and anion radicals.*

Glucose oxidase has an ionisation such as that shown in Figure 4.2 with a pK ~7.5. The other known flavoproteins do not show any ionisation. Instead they exhibit either a stabilised blue or red radical form (Massey & Palmer, 1966). A tentative explanation to this behaviour was presented: a positive charge at the active site of oxidases would allow sulfite binding and stabilise the anionic semiquinone while the

presence of a negative charge in the dehydrogenases would explain the lack of sulfite reactivity and the preferred formation of the neutral semiquinone. An example of this was presented in the case of D-amino acid oxidase. In addition to giving the red radical form, there is evidence to support a positively charged amino acid residue close to the isoalloxazine ring system of the flavin which is responsible for its strong binding of benzoate (a competitive inhibitor) and other carboxylic acids (Yagi & Ozawa, 1962; Massey & Ganther, 1965). The positive charge would stabilise the anionic semiquinone and may also be responsible for the binding of sulfite to the enzyme and facilitating its attack on the N-5 position of the oxidised flavin. Conversely, if a negatively charged amino acid residue was in the vicinity of the flavin, this would (*a*) stabilise the blue semiqunone, (*b*) repel sulfite and hinder its addition to N-5, (*c*) hinder the reaction of oxygen with reduced flavin. Of course, the presence of a positively or negatively charged group near the flavin should not really have any influence over the reactivity of its reduced form with molecular oxygen. Here it was postulated that reduced flavin may interact with O_2 at carbon atoms 1a or 4a, previously implicated by Mager & Berends, 1966 and Hemmerich *et al.*, 1967. These oxygen adducts could then break down in several possible ways, for example, yielding oxidised flavin with the elimination of H_2O_2.

4.1.3 Sulfite Binding to a Flavodehydrogenase

Baker's yeast L-lactate dehydrogenase (flavocytochrome b_2) is a typical flavodehydrogenase that accepts two electrons from its substrate but has a monoelectronic acceptor (as discussed previously in section 1.5.1). The flavin forms a red semiquinone (Capeillère Blandin *et al.*, 1975) and a reversible covalent complex with sulfite (Lederer, 1978). This sulfite-complex was observed by Lederer (1978) through the use of difference spectroscopy, a convenient tool for looking at the flavin since it is usually hidden under the intense heme absorbance. The technique of difference spectroscopy utilises a dual-beam spectrometer with a reference cell and a sample cell. Equal volumes of enzyme are added to each cell. Upon addition of progressive aliquots of sulfite solution to the sample cell whilst adding equal volumes of buffer to the reference cell, Lederer acquired a typical difference spectrum of oxidised flavin with two maxima at 454 and 377 nm. Differential titrations yielded a $K_d = 1.5 \pm 0.4$ μM and $\Delta\varepsilon_{454} = 10\,500 \pm 500$ $M^{-1}cm^{-1}$. Steady-state studies carried out

on the enzymatic activity in the presence of sulfite showed it behaved as a kinetic inhibitor of lactate, with a K_i of 1.4 ± 0.5 μM.

Since flavocytochrome b_2 forms a red semiquinone and reacts with sulfite it does not fit in with the classification proposed by Massey *et al*, 1969. Its reactivity with oxygen is low and in fact the rate of autoxidation has been estimated to represent between just 0.7% and 2% the rate of reoxidation by ferricyanide (Boeri & Rippa, 1961).

4.1.4 The Crystallographic Structure of the Flavocytochrome b_2-Sulfite Complex

The structure of Flavocytochrome b_2 from *Saccharomyces cerevisiae* was obtained to 2.4 Å (Xia & Mathews, 1990) and is a homotetramer with a molecular weight of 4 x 57.5 kDa. Each monomer consists of two distinct domains, one which carries an FMN and the other, the b_2-heme. For a fuller description of this structure see section 1.5.1. More recently, the *Escherichia coli* recombinant flavocytochrome b_2 with bound sulfite has been solved (Tegoni & Cambillau, 1994). The crystals were obtained under different conditions to the native enzyme but were found to be isostructural. The X-ray structure was solved to 2.6 Å where it was found that few differences existed between the native and recombinant structures. The main features of the heme and FMN domain architecture were identical: subunit 1 contains the heme domain (resides 6-99), the interdomain hinge region (residues 100-190), the β-barrel (residues 191-465), and an extended C-terminal segment forming the tail (466-511). In addition to this the heme domain is disordered in subunit 2. This further confirms the intrinsic mobility of the heme domain which is observed in the native enzyme (Labeyrie *et al.*, 1988).

At the active site, one molecule of sulfite was visible in both subunits. In subunit 1 the sulfite molecule replaces a water molecule while in subunit 2 it replaces the pyruvate. The sulfur is covalently bound to the N-5 of the FMN with a distance of 1.8 Å. The structures of the FMN molecules in both subunits are similar although they did deviate slightly in planarity in comparison to the native protein. The high affinity of sulfite and the strong inhibition it exerts on the catalytic activity of flavocytochrome b_2 (Lederer, 1978) appeared to be in good agreement with the interactions occurring at the active site in the crystal structure. The oxygen atoms of the SO_3^{2-} are all hydrogen-bonded to the amino acid residues involved in catalysis.

These are Tyr143, Tyr254, His373 and Arg376. This leads to a highly structured active site.

4.2 Results

4.2.1 Pre-Steady-State Kinetics

Stopped-flow kinetics were carried out on the wild-type, open and closed enzymes to measure their reaction rates with sulfite. Reduction of the flavin by an excess of sulfite (0.1-10 mM after mixing) was monitored at 450 nm, which allows direct observation of the flavin chromophore. An example of the stopped-flow flavin reduction trace fitted to a double exponential function is shown in Figure 4.3. Resulting values of k_{obs} showed a linear dependence on the concentration of sulfite, as shown in Figures 4.4 and 4.5 for the open/closed and wild-type enzymes respectively. Since the reaction is second-order it is clear that sulfite binding at the active site is slower than electron transfer to the FMN and therefore k_2 is a reflection of the "on-rate" for sulfite binding. Table 4.1 lists the second-order rate constant, k_{on}, for sulfite binding.

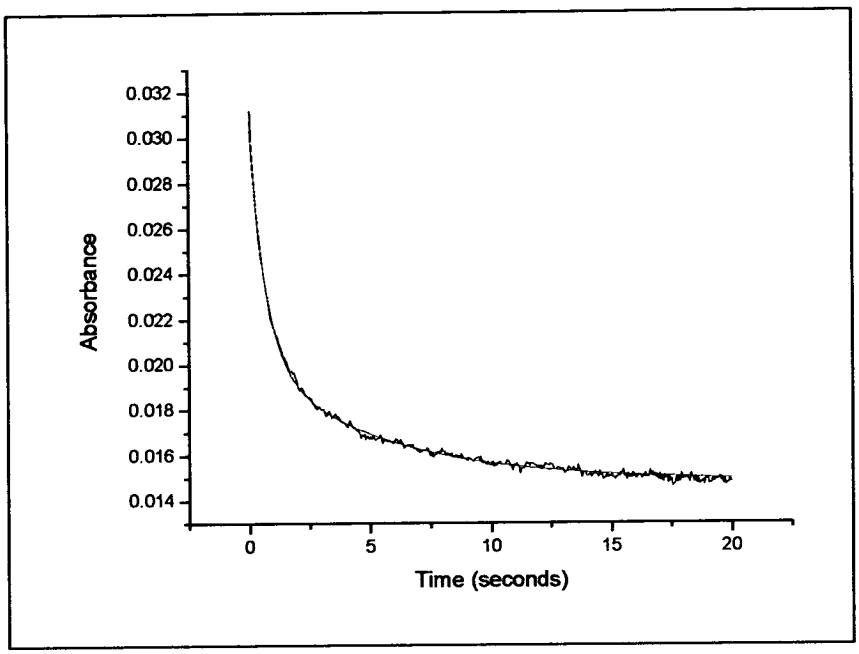

Figure 4.3: *Example trace of the flavin reduction observed in the closed enzyme: generated by mixing 10 mM sulfite with 8.4 μM enzyme in 10 mM Tris/HCl buffer, pH 7.5, I 0.10. The trace is fitted to a double exponential function (red line). The more significant fast phase gives an observed rate constant of 1.7 ± 0.2 s^{-1}.*

Enzyme	k_{on} ($mM^{-1}s^{-1}$)
Wild Type	24.6 ± 6.3 $mM^{-1}s^{-1}$
Open	10.5 ± 2.0 $mM^{-1}s^{-1}$
Closed	0.17 ± 0.02 $mM^{-1}s^{-1}$

Table 4.1: *k_{on} for sulfite binding to the various enzyme forms.*

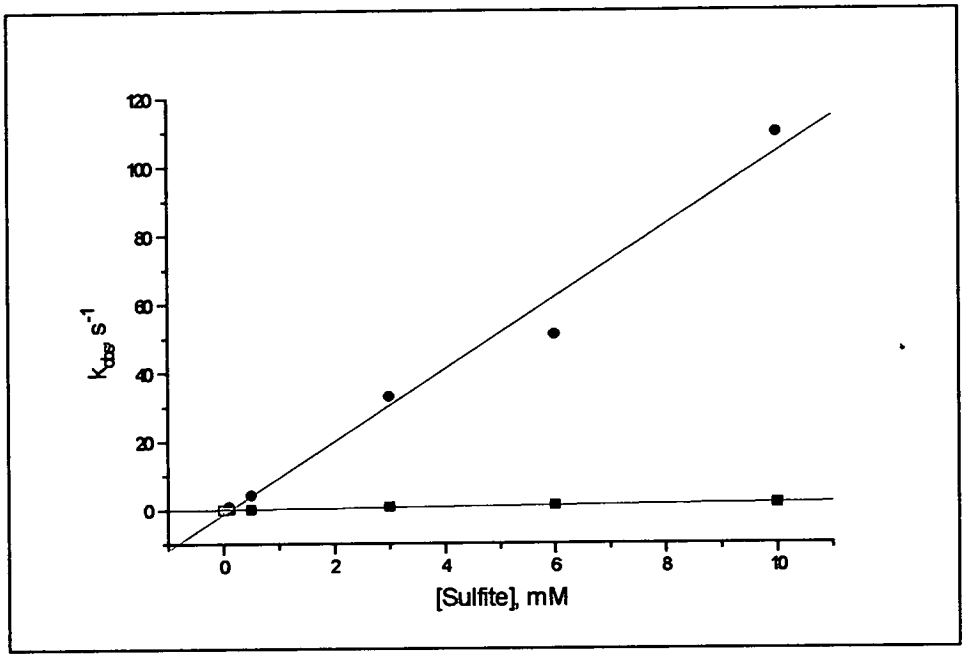

Figure 4.4: *Plot of the observed rate constants against sulfite concentration. The second-order rate constant for sulfite binding to the closed (black line) and open (red line) forms of N42C:K324C flavocytochrome b_2 is derived from fitting the data points to a straight line equation. The gradients give a k_{on} of 0.17 ± 0.02 $mM^{-1}s^{-1}$ and 10.50 ± 1.98 $mM^{-1}s^{-1}$ for the closed and open enzymes respectively.*

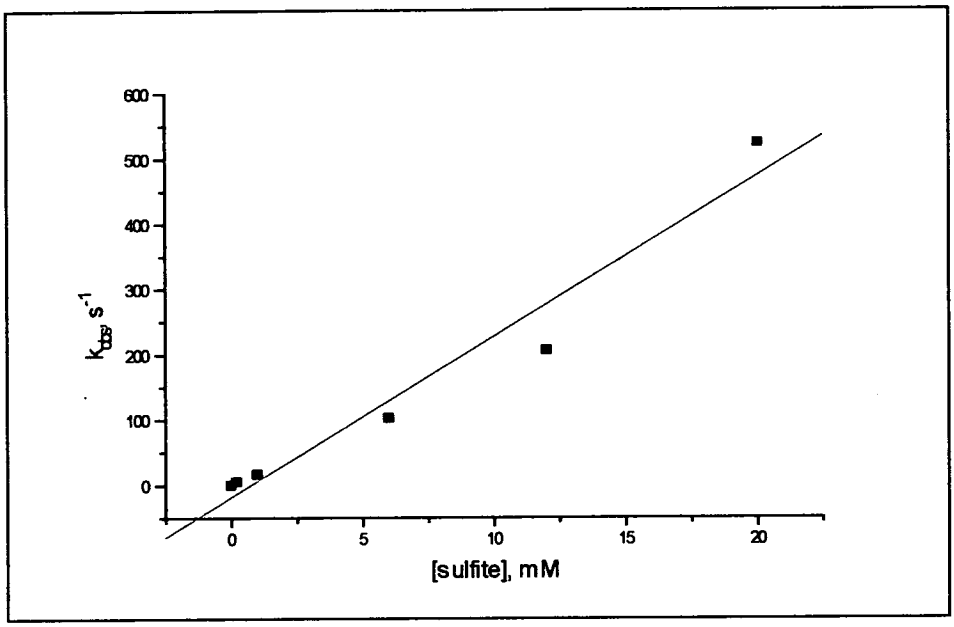

Figure 4.5: *Plot of the observed rate constants against sulfite concentration. The second-order rate constant for sulfite binding to wild-type flavocytochrome b_2 is derived from fitting the data points to a straight line equation. The gradient gives a k_{on} of 24.6 ± 6.3 $mM^{-1}s^{-1}$.*

4.2.2 Determination of the Dissociation Constant (K_d) for Sulfite

Direct observation of the flavin is difficult since it tends to be obscured under the intense heme chromophore (the Soret band has ε_{ox} = 129.5 $mM^{-1}cm^{-1}$ at 413 nm). Figure 4.6 shows the effect of adding a few grains of solid sodium sulfite to a solution of the closed enzyme. This did not appear to affect the heme chromophore. As such, difference spectroscopy was used which involved the progressive addition of a sulfite solution to the reference cell. These titrations yielded difference spectra as shown in Figure 4.7, with maxima occurring at approximately 460 nm and 370 nm. Due to baseline drift, and to avoid any impact of the heme absorbance, the change in absorbance due to the flavin was taken as the mean of the difference between absorbances at 520 nm and 470 nm. These were ideal absorbances to choose since they are right on the edge of the flavin peak.

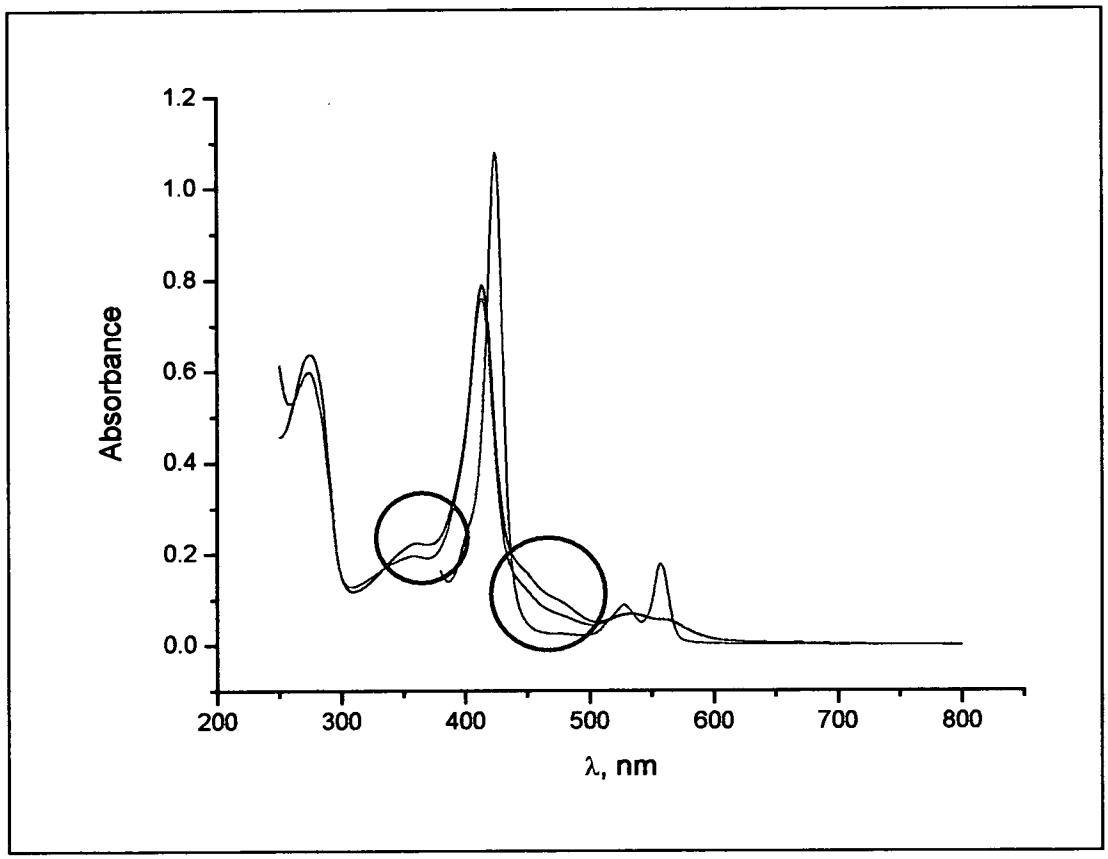

Figure 4.6: *Effect of sulfite binding on the spectrum of the closed form of the N42C:K324C mutant enzyme. The black line represents 5.1 μM oxidised enzyme; the red line is after the addition of a few grains of solid sodium sulfite; the green line is after the addition of solid sodium dithionite. The purple circles highlight the regions where the largest spectral alterations are observed on addition of sodium sulfite.*

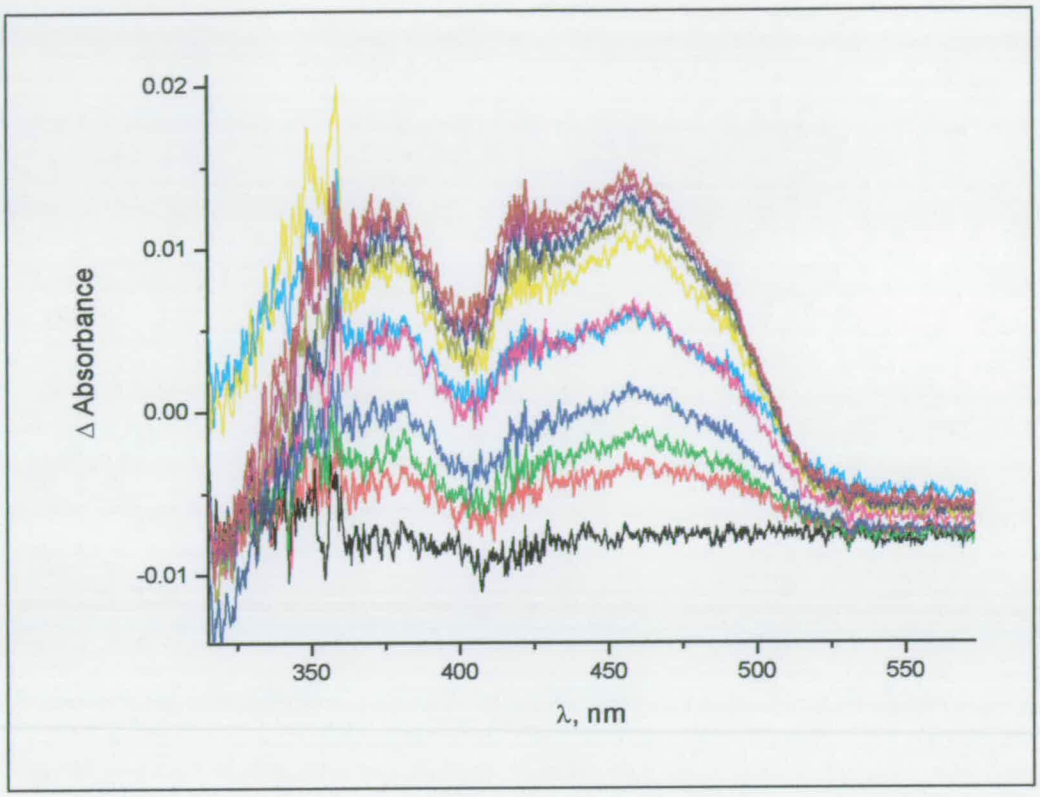

Figure 4.7: *Difference spectrum of wild type enzyme (4.97 μM) vs wild type enzyme (4.97 μM) with sulfite. Small aliquots of a 1mM sulfite stock solution were added to the sample cell (up to a total of 20 μM) whilst equal volumes of buffer were added to the reference cell. Minima are observed at approximately 460 nm and 370 nm.*

K_d values were found to be 0.8 ± 0.2 μM, 4.3 ± 0.9 μM, and 25.9 ± 3.6 μM for wild type enzyme, open enzyme and closed enzyme respectively (see Figures 4.8, 4.9 and 4.10).

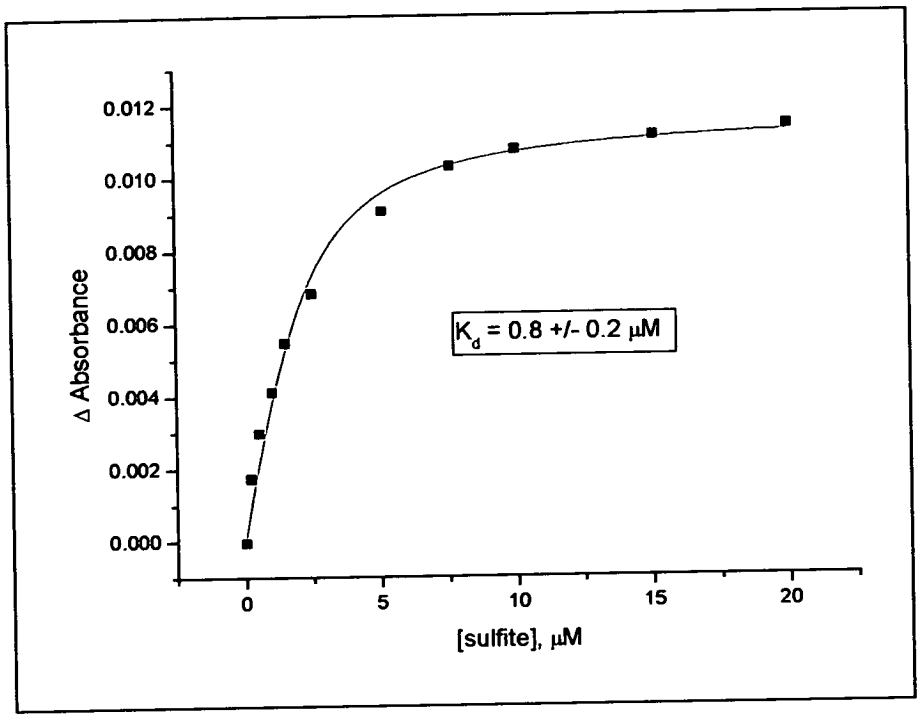

Figure 4.8: *Plot of the change in absorbance between 520 and 470 nm vs. sulfite concentration (μM). From this plot, the K_d for wild-type enzyme is obtained.*

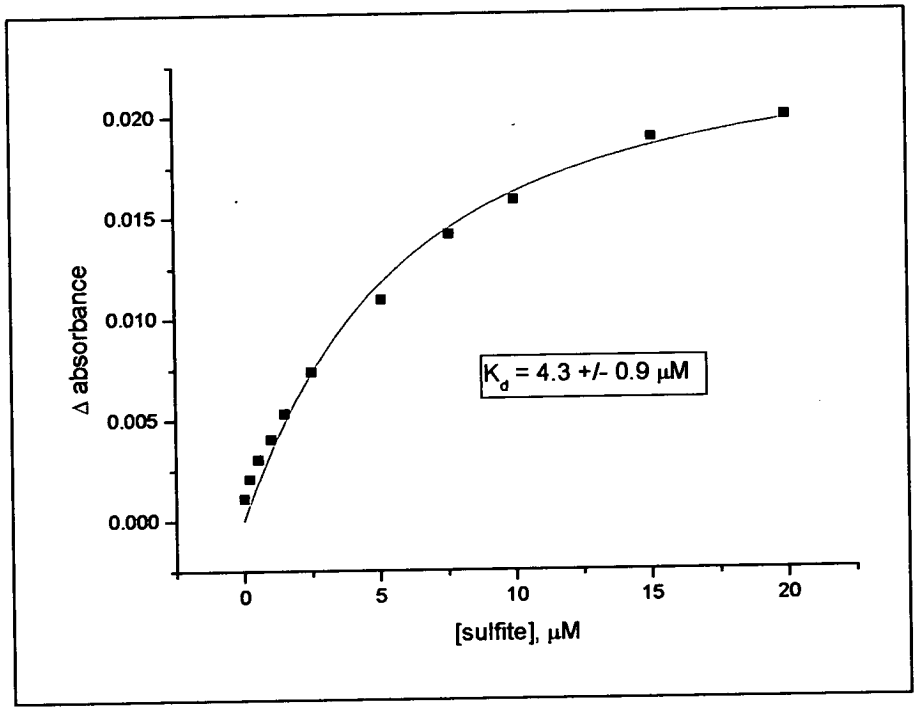

Figure 4.9: *Plot of the change in absorbance between 520 and 470 nm vs. sulfite concentration (μM). From this plot, the K_d for the open form of the N42C:K324C mutant enzyme is obtained.*

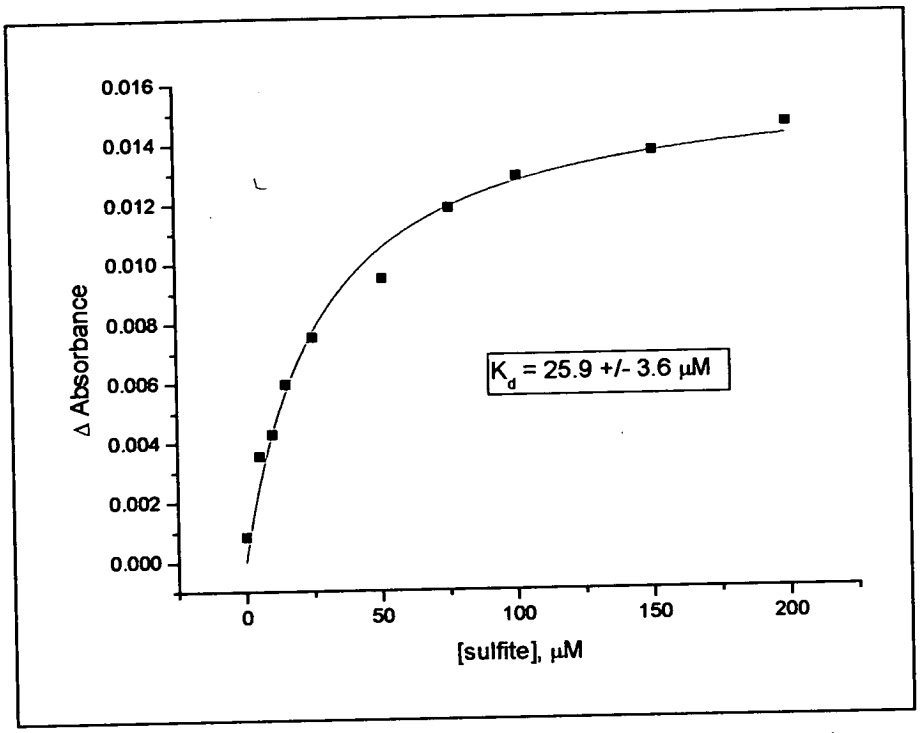

Figure 4.10: *Plot of the change in absorbance between 520 and 470 nm vs. sulfite concentration (μM). From this plot, the K_d for the closed form of the N42C:K324C mutant enzyme is obtained.*

Having experimentally obtained k_{on} and K_d for the open and closed forms of the mutant enzyme as well as for wild-type enzyme, the k_{off} value (the rate constant for the sulfite dissociating from the flavin) can be obtained simply from the reaction given in Figure 4.11 and Equation 4.1;

$$\text{FMN---N-5} + SO_3^{2-} \underset{k_{off}}{\overset{k_{on}}{\rightleftharpoons}} \text{FMN---N-5---}SO_3^{2-}$$

Figure 4.11: *Equation representing the binding of SO_3^{2-} to the N-5 position of the flavin.*

$$K_d = \frac{k_{off}}{k_{on}} \qquad \textbf{Equation 4.1}$$

Table 4.2 lists these values:

	K_d (μM)	k_{on} ($mM^{-1}s^{-1}$)	k_{off} (s^{-1})
Wild-type	0.8	24.6	0.020
Open	4.3	10.5	0.045
Closed	25.9	0.17	0.004

Table 4.2: *K_d, k_{on} and k_{off} for sulfite binding to the closed and open mutant enzyme as well as wild-type enzyme.*

4.3 Discussion and Conclusions

The k_{on} for sulfite binding to flavin in the wild-type enzyme and the open form of the mutant enzyme has been experimentally determined to be 24.6 ± 6.3 $mM^{-1}s^{-1}$ and 10.50 ± 1.98 $mM^{-1}s^{-1}$ respectively. In stark contrast, the closed, disulfide-bridged enzyme has a k_{on} of 0.17 ± 0.02 $mM^{-1}s^{-1}$, an order of magnitude smaller. This is a very clear indication that the rate of sulfite entry to the active site is dramatically slowed by formation of the disulfide bridge. Consider now the k_{off} values obtained for wild-type enzyme and the open form of the mutant enzyme. These are 0.020 s^{-1} and 0.045 s^{-1} respectively. Strikingly, the k_{off} value obtained for the closed form of the mutant enzyme is 0.004 s^{-1}, some 11-fold lower as compared to the open form of the mutant enzyme. This suggests that once sulfite has complexed with the flavin N-5, it is much more difficult for it to dissociate in the disulfide-bridged form of the enzyme.

As illustrated in Equation 4.1, the dissociation constant can be regarded as an equilibrium constant. In this case, it gives an indication of the equilibrium that exists between sulfite binding to and dissociating from the N-5 position of the flavin. The K_d values obtained for the wild-type enzyme and open form of the mutant enzyme are an order of magnitude smaller than that of the closed form of the mutant enzyme. This signifies that the equilibrium for the wild-type and open form of the mutant enzyme lies to the right hand side of the reaction shown in Figure 4.11, i.e. they favour the binding of sulfite to the N-5 of the flavin. The equilibrium for the closed

form of the mutant enzyme lies to the left hand side of this reaction because it cannot bind so readily to the N-5 of the flavin.

The crystal structure of the N42C:K324C mutant enzyme can shed some light on this situation. Figure 4.12 illustrates the active site of the mutant enzyme in the disulfide-bridged form. It can be seen that the propionate of ring A on the b_2-heme protudes into this space liberating a significant amount of negative charge over this area. It is reasonable to assume that the negative charge from the oxygen atoms of the b_2-heme propionate will repel the negatively charged oxygen atoms of a sulfite molecule as well as the carboxylate group of L-lactate. Hence, binding, and indeed subsequent dissociation of SO_3^{2-} with the flavin N-5 may prove more difficult. In addition, it is known that in subunit 1 of the wild-type crystal structure, where the cytochrome domain is ordered, the b_2-heme propionate (from ring A) interacts with two water molecules and Tyr143 (Xia and Mathews, 1990). In the case of the N42C:K324C mutant crystal structure, this is not found to be the case. Here, the propionate only hydrogen bonds to one active site water molecule, Wat146. Since Tyr143 is not stabilising the negative charge over the heme propionate, this could also be a contributing factor towards the difficulty of sulfite and to access the flavin active site.

Sulfite obviously does access the active site in the disulfide-bridged form of the mutant enzyme, albeit rather slowly. Thus, an investigation of the active site of the crystal structure of the N42C:K324C mutant enzyme has provided a significant amount of insight towards the accessibility problem on a molecular level. However, it does not provide a huge amount of information regarding the protein dynamics, or how the restricted mobility about the cytochrome domain could be hindering access of sulfite to the active site. Various studies have been carried out to determine the importance of the inter-domain hinge for electron transfer through flavocytochrome b_2 (White *et al.*, 1993, Sharp *et al*, 1994, 1996a, 1996b). An interspecies hybrid enzyme was constructed whereby the hinge region from the *S. cerevisiae* enzyme had been replaced with that from the *H. anomola* flavocytochrome b_2 (White *et al.*, 1993). The hinge region from *H. anomola* is six residues shorter and considerably more acidic than that from the *S. cerevisiae* enzyme. This hinge-swap enzyme remained a good L-lactate dehydrogenase, however, the major effect of the hinge-swap mutation was to dramatically lower the enzymes effectiveness as a cytochrome *c* reductase. Since the

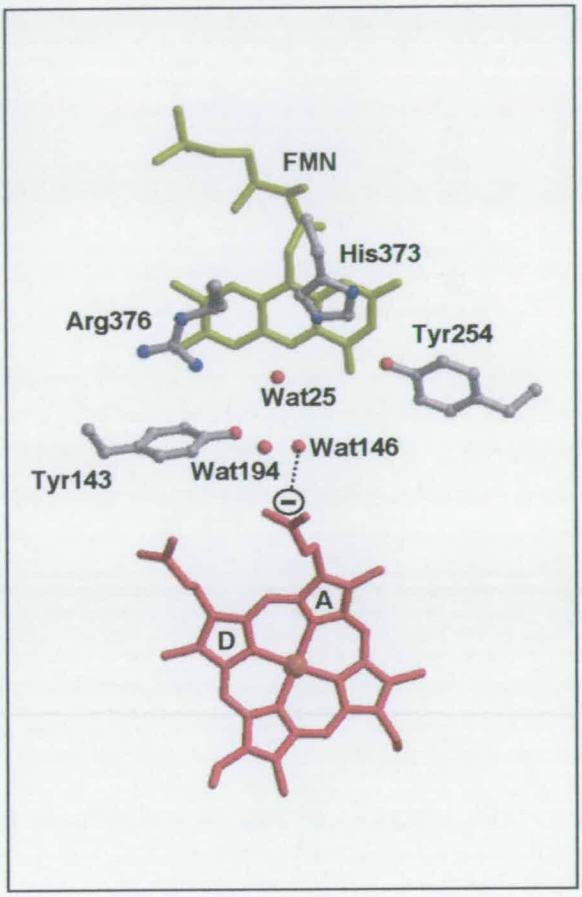

Figure 4.12: *The active site of the N42C:K324C flavocytochrome b_2 (subunit A), illustrating the negative charge protruding from the b_2-heme propionate on ring A. The propionate only makes contact with Wat146 which lies at a distance of 2.7 Å.*

hinge region was six residues shorter than in the wild-type enzyme, this would restrict hinge bending and thus prevent efficient recognition between the flavin and cytochrome domains. It would not, however, restrict access of substrate to the active site. Furthermore, subtle mutations to the hinge region were carried out by Sharp *et al.* (1994, 1996a, 1996b), whereby deletions and insertions of residues were made to the hinge. Three-, six- and nine- amino acid deletions were made to the hinge region which had no effect upon its net charge. Again, the mutant enzymes remained good L-lactate dehydrogenases while the global effect of these deletions was to reduce the enzymes effectiveness as a cytochrome *c* reductase. An interesting observation regarding the kinetic behaviour of the enzymes with six and nine amino acids deleted

was the marked substrate inhibition exhibited by these enzymes in contrast to the wild-type and 3-amino acid deletion mutant enzyme. It is likely that a shorter hinge region will have the effect to restrict the arch of the hinge thus by directing the cytochrome domain away from the flavin-binding domain and allowing a greater accessibility of L-lactate to the active site. Insertions of three- and six- amino acids were also made to the hinge to elongate this region. Once again, the mutant enzymes remained good L-lactate dehydrogenases while lowering the effectiveness of the enzyme as a cytochrome *c* reductase. The hinge insertion enzymes also exhibit severe substrate inhibition at relatively low L-lactate concentrations. This inhibition was the strongest observed for all the hinge-modified enzymes and again reflected the greater accessibility of the substrate to the active site, presumably in this case, by allowing the cytochrome domain to 'swing' further from the flavodehydrogenase domain.

It is thus apparent that in the case of the N42C:K324C mutant flavocytochrome b_2, there are two main reasons as to why accessibility of the active site is restricted. Firstly, cross-linking the cytochrome and flavin-binding domains prevents mobility about the cytochrome domain, essentially 'cordoning off' the usual pathway taken by the substrate to the active site. Secondly, the active site itself provides a somewhat inhospitable environment for the binding of sulfite and substrate since the free b_2-heme propionate will repel the entry of these negatively charged molecules to the active site. On cleavage of the disulfide bond by DTT, the enzyme is once again able to behave in its native manner, indicating its requirement for dynamic flexibility about the hinge region.

Chapter 5

Kinetic Characterisation of the N42C:K324C Mutant Flavocytochrome b_2

Chapter 5

Kinetic Characterisation of the N42C:K324C Mutant Flavocytochrome b_2

5.1 Introduction

This chapter reports the kinetic behaviour of the N42C:K324C mutant enzyme when L-lactate and S-2-hydroxybutyrate are used as substrates and with ferricyanide, ($[Fe(CN)_6]^{3-}$), and cytochrome *c* as electron acceptors. As mentioned in section 1.5.2.1, flavocytochrome b_2 acts physiologically as a L-lactate dehydrogenase but can utilise several other 2-hydroxy-acids as substrates, including S-2-hydroxybutyrate (Daff *et al*, 1994). S-2-hydroxybutyrate is used to further probe the accessibility of the active site since it possesses slightly more steric bulk than L-lactate in that an ethyl group replaces the methyl group.

5.2 Results

5.2.1 Steady-State Kinetics

Steady-state experiments with the N42C:K324C mutant enzyme were carried out using both the physiological electron acceptor, cytochrome *c*, and an artificial one-electron acceptor, $[Fe(CN)_6]^{3-}$. Data were obtained as described in section 2.16 and the resulting k_{cat} and K_m values are compared with those for the wild-type enzyme in Table 5.1. Experiments carried out in the presence of DTT have been corrected for any background activity. Michaelis-Menten plots obtained for both the open and closed forms of the mutant enzyme, with both electron acceptors are illustrated in Figure 5.1.

	Electron Acceptor: $[Fe(CN)_6]^{3-}$		
Enzyme	**k_{cat} (s^{-1})**	**K_m (mM)**	**$10^5 \times k_{cat}/K_m$ ($M^{-1}s^{-1}$)**
Wild-Type*	400 ± 10	0.49 ± 0.05	8.2
Open	76 ± 4	1.8 ± 0.3	0.43
Closed	5.1 ± 1.6	0.72 ± 0.24	0.07
	Electron Aceptor: Cytochrome *c*		
	k_{cat} (s^{-1})	**K_m (mM)**	**$10^5 \times k_{cat}/K_m$ ($M^{-1}s^{-1}$)**
Wild-Type*	207 ± 10	0.24 ± 0.04	8.6
Open	13 ± 1	1.2 ± 0.2	0.11
Closed	0.84 ± 0.14	0.33 ± 0.09	0.03

Table 5.1: *Steady-state kinetic results for the N42C:K324C mutant enzyme using L-lactate as substrate. All experiments were carried out in 10 mM TrisHCl, pH 7.5, I 0.10 at 25 °C. Acceptors were used at the following saturating concentrations: $[Fe(CN)_6]^{3-}$, 5 mM; cytochrome c: 100 μM. Values of k_{cat} represent the rate constant for electron transfer, at saturating substrate concentration per second per molecule of enzyme. Since L-lactate is a 2-electron donor, k_{cat} values can be halved to give rates in terms of substrate molecules consumed..*

**Miles et al., 1992*

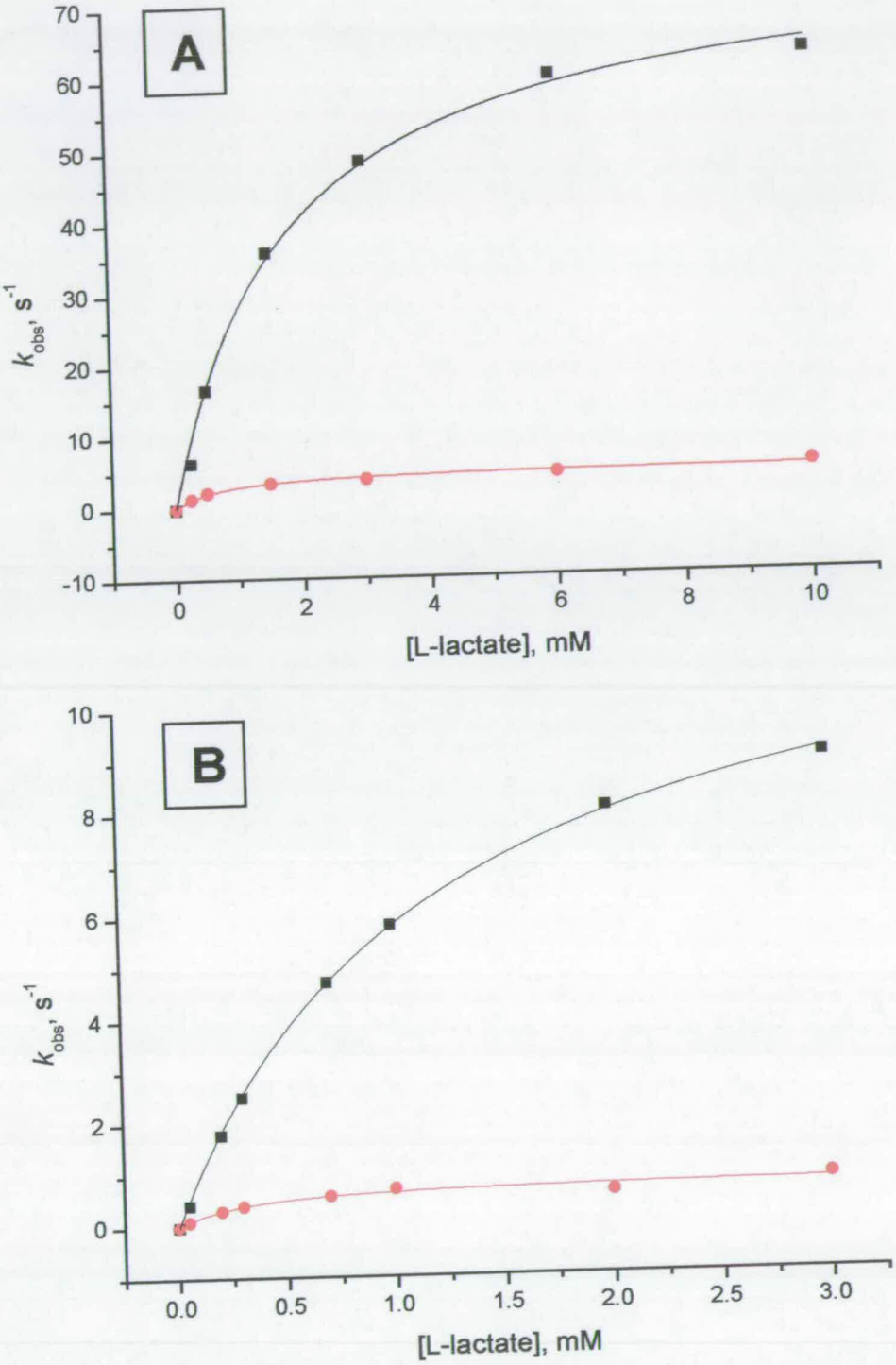

Figure 5.1: *Plots of observed rate constant vs. L-lactate concentration. (A) Michaelis-Menten curves for the closed (red line) and open (black line) N42C:K324C mutant enzymes with $[Fe(CN)_6]^{3-}$ as the electron acceptor. (B) Michaelis-Menten curves of the closed (red line) and open (black line) N42C:K324C mutant enzymes with cytochrome c as the electron acceptor.*

5.2.2 Pre-Steady-State Kinetics of Flavin and Heme Reduction

Stopped-flow kinetic experiments were carried out on both the closed and open forms of the N42C:K324C mutant enzyme. FMN reduction was monitored at 438.3 nm, an isosbestic point for the b_2-heme. The b_2-heme reduction was monitored at 557 nm where the FMN absorbance is essentially zero. Experimental details are described in section 2.17.3.

Both L-lactate and S-2-hydroxybutyrate were used as substrates. Figure 5.3 indicates the traces obtained for b_2-heme reduction for the closed form of the mutant enzyme using L-lactate and S-2-hydroxybutyrate. No data were obtained for FMN reduction for the closed enzyme since little or no absorption change was observed. Figures 5.4a and 5.4b illustrate FMN reduction and b_2-heme reduction for the open form of the mutant enzyme using L-lactate and S-2-hydroxybutyrate respectively.

The resulting kinetic parameters are summarised in Table 5.2 where they are compared with values for the wild-type enzyme. As noted in previous work (Miles *et al.*, 1992, Capellière-Blandin, 1991, Pompon *et al.*, 1980), in most cases biphasic traces were observed for b_2-heme and flavin reduction with the rapid phase corresponding to at least 80 % of the absorbance change. It has been well documented that the rapid phase corresponds to the initial reduction of FMN and b_2-heme groups by one L-lactate molecule, whereas the slow phase corresponds to entry of a third electron into the flavocytochrome b_2 protomer (Capellière-Blandin, 1991; Pompon *et al.*, 1980; Pompon, 1980). This occurs because full reduction of flavocytochrome b_2, in the absence of electron acceptors, requires three electrons per protomer, i.e. six lactate molecules per tetramer (Pompon *et al.*, 1980). This is shown diagrammatically in Figure 5.2. Rate constants for the slow phase are about 20-fold lower than those for the rapid phase and indicate, as previously reported (Pompon *et al.*, 1980; Capellière-Blandin *et al.*, 1975) that the slow phase is kinetically irrelevant during catalytic turnover of the enzyme. Thus, in the presence of an electron acceptor, flavocytochrome b_2 acts as a two-electron transferase. Therefore, it is the limiting rate constants, k_{lim}, for the rapid phase corresponding to the initial reduction of FMN and b_2-heme groups by one L-lactate molecule that are reported in Table 5.2.

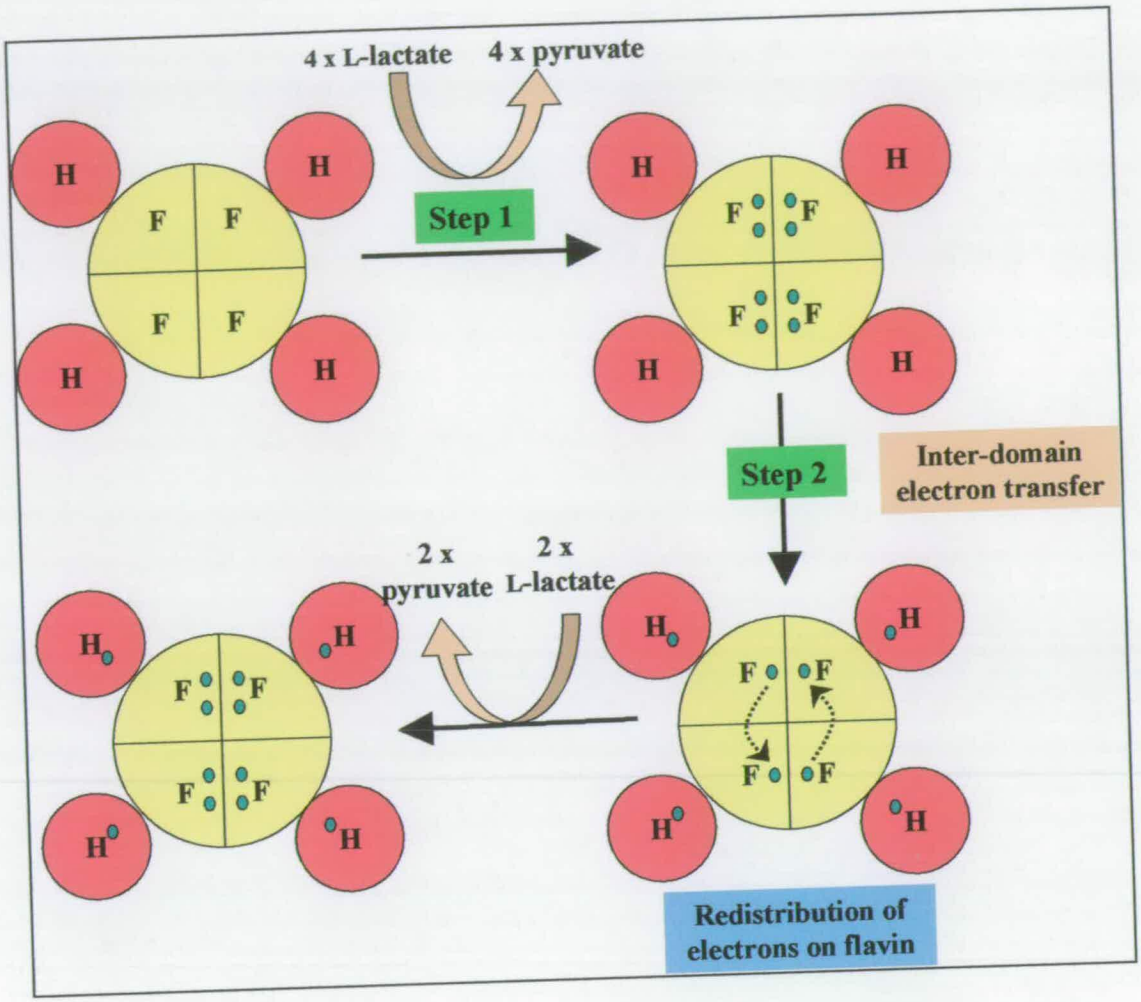

Figure 5.2: *Electron transfer within flavocytochrome b_2. F = FMN, H = b_2-heme. Electrons are represented by blue dots. The figure corresponds to the tetrameric enzyme. Step 1: reduction of all four FMN molecules by four molecules of L-lactate. Step 2: Fast inter-domain electron transfer from flavin to b_2-heme, leaving the FMN in its semiquinone state. This is followed by a redistribution of the electrons on the flavins, leaving two flavin molecules fully-reduced and two oxidised. This is now followed by complete reduction of the enzyme by two further molecules of L-lactate.*

Enzyme	L-lactate	
	Flavin Reduction, k_{lim} (s^{-1})	b_T-heme Reduction, k_{lim} (s^{-1})
Wild-Type*	600 ± 60	445 ± 50
Open	440 ± 80	283 ± 3
Closed	unmeasurable	0.61 ± 0.06
Enzyme	**S-2-hydroxybutyrate**	
	Flavin Reduction, k_{lim} (s^{-1})	b_T-heme Reduction, k_{lim} (s^{-1})
Wild-Type	47 ± 5	50 ± 5
Open	43 ± 7	48 ± 4
Closed	unmeasurable	1.1 ± 0.1

Table 5.2: *Pre-steady-state rate constants for flavin and heme reduction at saturating substrate concentrations (10 mM L-lactate or S-2-hydroxybutyrate). All experiments were carried out in 10 mM TrisHCl, pH 7.5, I 0.10 at 25 °C.*

**Miles et al., 1992*

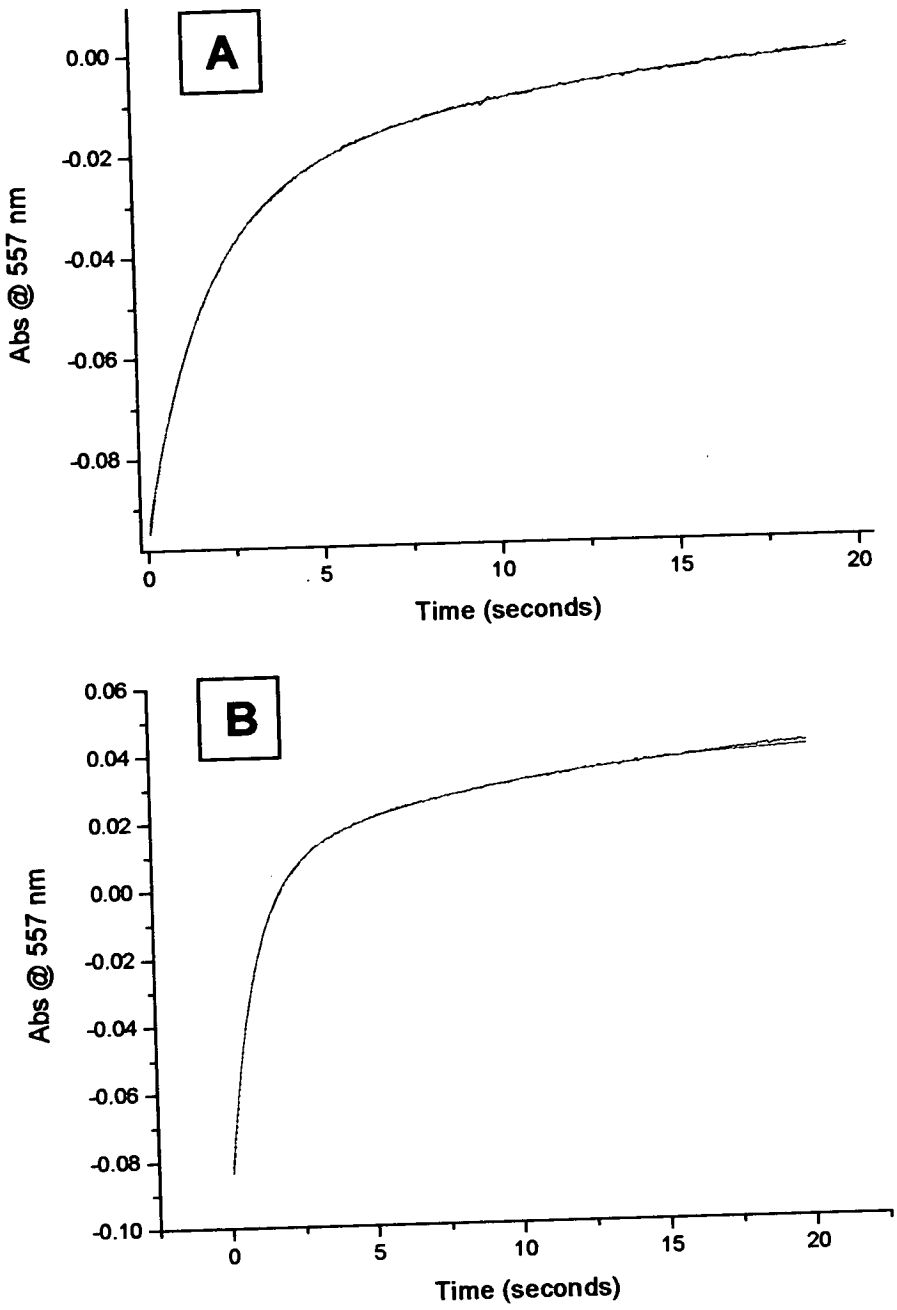

Figure 5.3: *Stopped-flow traces obtained for b_T-heme reduction in the closed form of the mutant enzyme. L-lactate (Panel A) and S-2-hydroxybutyrate (Panel B) are the substrates at a saturating concentration of 10 mM. All experiments were carried out in 10 mM TrisHCl, pH 7.5, I 0.10 at 25 °C. The black line shows the data while the red line shows the fit to an appropriate exponential function.*

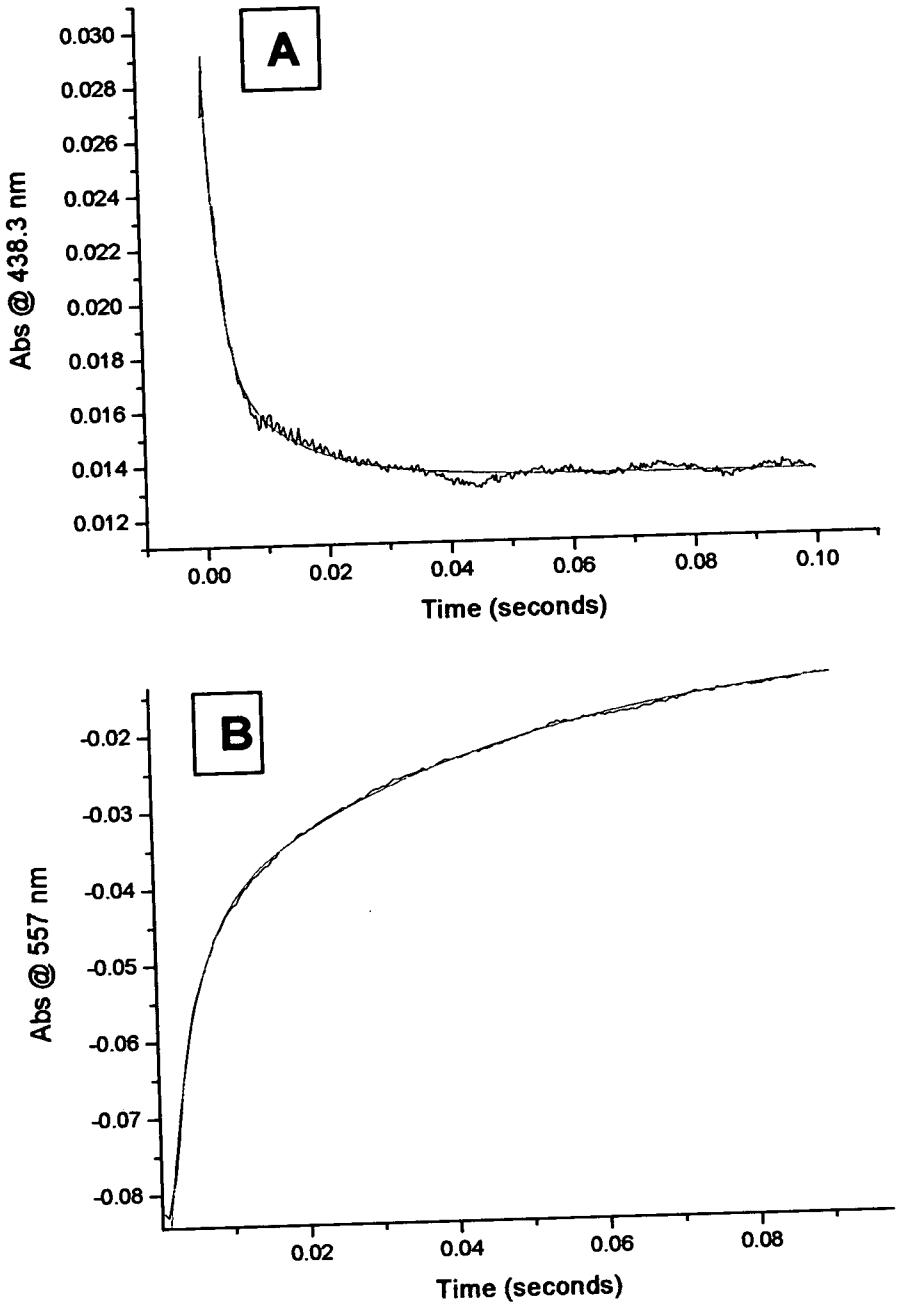

Figure 5.4a: *Stopped-flow traces obtained for FMN and b_T-heme reduction in the open form of the mutant enzyme. L-lactate is the substrate at a saturating concentration of 10 mM. All experiments were carried out in 10 mM TrisHCl, pH 7.5, I 0.10 at 25 °C. The black line shows the data while the red line shows the fit to a double exponential function. Panel A shows flavin reduction to its hydroquinone form while Panel B shows reduction of the b_T-heme.*

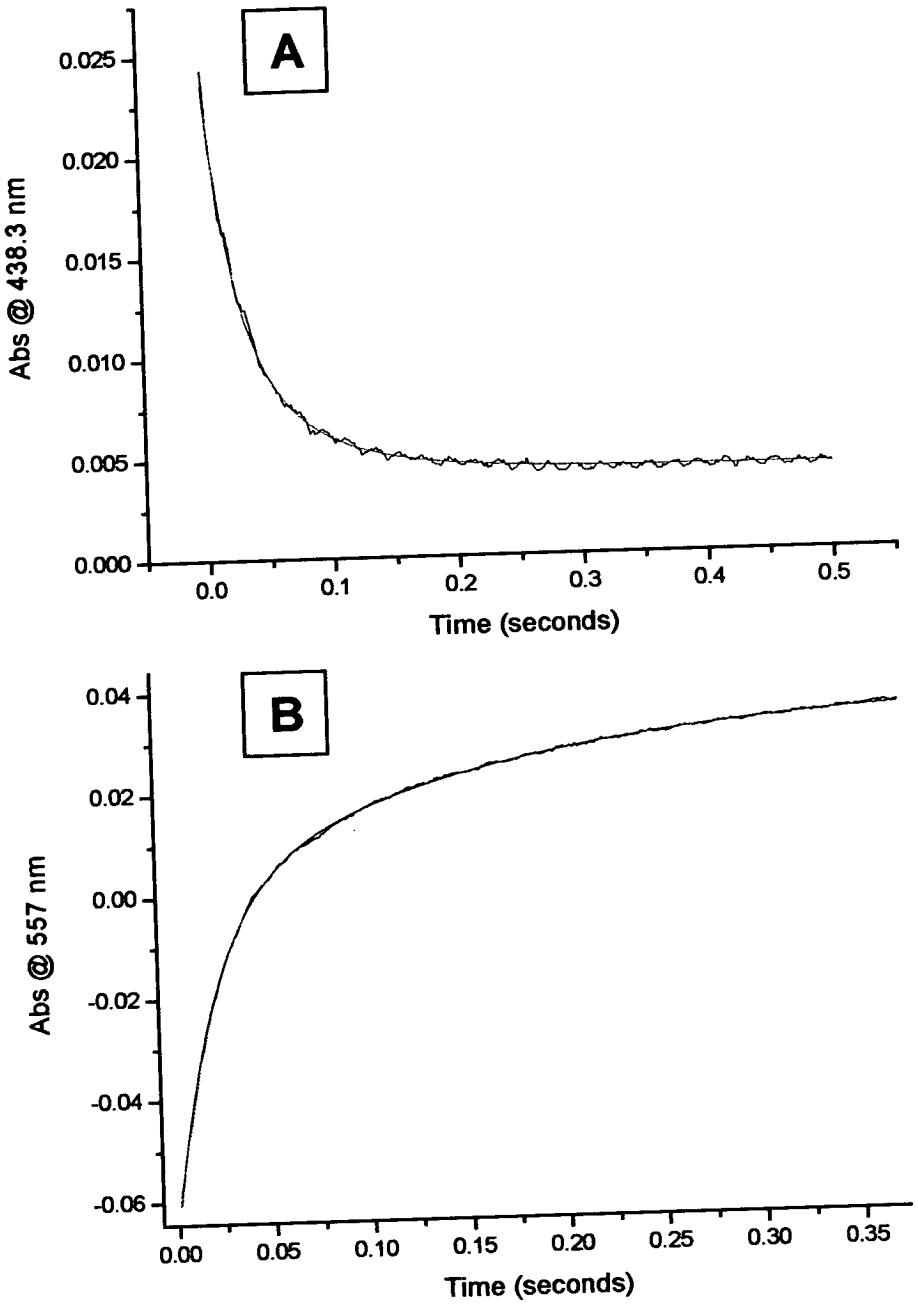

Figure 5.4b: *Stopped-flow traces obtained for FMN and b_2-heme reduction in the open form of the mutant enzyme. S-2-hydroxybuyrate is the substrate at a saturating concentration of 10 mM. All experiments were carried out in 10 mM TrisHCl, pH 7.5, I 0.10 at 25 °C. The black line shows the data while the red line shows the fit to a double exponential function. Panel A shows flavin reduction to its hydroquinone form while Panel B shows reduction of the b_2-heme.*

The observed rate constants at saturating concentrations of substrate (k_{lim}) are given in Table 5.2. As can be seen from this table, as well as Figures 5.4a and 5.4b, the open form of the mutant enzyme displays behaviour that is very similar to wild-type enzyme. However, the closed form of the mutant enzyme displays some interesting features. Flavin reduction could not be reliably obtained due to little or no absorbance change being observed. In addition, the b_2-heme reduction k_{lim} values were reduced considerably on formation of the disulfide bridge to 0.61 ± 0.01 s^{-1} and 1.10 ± 0.01 s^{-1} for L-lactate and S-2-hydroxybutyrate respectively.

5.2.3 Obtaining the Second-Order Rate Constant (k_2) for Cytochrome *c* Reduction

The bimolecular reaction between N42C:K324C flavocytochrome b_2 and cytochrome *c* was studied spectrophotometrically by following the reduction of a sub-stoichiometric amount of cytochrome *c* by an excess of the reduced N42C:K324C enzyme at 416.5 nm, a flavocytochrome b_2-heme isosbestic point. The conditions are detailed in section 2.17.4. The traces generated were fitted to single exponential functions and are shown in Figure 5.5. Derivation of the second-order rate constant for cytochrome *c* reduction was carried out by plotting the observed rate constant (k_{obs}) against N42C:K324C mutant enzyme concentration, with the enzyme in both its open and closed form (Figure 5.6).

The second-order rate constants (k_2) were found to be 2.0 ± 0.2 $\mu M^{-1}s^{-1}$ and 2.8 ± 0.3 $\mu M^{-1}s^{-1}$ for the closed and open forms of the enzyme respectively. This is some 15-fold lower than wild type enzyme (34.8 ± 0.9 $\mu M^{-1}s^{-1}$)(Daff *et al.*, 1996b). Clearly, there is very little difference between the second-order rate constants for the open and closed forms of the enzyme. This indicates that the reduction of cytochrome *c* takes place in a similar manner, regardless of whether the disulphide bridge is formed or not. However, it is also apparent that the efficiency of this process is compromised relative to the wild-type enzyme by the introduction of the cysteine residues at positions 42 and 324, as judged by the 15-fold decrease in k_2.

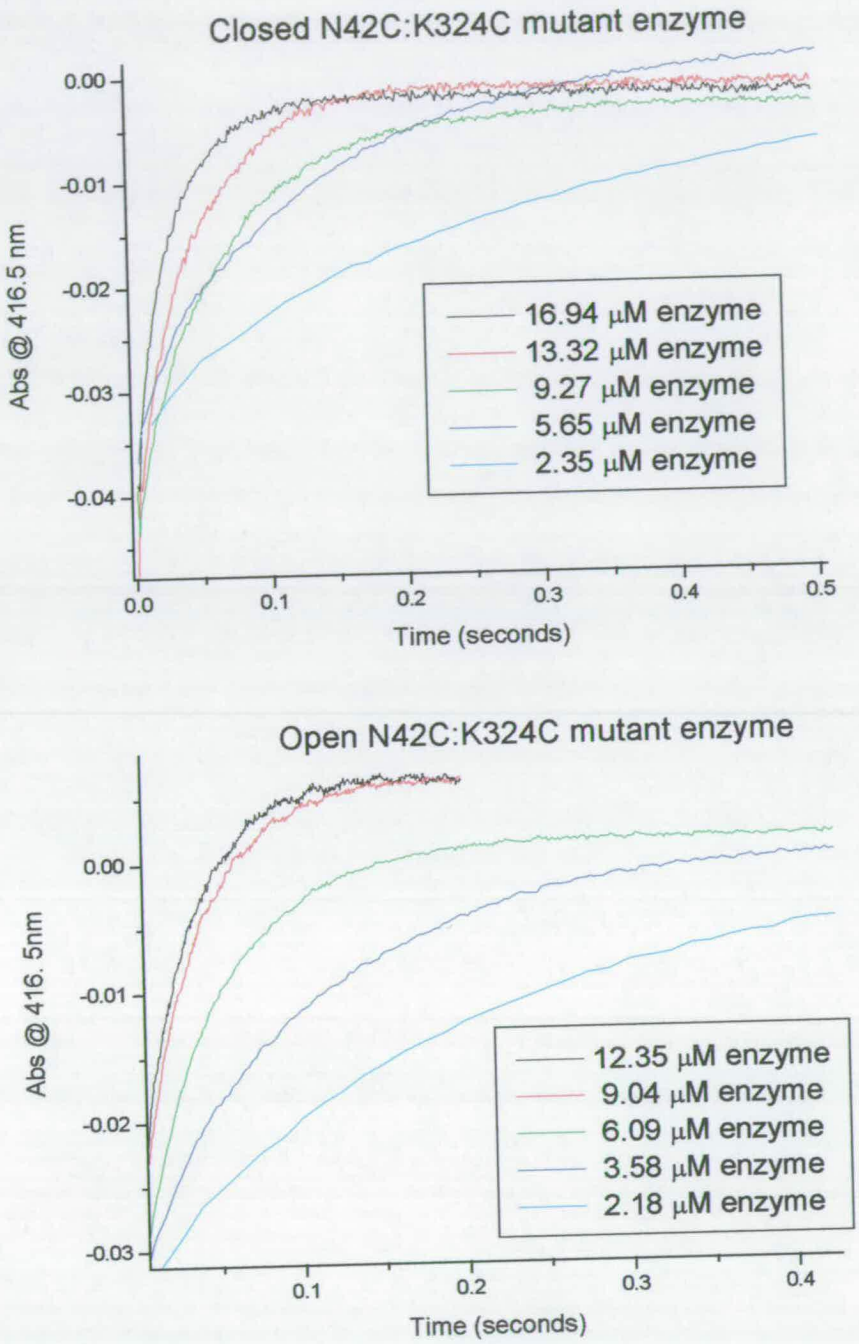

Figure 5.5: *Stopped-flow traces obtained from the bimolecular reaction between a sub-stoichiometric amount of cytochrome c and reduced N42C:K324C mutant enzyme. Those traces obtained from the closed form of the enzyme are shown on the left hand side, while those from the open form of the enzyme are shown to the right hand side. All experiments were carried out in 10 mM TrisHCl, pH 7.5, I 0.10 at 25 °C.*

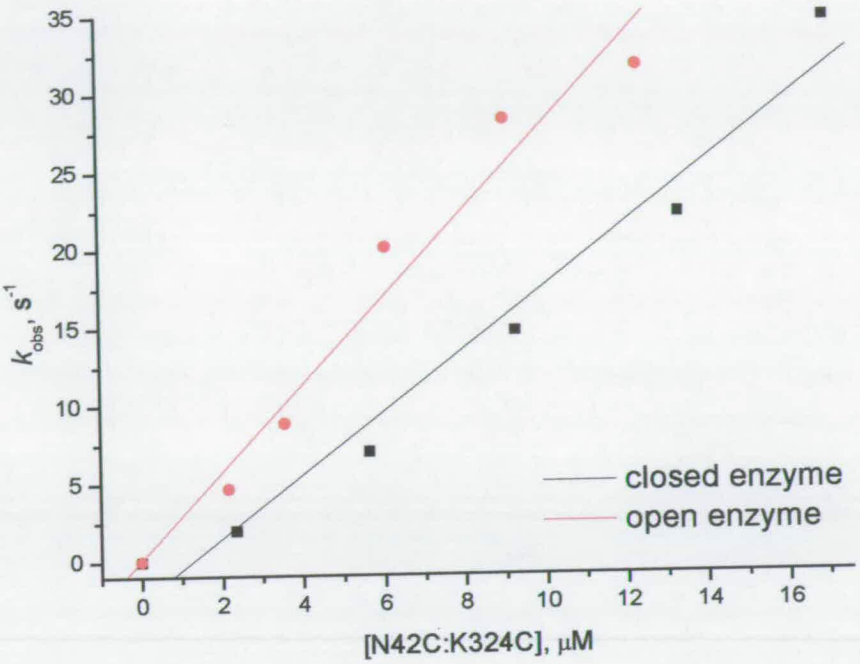

Figure 5.6: *Plot of the observed rate constant vs the concentration of pre-reduced N42C:K324C mutant enzyme in their closed and open forms. The data points are fitted to a straight line to give a second-order rate constant of 2.0 ± 0.2 $\mu M^{-1}s^{-1}$ and 2.8 ± 0.3 $\mu M^{-1}s^{-1}$ for the closed and open enzymes respectively.*

5.3 Discussion and Conclusions

5.3.1 Steady-State Kinetics

Results from steady-state kinetic measurements on the N42C:K324C mutant enzyme, using L-lactate as the substrate and with $[Fe(CN)_6]^{3-}$ and cytochrome *c* as electron acceptors are presented in Table 5.1, where they are compared with previously reported values for wild-type enzyme. Firstly, and as expected, the open, disulfide cleaved form of the mutant enzyme can still function as an L-lactate dehydrogenase as judged by the results with $[Fe(CN)_6]^{3-}$ as electron acceptor (only a 5-fold decrease in the k_{cat} value as compared to wild-type enzyme). Using cytochrome *c* as the electron acceptor exhibits a more pronounced decrease in k_{cat} (some 16-fold) for the open form

of the mutant enzyme as compared to wild-type enzyme. This phenomenon has been previously observed in flavocytochrome b_2 where other point mutations have been made (Diêp LÊ *et al.*, 2003). Interestingly, two of these mutations (F39A and P44A), also show a decreased k_{cat} value with cytochrome *c* as electron acceptor. Both these mutations lie in close proximity to the substituted asparagine residue in the N42C:K324C mutant enzyme. This tends to indicate a disruption of one of the monoelectronic transfer steps, either flavin to b_2-heme or b_2-heme to cytochrome *c*.

However, the most significant differences are seen between the open and closed (disulfide bridged) forms of the mutant enzyme. On formation of the disulfide bridge, a 15-fold decrease in k_{cat} relative to the open form of the mutant enzyme is observed using both electron acceptors. In addition, the catalytic efficiency (as indicated by k_{cat}/K_m) of the closed mutant enzyme with $[Fe(CN)_6]^{3-}$ as electron acceptor represents approximately only 16 % that of the open form of the mutant enzyme. The catalytic efficiency of the closed form of the mutant enzyme when cytochrome *c* is used as the electron acceptor, is only 27 % that of the open form of the mutant enzyme.

This result has important implications for our understanding of the electron flow through the N42C:K324C flavocytochrome b_2. It has been previously shown that ferricyanide can accept electrons from both the FMN and b_2-heme of flavocytochrome b_2, (Iwatsubo *et al.*, 1977; Tegoni *et al.*, 1990) however cytochrome *c* receives electrons only from the b_2-heme (Morton *et al.*, 1961; Ogura & Nakamura, 1966; Capellière-Blandin *et al.*, 1980). Thus, if the formation of the disulfide bridge had significantly affected either the FMN to b_2-heme or the b_2-heme to cytochrome *c* electron transfer rates then the k_{cat} value seen with cytochrome *c* would have decreased more than that seen with ferricyanide. The fact that both electron acceptors show a 15-fold decrease in k_{cat} indicates that it is the rate of FMN reduction by L-lactate that is primarily affected by disulfide bridge formation.

5.3.2 Pre-Steady-State Kinetics of Flavin and Heme Reduction

While steady-state kinetic analyses are an efficient and effective means to study the overall turnover of the N42C:K324C mutant enzyme, they do not give much information about the individual steps that make up the catalytic cycle. As such, the reduction of the FMN and b_2-heme was monitored directly using stopped-flow spectrophotometry. The resulting kinetic parameters are given in Table 5.2.

It is apparent from Table 5.2 that the open form of the mutant enzyme shows similar rate constants to that seen for the wild-type enzyme. Indeed, k_{lim} values for the FMN and b_2-heme reduction in the open form of the N42C:K324C flavocytochrome b_2 are around 60-70% of the values seen for wild-type. However, results for the closed form of the mutant enzyme are dramatically different, with the rate constant for b_2-heme reduction being more than 450-fold less and 43-fold less in the closed form than in the open form when using L-lactate and S-2-hydroxybutyrate as substrates respectively. In fact, the formation of the disulfide bridge makes it impossible to measure the rate constant for FMN reduction directly. The obvious explanation for this is that FMN reduction is very slow in the closed form and so the flavin is reoxidised immediately by electron transfer to the b_2-heme. The k_{lim} for b_2-heme reduction by L-lactate and S-2-hydroxybutyrate in the closed form, as measured from a fit of the heme reduction trace, is 0.61 s^{-1} and 1.1 s^{-1} respectively. However, as previously shown (Daff *et al.*, 1996a), fitting of the data to a simple exponential equation is an approximation. If flavin to b_2-heme electron transfer is much faster than flavin reduction by substrate the rate constant for b_2-heme reduction will be limited by the rate of formation of reduced flavin. This is illustrated in Figure 5.7. Therefore, the k_{lim} values of 0.61 s^{-1} and 1.1 s^{-1} seen for b_2-heme reduction in the closed form of the N42C:K324C mutant enzyme, simply reflects the rate constant for FMN reduction which rate limits the reaction. Thus the stopped-flow data are consistent with the steady-state data in indicating that the formation of the disulfide bridge substantially lowers the rate of FMN reduction.

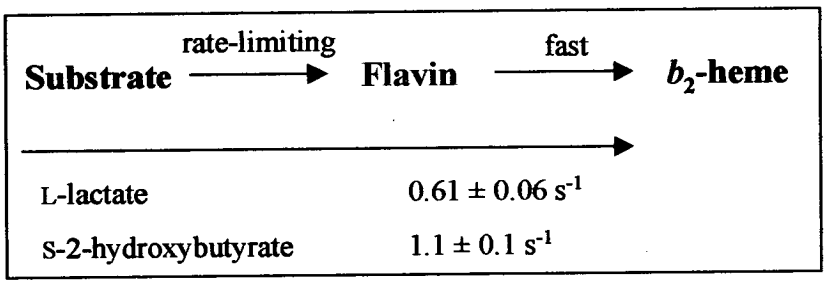

Figure 5.7: *Schematic detailing the rate-determining and fast electron transfer steps in the closed form of the N42C:K324C mutant enzyme. The arrows indicate the direction of the flow of electrons.*

In summary, steady-state and pre-steady-state results with L-lactate and S-2-hydroxybutyrate indicate that flavin reduction is rate-limiting in the N42C:K324C mutant enzyme. Together with the evidence from the sulfite binding experiments discussed in Chapter 4, this confirms that cross-linking the flavin and b_2-heme domains is restricting access of substrate to the active site.

5.3.3 The Interaction with Cytochrome *c*

As was mentioned in section 5.2.3, the traces for the reduction of cytochrome *c* by pre-reduced N42C:K324C flavocytochrome b_2 fit well to a single exponential function. This suggests that the reaction involves only one rate-determining step. Since this is a bimolecular reaction, there are two possible mechanisms. The first involves a fast, yet reversible interaction between the b_2-heme domain of flavocytochrome b_2 and cytochrome *c*, followed by a slower electron transfer step from the b_2-heme to cytochrome *c*. In this case a hyperbolic curve would be observed which would saturate at the limit of the electron transfer rate. Alternatively, the binding and subsequent dissociation between flavocytochrome b_2 and cytochrome *c* can be relatively slow in comparison to the subsequent faster electron-transfer rate from the b_2-heme to cytochrome *c*. Here, a linear plot would be observed. Both these possibilities are modelled in Figure 5.8.

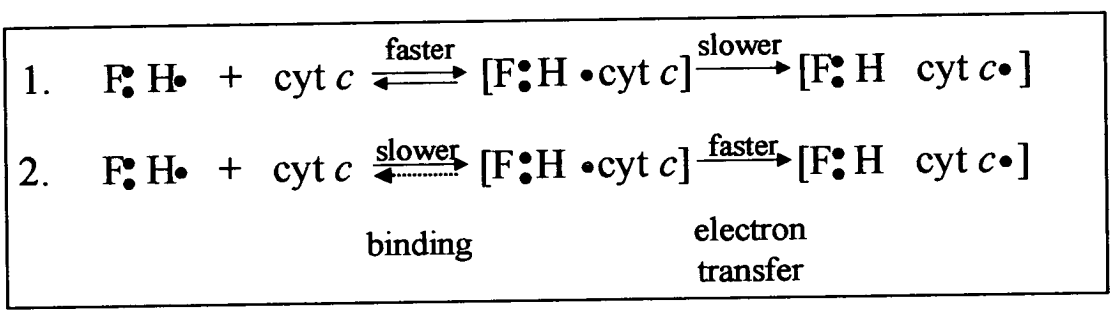

Figure 5.8: *Reduction of cytochrome c by excess flavocytochrome b_2. Both models are valid possibilities since the cytochrome c reduction traces follow single exponential functions. Model 1; cytochrome c binding is fast and reversible, followed by relatively slower electron transfer. Model 2; binding (and dissociation) of cytochrome c to the b_2-heme domain of flavocytochrome b_2 is slower in comparison to electron transfer. F:FMN, H; b_2-heme, cyt c; cytochrome c, the dark blue dots represent electrons.*

The linear plots observed for cytochrome *c* reduction by both the closed and open forms of the mutant enzyme (Figure 5.6), indicates that model 2 operates, i.e. the rate of binding to cytochrome *c* is slow in contrast to the subsequently faster rate of electron transfer. This was also found to be the case in wild-type flavocytochrome b_2 (Capeillère-Blandin *et al.*, 1982; Daff *et al.*, 1996b).

There is very little difference between the second-order rate constants for the closed and open forms of the enzyme (2.0 ± 0.2 $\mu M^{-1}s^{-1}$ and 2.8 ± 0.3 $\mu M^{-1}s^{-1}$ respectively). This indicates that the reduction of cytochrome *c* takes place in the same manner, regardless of whether the disulphide bridge is formed or not and thus domain movement does not appear to play any significant role in the recognition of cytochrome *c*. However, it is also apparent that the efficiency of this process is compromised by the introduction of the cysteine residues at postions 42 and 324, as judged by this 15-fold decrease in k_2 relative to wild-type enzyme (34.8 ± 0.9 $\mu M^{-1}s^{-1}$)(Daff *et al.*, 1996b). Short *et al.* (1998) proposed a location for this cytochrome *c* binding which involved a triangle of electrostatic interactions between the acidic residues Glu63, Asp72 and Glu237 from flavocytochrome b_2 and basic residues Lys13, Lys27 and Lys79 on cytochrome *c*. In addition to this, it was thought that a possible σ–tunneling pathway for electron transfer could run through this triangle of interactions. The pathway would start at the imidazole ring of His66, a ligand to the b_2-heme-iron of flavocytochrome b_2 and then run through the backbone of Ala67 and end at the ring of Pro68, which would be in van der Waals contact with the cytochrome *c* heme. However, an inspection of the crystal structure of the native enzyme shows that none of the above mentioned residues are particularly close to the site of the engineered cysteine residues. The distance between the α-carbon atoms of Cys42 and Glu63 is 16 Å, perhaps too far to have any obvious impact on the rate of binding of the mutant enzyme to cytochrome *c*. As such, the reasons to why the second-order rate constant should be the same for both the closed and open forms of the mutant enzyme, yet still 15-fold lower compared to wild-type enzyme, remain elusive.

Chapter 6

Overall Conclusions and Future Work

Chapter 6

Overall Conclusions and Future Work

The main conclusions presented in this thesis are as follows;

- The crystal structure of the N42C:K324C mutant enzyme has been solved to 3.0 Å resolution, confirming the existence of the imposed disulfide-bridge. The major effect of 'fixing' these two domains was the presence of an ordered cytochrome domain in each of the four subunits of the tetramer. It was also interesting to note that despite the crystallising conditions containing 50 mM pyruvate, none was observed at the active site in the crystal structure.

- Steady-state kinetic analyses indicate that it is the rate of FMN reduction by L-lactate that is primarily affected by disulfide-bridge formation.

- Pre-steady-state kinetic analyses are consistent with the steady-state data. FMN reduction has been rate-limited by the formation of the disulfide bridge and thus the flavin is re-oxidised immediately by subsequent electron transfer to the b_2-heme.

- The second-order rate constant for the reaction with sulfite was found to be some 60-fold lower in the disulfide-bridged form of the mutant enzyme as compared to the open form of the mutant enzyme. Clearly, the rate of sulfite entry to the active site is dramatically slowed by formation of the disulfide-bridge.

- Binding experiments with sulfite were carried out. The K_d for the closed form of the mutant enzyme is some 6-fold higher than for the open form, indicating that binding of sulfite to the flavin is not favoured in the disulfide-bridged enzyme.

- The bimolecular reaction between N42C:K324C flavocytochrome b_2 and cytochrome *c* was studied spectrophotometrically. The second-order rate constants for the closed and open forms of the mutant enzyme were found to be very similar, but still 15-fold lower than wild-type enzyme. This suggests that domain movement plays no role in cytochrome *c* reduction, but the imposed cysteine mutations affect the efficiency of this process.

A question was posed in section 1.6 - why is there inter-domain mobility in flavocytochrome b_2 and is it important for catalysis? From the above conclusions it would appear that the role of inter-domain mobility is to allow the b_2-heme domain to move away from the flavin-binding domain in order for substrate to effectively access the active site. Cross-linking the b_2-heme and flavin-binding domains prevents mobility about the cytochrome domain and essentially 'cordons off' the usual pathway taken by the substrate to the active site. On cleavage of the disulfide bond by DTT, the enzyme is once again able to behave in its native manner, indicating its requirement for dynamic flexibility about the hinge region.

It would be interesting to carry out the following work;

- The second-order rate constants for the closed and open forms of the N42C:K324C mutant enzyme were found to be very similar in the bimolecular reaction with cytochrome *c*. This indicates that domain movement plays no role in cytochrome *c* reduction. However, the second-order rate constants were found to be 15-fold lower than wild-type enzyme. It is likely that the imposed cysteine mutations affect the efficiency of this process. As such, it would be interesting to analyse the effects of the single N42C and K324C mutations. Would either of these mutations account for the 15-fold decrease in second-order rate constant observed with this reaction?

References

Anfinsen, C.B. (1973) *Science*, **181**, 223

Appleby, C.A., Morton, R.K. (1954) *Nature*, **173**, 749-752

Bach, S.J., Dixon, M., Keilin, D. (1942) *Nature*, **149**, 21

Bader, M., Muse, W., Ballou, D.P., Gassner, C., Bardwell, J.C. (1999) *Cell*, **98**, 217-227

Balme, A., Brunt, C.E., Pallister, R.L., Chapman, S.K., Reid, G.A. (1995) *Biochem. J.*, **309**, 601-605

Bardwell, J.C., McGovern, K., Beckwith, J. (1991) *Cell*, **67**, 581-589

Becker, W., Pfeil, E. (1966) *Biochem. Z.*, **346**, 301

Bell, C. (1997) PhD Thesis

Beratan, D.N., Betts, J.N., Onuchic, J.N. (1991), *Science*, **252**, 1285–1288

Beratan, D.N., Betts, J.N., Onuchic, J.N. (1992), *J. Phys. Chem*, **96**, 2852-2855

Black, M.T., White, S.A., Reid, G.A., Chapman, S.K. (1989a) *Biochem. J.*, **258**, 255-259

Black, M.T., Gunn, F.J., Chapman, S.K., Reid, G.A. (1989b) *Biochem. J.*, **263**, 973-976

Boeri, E., Rippa, M. (1961) *Archives of Biochemistry and Biophysics*, **94**, 336-341

Brunt, C.E., Cox, M.C., Thurgood, A.G.P., Moore, G.R., Reid, G.A., Chapman, S.K. (1992) *Biochem. J.*, **283**, 87-90

Brunt, C.E. (1993) PhD Thesis

Campbell, N.A., (1996) *Biology*, 4th Edition, The Benjamin/Cummings Publishing Company, Inc.

Capeillère-Blandin, C. (1975) *Eur. J. Biochem.*, **56**, 91-101

Capeillère-Blandin (1982) *Eur. J. Biochem.*, **128**, 533-542

Capellière-Blandin, C. (1991) *Biochem. J.*, **274**, 207-217

Capellière-Blandin, C., Bray, R.C., Iwatsubo, M., Laberyie, F. (1975) *Eur. J. Biochem.*, **54**, 549-566

Capeillère-Blandin, C., Iwatsubo, M., Testylier, G., Labeyrie, F. (1980) *Flavins Flavoproteins, Proc. Int. Symp.*, 6th, 617-630

Capeillère-Blandin, C., Barber, M.J., Bray, R.C. (1982) *Developments in Biochemistry (Flavins Flavoproteins)*, **21**, 838-43

Capeillère-Blandin, C., Albani, J. (1987) *Biochem J.*, **245**, 159-165

Chapman, S.K., Reid, G.A., Daff, S.N., Sharp, R.E., White, P., Manson, F.D.C., Lederer, F. (1994) *Biochem. Soc. Trans.*, **22**, 713-718

Chapman, S.K., Daff, S., Munro, A.W., (1997) *Structure and Bonding*, **88**, 39-70

Cherrier, M.V., Martin, L., Cavazza, C., Jacquamet, L., Lemaire, D., Gaillard, J., Fontecilla-Camps, J.C., (2005), *J. Am. Chem. Soc.*, **127**, 10075-10082

Collet, J.F., Bardwell, J.C. (2002) *Molecular Microbiology*, **44(1)**, 1-6

Creighton, T.E. (1988) *BioEssays*, **8(2)**, 57-63

Cunane, L.M., Barton, J.D., Chen, Z-W., Welsh, F.E., Chapman, S.K., Reid, G.A., Mathews, F.S. (2002) *Biochemistry*, **41**, 4264-4272

Cuozzo, J.W., Kaiser, C.A. (1999) *Nat. Cell. Biol.*, **1**, 130-135

Daff, S., Manson, F.D.C., Reid, G.A., Chapman, S.K. (1994) *J. Biochem.*, **301**, 829-834

Daff, S., Ingledew, W.J., Reid, G.A., Chapman, S.K. (1996a) *Biochemistry*, **35**, 6345-6350

Daff, S., Sharp, R.E., Short, D.M., Bell, C., White, P., Manson, F.D.C., Reid, G.A., Chapman, S.K. (1996b) *Biochemistry*, **36**, 6351-6357

Daum, G., Böhni, P.C., Schatz, G. (1982) *J. Biol. Chem.* **252**, 13028-13033

Deisenhofer, J., Epp, O., Miki, K., Huber, R., Michel, H., (1985), *Nature*, **318**, 618-624

Diêp Lê, K.H, Mayer, M., Lederer, F. (2003) *Biochem. J.*, **373**, 115-123

Dubois, J., Chapman, S.K., Mathews, F.S., Reid, G.A., Lederer, F. (1990) *Biochemistry*, **29**, 6393-6400

Falke, J.J., Koshland, D.E. (1987) *Science*, **237**, 1596-1600

Ferari, D.M., Soling, H.D. (1999) *Biochem. J.*, **339**, 1-10

Franco, L., Montero, F., Rodriguez-Molina, J.J. (1977) *FEBS Letters*, **78**, 317-320

Frand, A.R., Kaiser, C.A. (1998) *Mol. Cell*, **1**, 161-170

Frew, J.E., Jones, P. (1984) Structure and functional properties of peroxides and catalases. In: Sykes, A.G. (ed) *Advances in inorganic and bioinorganic mechanisms*, vol 3. Academic Press, London, p 175

Gething, M.J., Sambrook, J. (1992) *Nature*, **355**, 33-45

Gilbert, H.F. (1990) *Adv. Enzymol.*, **63**, 69-172

Gilbert, H.F. (1994) in *Mechanisms of Protein Folding* (ed. Pain, R.F), 104-135, (Oxford Univ. Press, Oxford, UK)

Gokhale, R.S., Agarwalla, S., Francis, V.S., Santi, D.V., Balaram, P. (1994) *J. Mol. Biol.*, **235**, 89-94

Golberger, R.F., Epstein, C.J., Anfinsen, C.B. (1963) *J. Biol. Chem.*, **238**, 628-635

Gondry, M., Lê, K.H.D., Manson, F.D.C., Chapman, S.K., Mathews, F.S., Reid, G.A., Lederer, F. (1995) *Protein Science*, **4**, 925-935

Guddat, L.W., Bardwell, J.C., Martin, J.L. (1998) *Structure*, **6**, 757-767

Guddat, L.W., Bardwell, J.C., Zander, T., Martin, J.L. (1997) *Protein Sci.*, **6**, 1148-1156

Guiard, B., Groudinsky, O., Lederer, F. (1974) *Proc. Nat. Acad. Sci. USA*, **71**, 2539-2543

Guillemette, J.G., Baker, P.D., Eltis, L.D., Lo, T.P., Smith, M., Brayer, G.D., Mauk, A.G. (1994) *Biochimie*, **76**, 592-604

Haumont, P.Y., Thomas, M.A., Labeyrie, F., Lederer, F. (1987) *Eur. J. Biochem.*, **169**, 539-546

Hazzard, J.T., Cusanovich, M.A., Tainer, J.A., Getzoff, E.D., Tollin, G. (1986) *Biochemistry*, **25**, 3318-3328

Hazzard, J.T., McDonough, C.A., Tollin, G. (1994) *Biochemistry*, **33**, 13445-13454

Hemmerich, P., Massey, V., Weber, G. (1967) *Nature*, 213, 728-30

Hinck, A.P., Truckses, D.M., Markley, J.L. (1996) *Biochemistry*, **35**, 1328-1338

Hwang, C., Sinskey, A.J., Lodish, H.F. (1992) *Science*, 257, 1496-1502

Iwatsubo, M., Mevel-Ninio, M., Labeyrie, F. (1977) *Biochemistry*, **16(16)**, 3558-3566

Jacq, C., Lederer, F. (1974) *Eur. J. Biochem.*, **41**, 311-320

Jameson, G.B., Ibers, J.A. (1994) *Biological and Synthetic Dioxygen Carriers*. In: Bertini, I., Gray, H.B., Lippard, S.J., Valentine, J.S. (eds) Bioinorganic Chemistry. University Science Books, Mill Valley CA, p253

Karpishin, T.B., Grinstaff, M.W., Komar-Panicucci, S., McLendon, G, Gray, H.B. (1994) *Structure*, **2**, 415-422

Kishigami, S., Ito, K. (1996) *Genes Cells*, **1**, 201-208

Labeyrie, F., Baudras, A. (1972) *Eur J. Biochem.*, **25**, 33-40

Labeyrie, F., Beloeil, J.C., Thomas, M.A. (1988) *Biochim. Biophys. Acta*, **953**, 134-141

Labeyrie, F., Groudinsky O., Jacquot-Armand, Y., Naslin, L. (1966) *Biochim. Biophys. Acta*, **128**, 492-503

Lancaster, J.R. (1988) *The Bioinorganic Chemistry of Nickel*, Ed., Wiley, New York, p337

Lederer, F. (1978) *Eur. J. Biochem.*, **88**, 425-431

Lederer, F. (1991) in *Chemistry and Biochemistry of Flavoenzymes*, Vol II, Chp 7, (Müller, F. ed., CRC Press, Boca Raton, Florida)

Lederer, F., Cortial, S., Becam, A.M., Haumont, P.Y., Perez, L. (1985) *Eur. J. Biochem.*, **152**, 419-428

Lederer, F., Mathews, F.S. (1987) in *Flavins & Flavoproteins* (McCormack, D.B., Edmondson, D.E. eds) p 33-142, Walter de Gruyter, Berlin

Leslie, A.G.W. (1992) Joint CCP4 + ESF-EAMCB, *Newsletter on Protein Crystallography*, No. 26

Mager, H. I. X., Berends, W. (1966) *Biochim. Biophys. Acta*, **118**, 440-441

Malatesta, F., Antonini, G., Sarti, P., Brunori, M. (1995) *Biophys. Chem.*, **54**:1

Marcus, R.A. (1956), *J. Chem. Phys.*, **24**, 966

Marcus, R.A., Sutin, N., (1985) *Biochim. Biophys. Acta*, **811**, 265-322

Martin, J.L., Bardwell, J.C., Kuriyan, J. (1993) *Nature*, **365**, 464-468

Massey V., Ganther, H. (1965) *Biochemistry*, **4**, 1161-1173

Massey V., Palmer, G. (1966) *Biochemistry*, **5**, 3181-3189

Massey, V., Müller, F., Feldberg, R., Schuman, M., Sullivan, P.A., Howell, L.G., Mayhew, S.G., Matthews, R.G., Foust, G.P. (1969) *J. Biol. Chem.*, **244**, 3999-4006

Mathews, F.S., Argos, P., Levine, M. (1972) *Cold Spring Harbour Symp. Quant. Biol.*, **36**, 387-395

Matsumara, M., Matthews, B.W. (1989a) *Science*, **243**, 792-794

Matsumara, M., Becktel, W.J., Levitt, M., Matthews, B.W. (1989b) *Proc. Natl. Acad. Sci. USA*, **86**, 6562-6566

Mattevi, A., Vanoni, M.A., Todone, F., Rizzi, M., Teplyakov, A., Coda, A., Bolognesi, M., Cutti, B. (1996) *Proc. Natl. Acad. Sci. USA*, **93**, 7496-7501

Matthews, R.G., Massey, V. (1969) *J. Biol. Chem.*, **244**, 1779-86

Mauk, A.G., Mauk, M.R., Moore, G.R., Northrup, S.H. (1995) *J. Bioen. Biomem.*, **27**, 311-330

Miles, C.S., Rouvière-Fourmy, N., Lederer, F., Mathews, S., Reid, G.A., Black, M.T., Chapman, S.K. (1992) *Biochem. J.*, **285**, 187-192

Miles, C.S., Lederer, F., Diêp Lê, K.H. (1998) *Biochemistry*, **37**, 3440-3448

Mizutani, H., Miyahara, I., Hirotsu, K., Nishima, Y., Shiga, K., Setoyama, C., Miura, R. (1996) *J. Biochem*, **120**, 14-17

Moore, G.R. (1996) *Hemeoproteins*. In:Bendall D.S. (ed) Protein electron transfer. Bios Scientific Publishers, Oxford, p189

Morton, R.K., Armstrong, J. McD., Appleby, C.A, **(1961)** *Haematin Enzymes, Symp. Intern. Union Biochem., Canberra, 1959*, 2, 501-523

Moser, C.C., Keske, J.M., Warncke, K., Farid, R.S., Dutton, P.L. (1992) *Nature*, **355**, 796-802

Mowat, C.G., Beaudoin, I., Durely, R.C., Barton, J.D., Pike, A.D., Chen, Z.W., Reid, G.A., Chapman, S.K., Mathews, F.S., Lederer, F. (2000) *Biochemistry*, **39**, 3266-3275

Mowat, C.G., Wehenkel, A., Green, A.J., Walkinshaw, M.D., Reid, G.A., Chapman, S.K. (2004) *Biochemistry*, **43**, 9519-9526

Müller, F., Massey, V. (1969) *J. Biol. Chem.*, **244**, 4007-4016

Murshudov, G.N., Vagin, A.A., Dodson, E.J. (1997) *Acta Crystallogr.* **D53**, 240-255

Nelson, J.W., Crieghton, T.E. (1994), *Biochemistry*, **33**, 5974-5983

Ogura, Y., Nakamura, T. (1966) *J. Biochem.*, **60**, 77-86

Oritz de Montellano, P.R. (1995) *Cytochrome P450*, 2nd edn. Plenum, New York

Page, C.C., Moser, C.C., Chen, X., Dutton, P.L. (1999) *Nature*, **402**, 47-52

Pajot, P., Claisse, M.L. (1974) *Eur. J. Biochem.*, **49**, 275-285

Pajot, P., Groudinsky, O. (1970) *Eur. J. Biochem.*, **12**, 158-164

Pettigrew, G.W., Moore, G.R. (1987) *Cytochromes c: Biological Aspects*, Rich, A. editor, Springer-Verlay

Pompon, D. (1980) *Eur. J. Biochem.*, **106**, 151-159

Pompon, D., Iwatsubo, M., Lederer, F. (1980) *Eur. J. Biochem.*, **104**, 479-488

Reid, G.A., White, S., Black, M.T., Lederer, F., Mathews, F.S., Chapman, S.K. (1988) *FEBS*, **178**, 329-333

Rothery, E.L., Mowat, C.G., Miles, C.S., Mott, S., Walkinshaw, M.D., Reid, G.A., Chapman, S.K. (2004) *Biochemistry*, **43**, 4983-4989

Roussel, A., Cambillau, C. (1991) TURBO-FRODO, in *Silicon Graphics Geometry Partners Directory 86*, Silicon Graphics, Mountain View, CA.

Salemme, F.R. (1976) *J. Mol. Biol.*, **102**, 563-568

Sharp, R.E., White, P., Chapman, S.K., Reid, G.A. (1994) *Biochemistry*, **33**, 5115-5120

Sharp, R.E., Chapman, S.K., Reid, G.A. (1996a) *Biochemistry*, **35**, 891-899

Sharp, R.E., Chapman, S.K., Reid, G.A. (1996b) *Biochem. J.*, **316**, 507-513

Short, D.M., Walkinshaw, M.D., Taylor, P., Reid, G.A., Chapman, S.K. (1998) *J. Biol. Inorg. Chem.*, **3**, 246-252

Smalley, J.F., Feldberg, S.W., Chidsey, C.E.D., Linford, M.R., Newton, M.D., Liu, Y-P. (1995) *J. Phys. Chem.*, **99**, 13141-13149

Steudel, R. (1975) *Angew. Chem. Internat. Ed.*, **14**, 655-664

Stryer, L. (1995) *Biochemistry*, 4th Edition, Freeman W.H. and Company, New York

Sworoda, B.E.P., Massey, V. (1966) *J. Biol. Chem.*, **241**, 3409-3416

Tegoni, M., Janot, J-M., Labeyrie, F. (1990) *Eur. J. Biochem.*, **190**, 329-342

Tegoni, M., White, S.A., Roussel, A., Mathews, F.S., Cambillau, C. (1993) *Proteins: Structure, Function and Genetics*, **16**, 408-422

Tegoni, M., Cambillau, C. (1994) *Protein Science*, **3**, 303-313

Tegoni, M., Begotti, S., Cambillau, C. (1995) *Biochemistry*, **34**, 9840-9850

Tegoni, M., Silvestrini, M.C., Guigliarelli, B., Asso, M., Brunori, M., Bertrand, P. (1998) *Biochemistry*, **37**, 12761-12771

Thomas, M-A., Favaudon, V., Pochon, F. (1983a) *Eur. J. Biochem.*, **135**, 569-576

Thomas, M-A., Gervais, M., Favaudon, V., Valat, P. (1983b) *Eur. J. Biochem.*, **135**, 577-581

Tu, B.P., Ho-Schleyer, S.C., Travers, K.J., Weisman, J.S. (2000) *Science*, **290**, 1571-1574

Urban, P., Lederer, F. (1985) *J. Biol. Chem.*, **260**, 11115-11122

Walker, M.C., Tollin, G. (1991) *Biochemistry*, **30**, 5546-5555

Walsh, C.T., Schonbrunn, A., Abeles, R. (1971) *J. Biol. Chem.*, **246**, 6855-6866

Walsh, C.T., Schonbrunn, A., Lockridge, O., Massey, V., Abeles, R. (1972) *J. Biol. Chem.*, **247**, 6004-6006

Walsh, C.T., Lockridge, O., Massey, V., Abeles, R. (1973) *J. Biol. Chem.*, **248**, 7049-7054

Well, J.A., Powers, D.B. (1986) *J. Biol. Chem.*, **261**, 6564-6570

White, P., Manson, F.D.C., Brunt, C.E., Chapman, S.K., Reid, G.A. (1993) *Biochem. J.*, **291**, 89-94

Wuttke, D.S., Bjerrum, M.J., Winkler, J.R., Gray, H.B (1992) *Science*, **256**, 1007-1009

Xia, Z-X., Mathews, F.S. (1990) *J. Mol. Biol.*, **212**, 837-863

Yagi, K., Ozawa, T. (1962) *Biochim. Biophys. Acta*, **56**, 420

Zapun, A., Missiakas, D., Raina, S., Creighton, T.E. (1995) *Biochemistry*, **32**, 5083-5092

Appendices

Appendix I

Amino Acid Sequence of Flavocytochrome b_2

The residues highlighted in red indicate an 80 amino acid N-terminal sequence that directs the protein into the mitochondrian of the cell where it is proteolytically processed to give the mature enzyme. In addition, when flavocytochrome b_2 is expressed in *E. coli*, the sequence commences at methionine-6 (highlighted in purple) of the mature *S. cerevisiae* protein (Black *et al.*, 1989a). The absence of the first five amino acids (highlighted in green) appears to have little or no effect on the physical properties of the enzyme (Black *et al.*, 1989a).

```
MLKYKPLLKI  SKNCEAAILR  ASKTRLNTIR  AYGSTVPKSK  SFEQDSRKRT    50
QSWTALRVGA  ILAATSSVAY  LNWHNGQIDN  EPKLDMNKQK  ISPAEVAKHN   100
KPDDCWVVIN  GYVYDLTRFL  PNHPGGQDVI  KFNAGKDVTA  IFEPLHAPNV   150
IDKYIAPEKK  LGPLQGSMPP  ELVCPPYAPG  ETKEDIARKE  QLKSLLPPLD   200
NIINLYDFEY  LASQTLTKQA  WAYYSSGAND  EVTHRENHNA  YHRIFFKPKI   250
LVDVRKVDIS  TDMLGSHVDV  PFYVSATALC  KLGNPLEGEK  DVARGCGQGV   300
TKVPQMISTL  ASCSPEEIIE  AAPSDKQIQW  YQLYVNSDRK  ITDDLVKNVE   350
KLGVKALFVT  VDAPSLGQRE  KDMKLKFSNT  KAGPKAMKKT  NVEESQGASR   400
ALSKFIDPSL  TWKDIEELKK  KTKLPIVIKG  VQRTEDVIKA  AEIGVSGVVL   450
SNHGGRQLDF  SRAPIEVLAE  TMPILEQRNL  KDKLEVFVDG  GVRRGTDVLK   500
ALCLGAKGVG  LGRPFLYANS  CYGRNGVEKA  IEILRDEIEM  SMRLLGVTSI   550
AELKPDLLDL  STLKARTVGV  PNDVLYNEVY  EGPTLTEFED  A           591
```

Appendix II

Overview of the Stratagene QuikChange® XL site-directed mutagenesis method. (Taken from Stratagenes' QuikChange® XL- SDM manual).

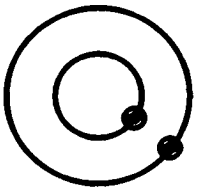

Step 1
Plasmid Preparation

Gene in plasmid with target site for mutation.

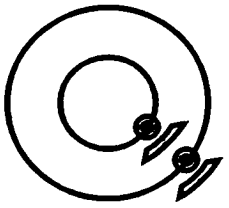

Step 2
Temperature cycling

The plasmid is denatured before annealing the oligonucleotide primers containing the desired mutation.

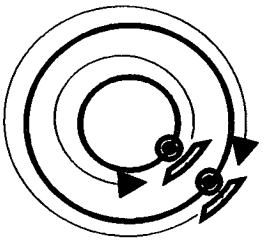

Using the nonstrand-displacing action of *Pfu*Turbo DNA polymerase, the mutagenic primers are extended and incorporated resulting in nicked circular strands.

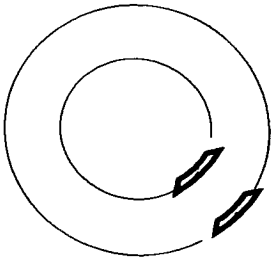

Step 3
Digestion

The methylated, nonmutated parental DNA is digested with *Dpn* I.

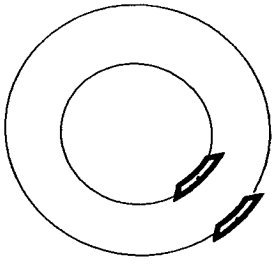

Step 4
Transformation

The circular, nicked dsDNA is transformed into the XL 10-Gold ultracompetent cells.

After transformation, the *E. coli* XL 10 Gold ultracompetent cells can repair the nicks in the mutated plasmid.

LEGEND

Parental DNA Plasmid

Mutagenic primer

Mutated DNA plasmid

Appendix III

Flavocytochrome b_2 DNA sequence with the sequencing primers highlighted in green. Primer b_2Seq1 anneals to the upstream vector sequence.

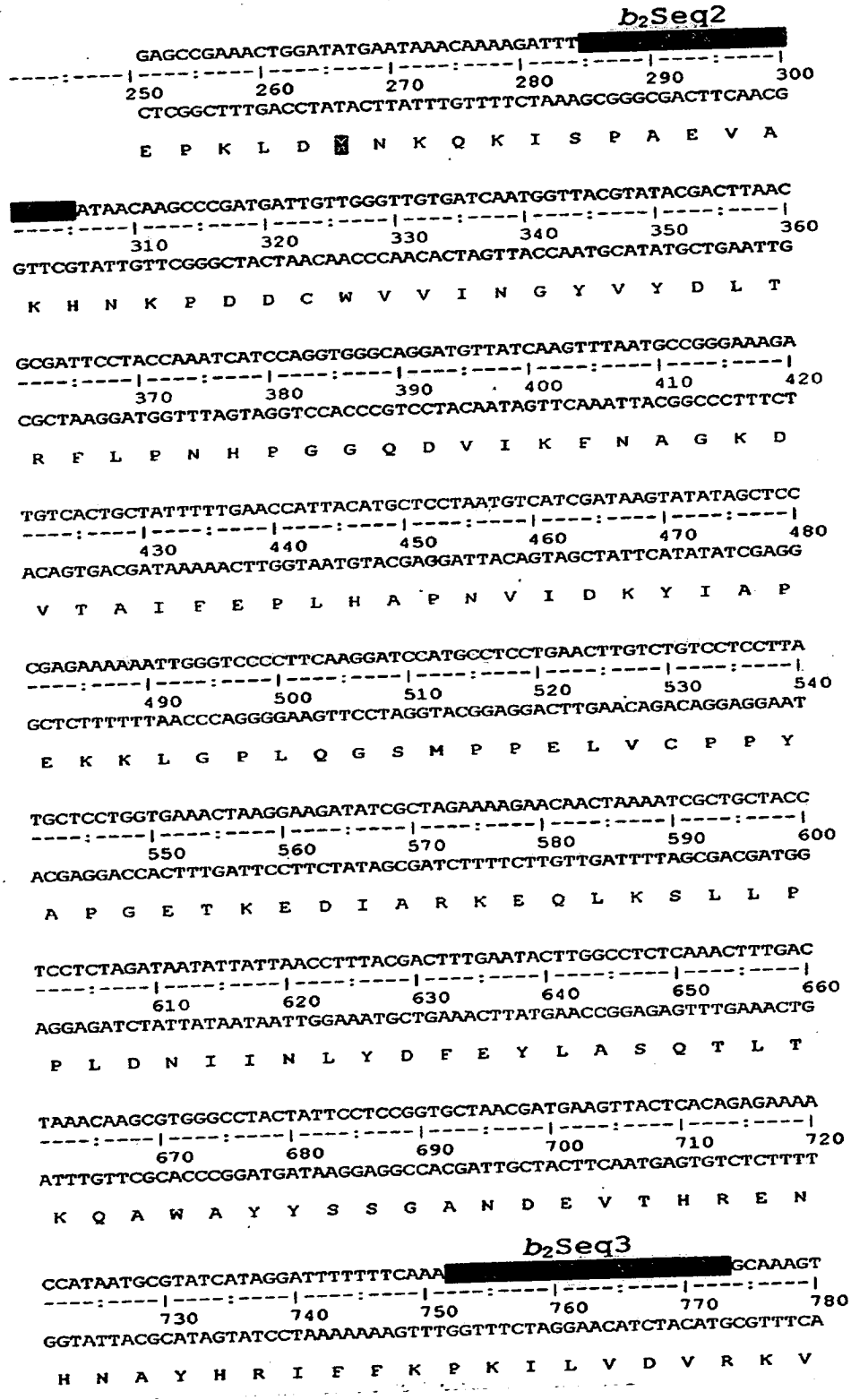

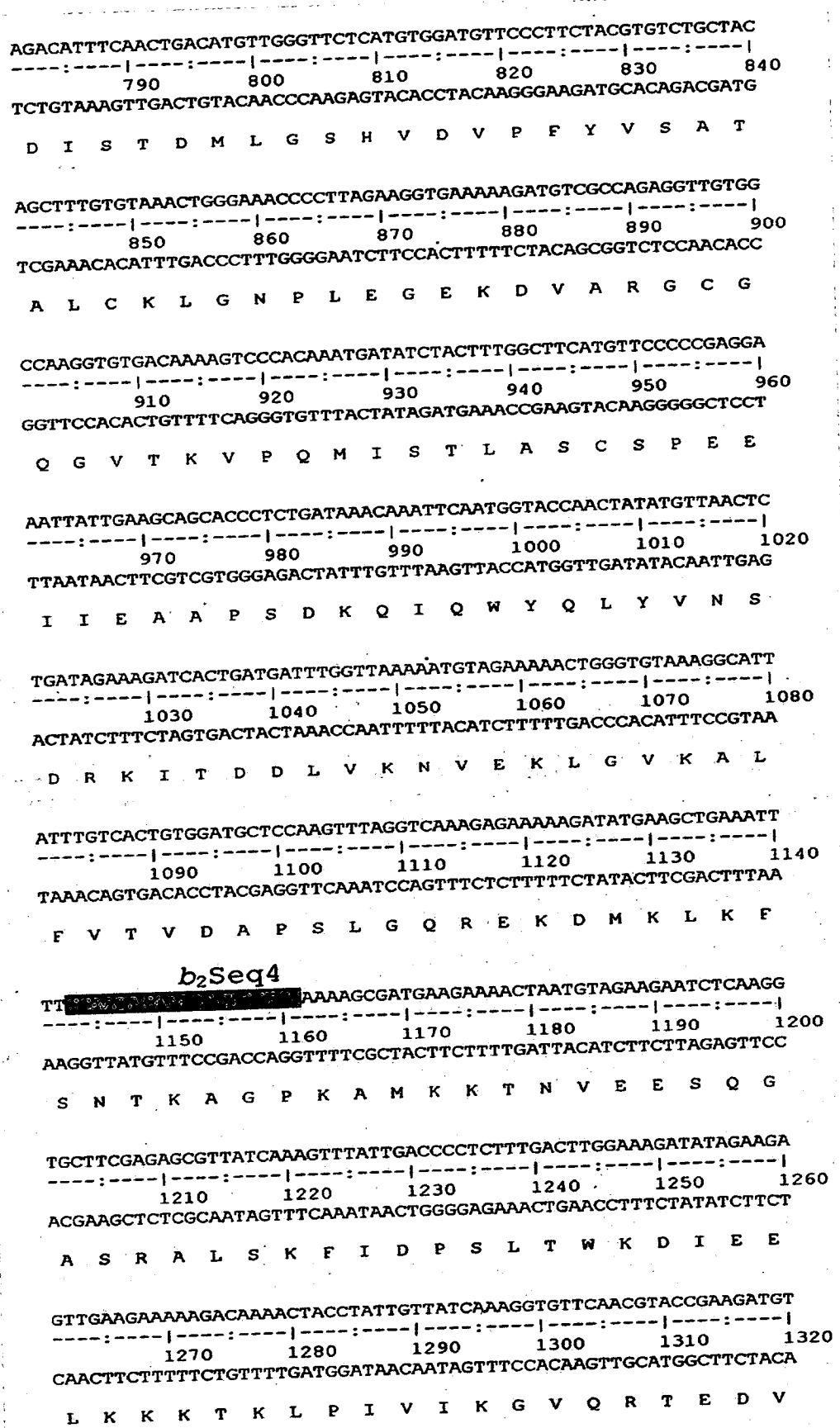
AGACATTTCAACTGACATGTTGGGTTCTCATGTGGATGTTCCCTTCTACGTGTCTGCTAC
790 800 810 820 830 840
TCTGTAAAGTTGACTGTACAACCCAAGAGTACACCTACAAGGGAAGATGCACAGACGATG
D I S T D M L G S H V D V P F Y V S A T
AGCTTTGTGTAAACTGGGAAACCCCTTAGAAGGTGAAAAAGATGTCGCCAGAGGTTGTGG
850 860 870 880 890 900
TCGAAACACATTTGACCCTTTGGGGAATCTTCCACTTTTTCTACAGCGGTCTCCAACACC
A L C K L G N P L E G E K D V A R G C G
CCAAGGTGTGACAAAAGTCCCACAAATGATATCTACTTTGGCTTCATGTTCCCCCGAGGA
910 920 930 940 950 960
GGTTCCACACTGTTTTCAGGGTGTTTACTATAGATGAAACCGAAGTACAAGGGGGCTCCT
Q G V T K V P Q M I S T L A S C S P E E
AATTATTGAAGCAGCACCCTCTGATAAACAAATTCAATGGTACCAACTATATGTTAACTC
970 980 990 1000 1010 1020
TTAATAACTTCGTCGTGGGAGACTATTTGTTTAAGTTACCATGGTTGATATACAATTGAG
I I E A A P S D K Q I Q W Y Q L Y V N S
TGATAGAAAGATCACTGATGATTTGGTTAAAAATGTAGAAAAACTGGGTGTAAAGGCATT
1030 1040 1050 1060 1070 1080
ACTATCTTTCTAGTGACTACTAAACCAATTTTTACATCTTTTTGACCCACATTTCCGTAA
D R K I T D D L V K N V E K L G V K A L
ATTTGTCACTGTGGATGCTCCAAGTTTAGGTCAAAGAGAAAAAGATATGAAGCTGAAATT
1090 1100 1110 1120 1130 1140
TAAACAGTGACACCTACGAGGTTCAAATCCAGTTTCTCTTTTTCTATACTTCGACTTTAA
F V T V D A P S L G Q R E K D M K L K F
b_2Seq4
TT[redacted]AAAAGCGATGAAGAAAACTAATGTAGAAGAATCTCAAGG
1150 1160 1170 1180 1190 1200
AAGGTTATGTTTCCGACCAGGTTTTCGCTACTTCTTTTGATTACATCTTCTTAGAGTTCC
S N T K A G P K A M K K T N V E E S Q G
TGCTTCGAGAGCGTTATCAAAGTTTATTGACCCCTCTTTGACTTGGAAAGATATAGAAGA
1210 1220 1230 1240 1250 1260
ACGAAGCTCTCGCAATAGTTTCAAATAACTGGGGAGAAACTGAACCTTTCTATATCTTCT
A S R A L S K F I D P S L T W K D I E E
GTTGAAGAAAAAGACAAAACTACCTATTGTTATCAAAGGTGTTCAACGTACCGAAGATGT
1270 1280 1290 1300 1310 1320
CAACTTCTTTTTCTGTTTTGATGGATAACAATAGTTTCCACAAGTTGCATGGCTTCTACA
L K K K T K L P I V I K G V Q R T E D V

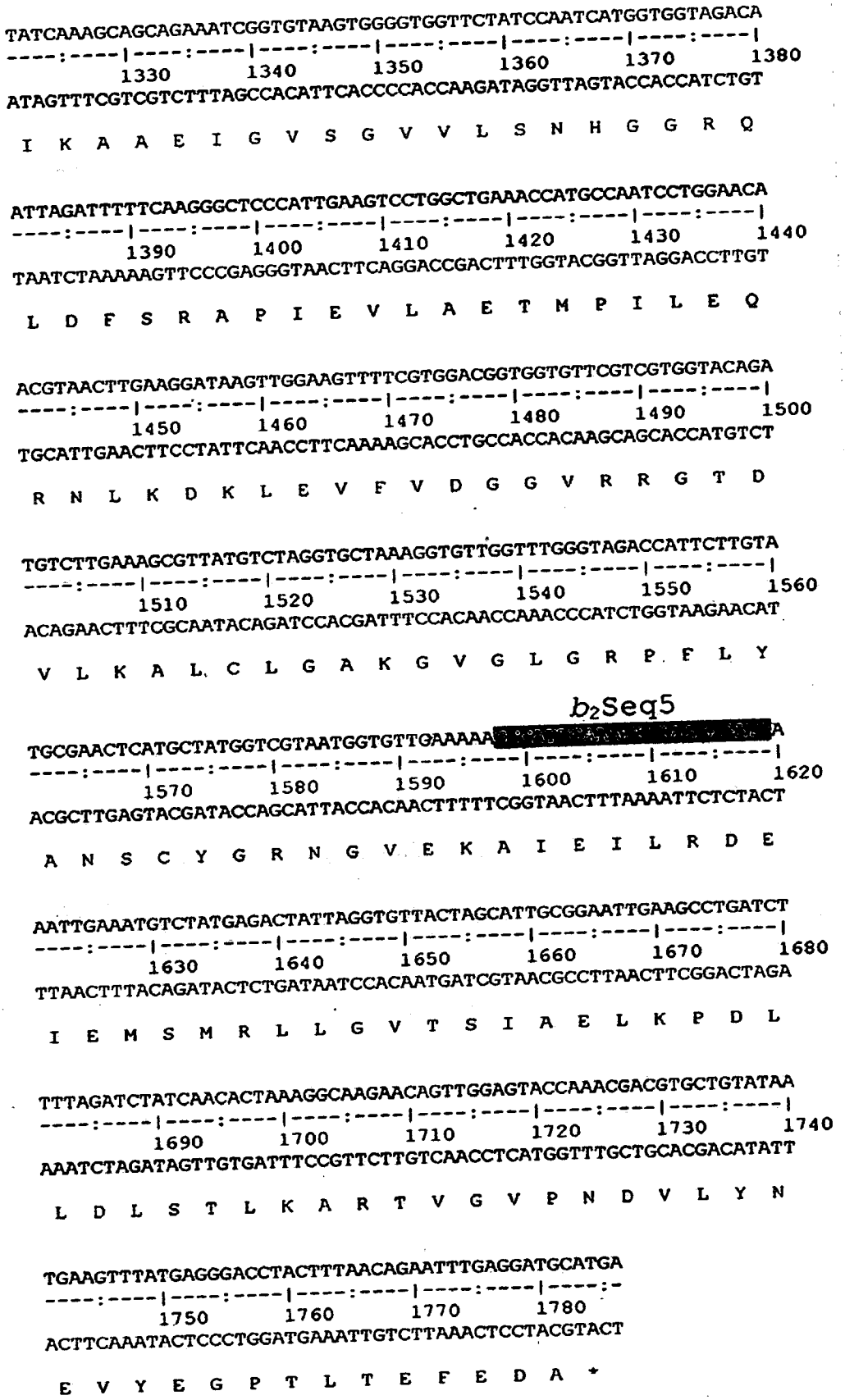
TATCAAAGCAGCAGAAATCGGTGTAAGTGGGGTGGTTCTATCCAATCATGGTGGTAGACA
1330 1340 1350 1360 1370 1380
ATAGTTTCGTCGTCTTTAGCCACATTCACCCCACCAAGATAGGTTAGTACCACCATCTGT
I K A A E I G V S G V V L S N H G G R Q
ATTAGATTTTTCAAGGGCTCCCATTGAAGTCCTGGCTGAAACCATGCCAATCCTGGAACA
1390 1400 1410 1420 1430 1440
TAATCTAAAAAAGTTCCCGAGGGTAACTTCAGGACCGACTTTGGTACGGTTAGGACCTTGT
L D F S R A P I E V L A E T M P I L E Q
ACGTAACTTGAAGGATAAGTTGGAAGTTTTCGTGGACGGTGGTGTTCGTCGTGGTACAGA
1450 1460 1470 1480 1490 1500
TGCATTGAACTTCCTATTCAACCTTCAAAAGCACCTGCCACCACAAGCAGCACCATGTCT
R N L K D K L E V F V D G G V R R G T D
TGTCTTGAAAGCGTTATGTCTAGGTGCTAAAGGTGTTGGTTTGGGTAGACCATTCTTGTA
1510 1520 1530 1540 1550 1560
ACAGAACTTTCGCAATACAGATCCACGATTTCCACAACCAAACCCATCTGGTAAGAACAT
V L K A L C L G A K G V G L G R P F L Y
b_2Seq5
TGCGAACTCATGCTATGGTCGTAATGGTGTTGAAAAA[redacted]A
1570 1580 1590 1600 1610 1620
ACGCTTGAGTACGATACCAGCATTACCACAACTTTTTCGGTAACTTTAAAATTCTCTACT
A N S C Y G R N G V E K A I E I L R D E
AATTGAAATGTCTATGAGACTATTAGGTGTTACTAGCATTGCGGAATTGAAGCCTGATCT
1630 1640 1650 1660 1670 1680
TTAACTTTACAGATACTCTGATAATCCACAATGATCGTAACGCCTTAACTTCGGACTAGA
I E M S M R L L G V T S I A E L K P D L
TTTAGATCTATCAACACTAAAGGCAAGAACAGTTGGAGTACCAAACGACGTGCTGTATAA
1690 1700 1710 1720 1730 1740
AAATCTAGATAGTTGTGATTTCCGTTCTTGTCAACCTCATGGTTTGCTGCACGACATATT
L D L S T L K A R T V G V P N D V L Y N
TGAAGTTTATGAGGGACCTACTTTAACAGAATTTGAGGATGCATGA
1750 1760 1770 1780
ACTTCAAATACTCCCTGGATGAAATTGTCTTAAACTCCTACGTACT
E V Y E G P T L T E F E D A *

Appendix IV

European Bioinformatics Institute (EBI) Pairwise Global and Local Alignment Tool

An example of the EBI Emboss Alignment using the K324C b_2 plasmid DNA. The wild-type DNA sequence of flavocytochrome b_2 is aligned with that from the K324C b_2 plasmid DNA. The mismatches in base pair alignment are shown by dots. The red circle indicates the DNA sequence of mismatching bases that represent the K→C mutation.

```
WILD-TYPE   649 GGCCAAGGTGTGACAAAAGTCCCACAAATGATATCTACTTTGGCTTCATG  698
                ||||||||||||||||||||||||||||||||||||||||||||||||||
K324C       101 GGCCAAGGTGTGACAAAAGTCCCACAAATGATATCTACTTTGGCTTCATG  150

WILD-TYPE   699 TTCCCCCGAGGAAATTATTGAAGCAGCACCCTCTGATAAACAAATTCAAT  748
                ||||||||||||||||||||||||||||||||||||||||||||||||||
K324C       151 TTCCCCCGAGGAAATTATTGAAGCAGCACCCTCTGATAAACAAATTCAAT  200

WILD-TYPE   749 GGTACCAACTATATGTTAACTCTGATAGAAAGATCACTGATGATTTGGTT  798
                ||||||||||||||||||||||||||||||||||||||||||||||||||
K324C       201 GGTACCAACTATATGTTAACTCTGATAGAAAGATCACTGATGATTTGGTT  250

WILD-TYPE   799 AAAAATGTAGAAAAACTGGGTGTAAAGGCATTATTTGTCACTGTGGATGC  848
                ||||||||||||||||||||||||||||||||||||||||||||||||||
K324C       251 AAAAATGTAGAAAAACTGGGTGTAAAGGCATTATTTGTCACTGTGGATGC  300

WILD-TYPE   849 TCCAAGTTTAGGTCAAAGAGAAAAAGATATGAAGCTGAAATTTTCCAATA  898
                ||||||||||||||||||||||||||||||||||||||||||||||||||
K324C       301 TCCAAGTTTAGGTCAAAGAGAAAAAGATATGAAGCTGAAATTTTCCAATA  350

WILD-TYPE   899 CAAAGGCTGGTCCAAAAGCGATGAAGAAAACTAATGTAGAAGAATCTCAA  948
                ||||||||||||||||||||||||||||||||||||||||||||||||||
K324C       351 CAAAGGCTGGTCCAAAAGCGATGAAGAAAACTAATGTAGAAGAATCTCAA  400

WILD-TYPE   949 GGTGCTTCGAGAGCGTTATCAAAGTTATTGACCCCTCTTTGACTTGGAA  998
                |||||||||||||||||||...|||||||||||||||||||||||||
K324C       401 GGTGCTTCGAGAGCGTTATCATGCTTATTGACCCCTCTTTGACTTGGAA  450

WILD-TYPE   999 AGATATAGAAGAGTTGAAGAAAAAGACAAAACTACCTATTGTTATCAAAG  1048
                ||||||||||||||||||||||||||||||||||||||||||||||||||
K324C       451 AGATATAGAAGAGTTGAAGAAAAAGACAAAACTACCTATTGTTATCAAAG  500
```

Appendix V

Enzyme Kinetics and Michaelis-Menten Theory

The reaction of a substrate binding to an enzyme, followed by release of a product molecule is composed of the following elementary steps;

$$E + S \underset{k_{-1}}{\overset{k_1}{\rightleftharpoons}} ES \xrightarrow{k_2} P + E$$

Here, E, S, ES and P represent the enzyme, substrate, enzyme-substrate complex and products respectively.

The ES complex will predominate when [S] becomes saturating, and consequently the second step of the reaction becomes rate limiting. This will prevent any further increase in the rate of the reaction on increasing the [S].

The rate of the reaction can be written as follows;

$$v = \frac{d[P]}{dt} = k_2 [ES] \qquad \text{Equation 1}$$

Therefore, the overall rate of production of ES is reliant upon the difference between the reaction rates which allow the appearance and disappearance of this complex.

$$\frac{d[ES]}{dt} = k_1[E][S] - k_{-1}[ES] - k_2 [ES] \qquad \text{Equation 2}$$

This, however, cannot be integrated without making two assumptions:

1 Equilibrium

$k_{-1} >> k_2$, such that the first step of the reaction reaches equilibrium.

$$K_s = \frac{k_{-1}}{k_1} = \frac{[E][S]}{dt} \qquad \text{Equation 3}$$

Where Ks is the dissociation constant of the first step in the enzymatic reaction.

2 Steady-state

This assumption requires the [S] to be in great excess over [E], which will allow [ES] to remain approximately constant until S has been used up. Therefore, the rate of synthesis of ES is equal to its rate of consumption over most of the course of the reaction, i.e. it remains in a steady-state according to equation 4;

$$\frac{d[ES]}{dt} = 0 \qquad \text{Equation 4}$$

However, [ES] and [E] do not tend to be easily quantifiable terms, thus the total enzyme concentration, $[E]_T$ is used;

$$[E]_T = [E] + [ES] \qquad \text{Equation 5}$$

The rate equation for the enzymatic reaction can now be derived as follows; combining equations 2, 4 and 5 gives,

$$k_1([E]_T - [ES])[S] = (k_{-1} + k_2)[ES]$$

$$\Rightarrow \quad [ES](k_{-1} + k_2 + k_1[S]) = k_1[E]_T[S]$$

$$[ES] = \frac{[E]_T[S]}{\left[\frac{k_{-1} + k_2}{k_1}\right] + [S]}$$ Where $\left[\frac{k_{-1} + k_2}{k_1}\right]$ is known as the Michaelis constant (K_m).

$$\Rightarrow \quad [ES] = \frac{[E]_T[S]}{K_m + [S]}$$ Equation 6

The terms $[E]_T$ and [S] can now be substituted into Equation 1 which equates to the initial velocity of the reaction;

$$v_o = \left(\frac{d[P]}{dt}\right)_{t = t_s} = k_2[ES] = \frac{k_2[E]_T[S]}{K_m + [S]}$$ Equation 7

The maximal rate is obtained when the catalytic sites of the enzyme are saturated with substrate, i.e. when [S] is much greater than K_m – so that $[S]/(K_m + [S])$ approaches 1. Therefore;

$$V_{max} = k_2[E]_T$$ Equation 8

Substituting Equation 8 into Equation 7 yields the **Michaelis-Menten** equation.

$$V = V_{max} \frac{[S]}{[S] + K_m}$$ Equation 9

Sulfite Binding

In the experiment where sulfite binds to the FMN in flavocytochrome b_2, E = S. Thus, as well as having an expression for [E] (Equation 5) and [ES] (Equation 6), an expression for [S] is also required:

$$[S] = [S]_T - [ES] \qquad \text{Equation 10}$$

In addition, V is replaced with ΔA, k_{cat} is replaced with A_{max} and K_m is replaced with K_d. Substitution and rearrangement of Equation 7 yields:

$$K_d = \frac{\left[-\frac{\Delta A}{A_{max}} + E_T \right] \left[S_T - E \right]}{\frac{\Delta A}{A_{max}}} \qquad \text{Equation 11}$$

Since $[ES] = [E]_T - [E]$ and $E = -\Delta A/A_{max} + E_T$, $[ES] = \Delta A/A_{max}$, thus:

$$K_d = \frac{\left[-\frac{\Delta A}{A_{max}} + E \right] \left[S - \frac{\Delta A}{A_{max}} \right]}{\frac{\Delta A}{A_{max}}} \qquad \text{Equation 12}$$

$$\Rightarrow$$

$$\frac{\Delta K_d}{A_{max}} = \left[\frac{\Delta A S}{A_{max}} + \left[\frac{\Delta A}{A_{max}} \right]^2 + ES - \frac{\Delta A E}{A_{max}} \right] \qquad \text{Equation 13}$$

$$\left[\frac{\Delta A}{A_{max}}\right]^2 - \Delta A \left[\frac{S + E + K_d}{A_{max}}\right] + ES = 0 \qquad \text{Equation 14}$$

This gives a quadratic equation in the form of:

$$\Delta A = \frac{-b \pm \sqrt{b^2 - 4ac}}{2a} \qquad \text{Equation 15}$$

Where $a = 1/A_{max} = 1$

$b = (-S - E - K_d)/A_{max} = -A_{max}(S + E + K_d)$

$c = ES = A_{max}^2 ES$ when multiplied by A_{max}^2

So:

$$\Delta A = \frac{A_{max}(S + E + K_d) \pm \sqrt{(A_{max}(S + E + K_d))^2 - 4 A_{max} ES}}{2} \qquad \text{Equation 16}$$

And finally,

$$\Delta A = A_{max}\left[\frac{(S + E + K_d) \pm \sqrt{[(S + E + K_d)^2 - 4ES]}}{2}\right] \qquad \text{Equation 17}$$

Where, S = [sulfite]

E = [flavocytochrome b_2]

K_d = Dissociation constant

A_{max} = Maximum absorbance change

ΔA = Change in absorbance

Appendix VI

Conferences and Courses Attended

7th, 8th and 9th Redox Enzymes Meeting, Firbush Point Field Centre, Perthshire

June 2003 (Delegate)

June 2004 (Speaker)

June 2005 (Delegate)

Inorganic Chemistry Section Meeting, Firbush Point Field Centre, Perthshire

April 2004 (Delegate)

Inorganic Biochemistry Discussion Group (IBDG), Imperial College, London

January 2004 (Delegate)

15th International Symposium on Flavins and Flavoproteins, Shonan Village Centre, Japan

April 2005 (Abstract and Poster Presented)

Inorganic Chemistry, Chemical Biology and Biophysical Chemistry Section Seminars

School of Chemistry Colloquia

Appendix VII

Publications

Mowat, C.G., Rothery, E., Miles, C.S., McIver, L., Doherty, M.K., Drewette, K., Taylor, P., Walkinshaw, M.D., Chapman, S.K., Reid, G.A. (2004) *Nature Structural & Molecular Biology*, **11**, 1023-1024

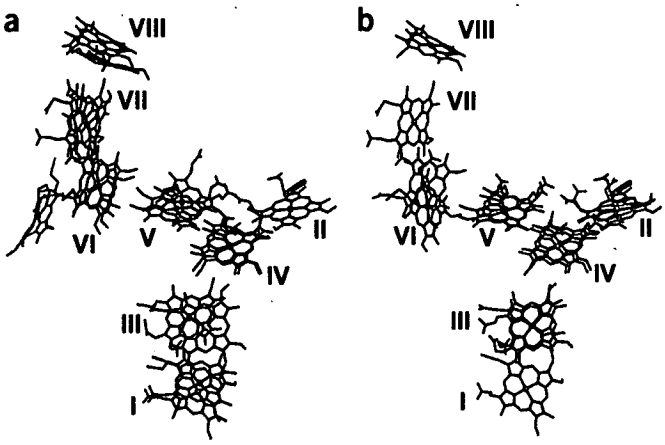

Figure 2 Heme arrangement in octaheme tetrathionate reductase. (**a**,**b**) Overlay of OTR hemes (red, labeled) with those in hydroxylamine oxidoreductase (**a**, blue; PDB entry 1FGJ) and nitrite reductase (**b**, green; PDB entry 1FS7). The active site heme of OTR is shown with thiocyanate present, whereas the active site hemes of hydroxylamine oxidoreductase and nitrite reductase are light blue and light green, respectively.

Thiocyanate is observed at the OTR active site, ligating the heme II iron through its sulfur atom with a Fe-S distance of 2.4 Å. The presence of this anion is almost certainly a consequence of crystallization in the presence of a high concentration of potassium thiocyanate but indicates the availability of this heme for binding a small molecule. The sulfur atom of thiocyanate is also found to be hydrogen-bonded to the terminal amino group of the side chain of Lys153 at a distance of 3.5 Å. This may indicate a possible role for Lys153 in substrate binding and/or activation. The nitrogen atom of the bound thiocyanate is hydrogen-bonded to a water molecule (Wat470) that is also hydrogen-bonded to the sulfur of Cys64. Cys64 is the only cysteine in OTR that is not involved in binding a heme group and its location in the active site of the enzyme (7.5 Å from the heme iron) indicates that it may play some role in catalysis. Purified OTR is an efficient tetrathionate reductase (E.R. *et al.*, unpublished results). The only previously identified tetrathionate reductase, from *Salmonella typhimurium*, is a membrane-bound molybdoenzyme[6]. The reduction of tetrathionate to produce two thiosulfate molecules may be mediated by disulfide exchange involving Cys64 followed by two-electron reduction via heme II. No other probable catalytic side chains are located in the region of the substrate-binding pocket. The reactivity of Cys64 is also demonstrated by the fact that in the structure of the enzyme this residue is apparently modified. Additional electron density adjacent to the cysteine sulfur was modeled as either an oxygen atom or a second sulfur atom but the data do not allow us to distinguish between these options. Modification of a cysteine to a sulfenic acid has been shown to be important for the activity of several enzymes[7] and a persulfide derivative is found in the thiosulfate oxidising enzyme, SoxAX, from *Rhodovulum sulfidophilum*[8], though this is stabilized by direct ligation to a heme iron.

The overall arrangement of the eight hemes of OTR is markedly similar to that observed for the hemes in hydroxylamine oxidoreductase from *Nitrosomonas europaea*[9]. Indeed, seven of the hemes are almost superimposable (in both position and orientation; r.m.s. deviation of heme irons of 2.6 Å) but the active site hemes of both enzymes are found on opposite sides of the seven-heme 'chain' (**Fig. 2a**). Similarly, the heme groups of the pentaheme nitrite reductase NrfA[7] are superimposable with five of the hemes of tetrathionate reductase (II–VI), with an r.m.s. deviation for heme iron alignment of 0.4 Å. In this case the active site hemes form part of this conserved arrangement, and the lysine ligands are found on the same side of each (**Fig. 2b**). Notably, although the conservation of the heme arrangement is marked, there is no conservation of protein architecture between OTR and either of the other enzymes. It is unclear to us how these observations can be interpreted in terms of protein evolution.

Note: Supplementary information is available on the Nature Structural & Molecular Biology website.

ACKNOWLEDGMENTS

We thank the UK Biotechnology and Biological Sciences Research Council for grant funding to G.A.R. and S.K.C. and the Wellcome Trust for their support to the Edinburgh Protein Interaction Centre. Synchrotron access at European Molecular Biology Laboratory Hamburg was supported by the European Commission (contract HPRI-CT-1999-00017).

COMPETING INTERESTS STATEMENT

The authors declare that they have no competing financial interests.

Received 26 May; accepted 10 August 2004
Published online at http://www.nature.com/nsmb/

1. Heidelberg, J.F. *et al. Nat. Biotechnol.* **20**, 1118–1123 (2002).
2. Gordon, E.H.J., Pealing, S.L., Chapman, S.K., Ward, F.B. & Reid, G.A. *Microbiology* **144**, 937–945 (1998).
3. Lo Conte, L., Brenner, S.E., Hubbard, T.J.P., Chothia, C. & Murzin, A. *Nucleic Acids Res.* **30**, 264–267 (2002).
4. Einsle, O. *et al. J. Biol. Chem.* **275**, 39608–39616 (2000).
5. Simon, J. *FEMS Microbiol. Rev.* **26**, 285–309 (2002).
6. Hensel, M., Hinsley, A.P., Nikolaus, T., Sawers, G. & Berks, B.C. *Mol. Microbiol.* **32**, 275–287 (1999).
7. Claiborne, A., Mallett, T.C., Yeh, J.I., Luba, J. & Parsonage, D. *Adv. Protein Chem.* **58**, 215–276 (2001).
8. Bamford V.A. *et al. EMBO J.* **21**, 5599–5610 (2002).
9. Igarashi, N., Moriyama, H., Fujiwara, T., Fukumori, Y. & Tanaka, N. *Nat. Struct. Biol.* **4**, 276–284 (1997).

Octaheme tetrathionate reductase is a respiratory enzyme with novel heme ligation

Christopher G Mowat[1,2], Emma Rothery[2], Caroline S Miles[1], Lisa McIver[1,2], Mary K Doherty[1,2], Katy Drewette[2], Paul Taylor[1], Malcolm D Walkinshaw[1], Stephen K Chapman[2] & Graeme A Reid[1]

We have isolated a soluble cytochrome from *Shewanella oneidensis* that contains eight covalently attached heme groups and determined its crystal structure. One of these hemes exhibits novel ligation of the iron atom by the ε-amino group of a lysine residue, despite its attachment via a typical CXXCH motif. This heme is most likely the active site for tetrathionate reduction, a reaction catalyzed efficiently by this enzyme.

Shewanella species exhibit marked respiratory flexibility and use a particularly wide range of electron acceptors for anaerobic respiration. The genome sequence of *Shewanella oneidensis* MR-1 (ref. 1) includes reading frames encoding many putative redox proteins likely to be involved in pathways leading to these acceptors. We identified a novel sequence that includes eight CXXCH motifs that are characteristic of *c*-type cytochromes, but with no homologs of known function. To obtain large amounts of this putative octaheme cytochrome (OTR) we overexpressed the native protein in *Shewanella frigidimarina* EG301 (ref. 2). Crystals of OTR were grown by the hanging-drop vapor diffusion and diffraction data were collected at multiple wavelengths (see **Supplementary Methods** online).

The electron density map, obtained using the anomalous iron signal to calculate phases, was of sufficient quality to allow unambiguous tracing of the polypeptide chain. This was aided by the positioning of the eight heme groups, their binding motifs and surrounding sequence. A data set at a resolution of 2.2 Å was used to refine the model to a final *R*-factor of 15.5% (see **Supplementary Table 1**). The quality of the final electron density map (**Fig. 1a**) allowed unambiguous fitting of the protein and its prosthetic groups. The single polypeptide of 442 amino acids folds into essentially two structural features (**Fig. 1b**). An N-terminal region comprising residues 1–240 is mainly α-helical and provides the framework for seven of the heme groups (hemes I–VII), as well as the active site residues mentioned below. The remainder of the protein is largely composed of β-strands that form a large sheet over the substrate-binding pocket. Two smaller helical regions involving residues 356–387 and 405–414 may have roles in enclosing the active site and in binding heme VIII, respectively. No matches were found in the SCOP database of protein folds[3] (http://www.ebi.ac.uk/msd/ssm); the structure of OTR therefore represents a novel protein fold.

From the sequence of OTR we expected that the protein would contain eight bis-histidine-ligated *c*-type heme groups. However, during model building it was apparent that the CXXCH motif (residues 74–78) for heme II does not provide a histidine ligand to the heme iron, a role taken by a lysine residue, Lys56 (**Fig. 1a**). It can also be seen that His78 is oriented away from heme II, with Trp41 lying between it and Lys56. Lysine heme ligation has only been observed previously in the pentaheme nitrite reductases from *Wolinella succinogenes*[4] and several other bacteria, but in these proteins the lysine ligand forms part of a CXXCK heme attachment motif. Notably, the predicted NrfA protein from *Campylobacter jejuni* has CXXCH rather than CXXCK at the active site heme[5]. The heme ligation in OTR raises the possibility that even in this NrfA, the heme could be ligated by a lysine.

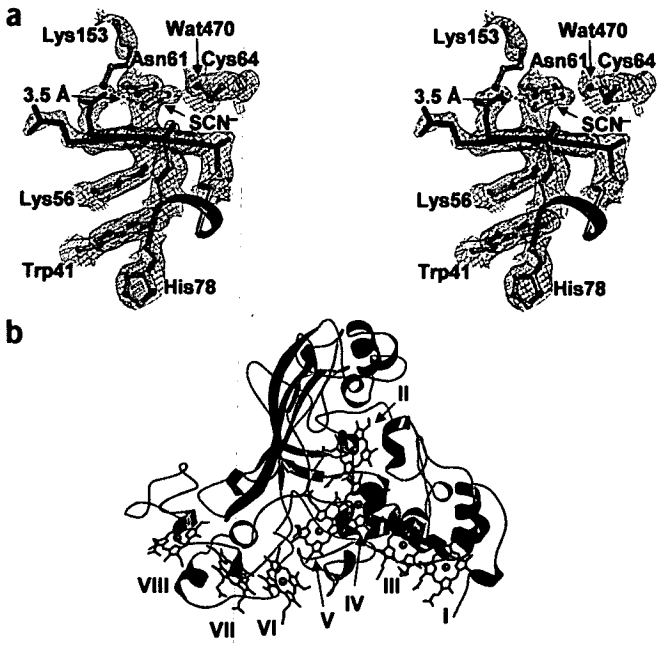

Figure 1 Structure of octaheme tetrathionate reductase. (**a**) Stereo view of the region surrounding heme II of OTR with final electron density. The $2F_o - F_c$ (cyan) map is contoured at 1 σ, whereas the $F_o - F_c$ (purple) map is contoured at 3 σ, indicating possible modification of Cys64. The hydrogen bond between the side chain of Lys153 and the S of thiocyanate is a dashed line. (**b**) Overall structure of octaheme tetrathionate reductase. Residues 1–240 are purple, and the remainder of the protein (residues 241–442) is green. The eight heme groups, labelled sequentially from the N terminus, are red and form a linear arrangement along one face of the protein. Thiocyanate is in atom-type colors bound to heme II at the active site of the enzyme. The OTR atomic coordinates have been deposited in the Protein Data Bank (accession code 1SP3).

[1]Institute of Cell and Molecular Biology, School of Biological Sciences, University of Edinburgh, Mayfield Road, Edinburgh EH9 3JR, UK. [2]School of Chemistry, University of Edinburgh, West Mains Road, Edinburgh EH9 3JJ, UK. Correspondence should be addressed to G.A.R. (graeme.reid@ed.ac.uk).

Published online 5 September 2004; doi:10.1038/nsmb827